Postzygotic barriers persist despite ongoing introgression in hybridizing *Mimulus* species

Samuel J. Mantel[1*] and Andrea L. Sweigart[1]

[1]Department of Genetics, University of Georgia, Athens, GA, 30602, USA

[*]Corresponding author:
Samuel Mantel
120 E. Green St.
Athens, GA 30602
smantel1@uga.edu

Abstract

The evolution of postzygotic isolation is thought to be a key step in maintaining species boundaries upon secondary contact. Yet the dynamics and persistence of hybrid incompatibilities in naturally hybridizing species is not well understood. Here, we explore these issues with genetic mapping in three independent populations of recombinant inbred lines between naturally hybridizing monkeyflowers *Mimulus guttatus* and *M. nasutus* from the sympatric Catherine Creek population. We discovered that the three *M. guttatus* founders differ dramatically in admixture history, with nearly a quarter of one founder's genome introgressed from *M. nasutus*. Comparative genetic mapping in the three RIL populations revealed three new putative inversions, each one segregating among the *M. guttatus* founders, two due to admixture. We also found strong, genome-wide transmission ratio distortion in all RILs, but patterns were highly variable among the three populations. At least some of this distortion appears to be explained by epistatic selection favoring parental genotypes, but tests of inter-chromosomal linkage disequilibrium also revealed multiple candidate Dobzhansky-Muller incompatibilities. We also mapped several genetic loci for hybrid pollen viability, including two interacting pairs that coincide with peaks of distortion. Remarkably, even with this limited sample of three *M. guttatus* lines, we discovered abundant segregating variation for hybrid incompatibilities with *M. nasutus,* suggesting this population harbors diverse contributors to postzygotic isolation. Moreover, even with substantial admixture, hybrid incompatibilities between Mimulus species persist, suggesting postzygotic isolation might be a potent force in maintaining species barriers in this system.

Introduction

Despite often being conceptualized as a single event, it has long been understood that speciation is a complex and dynamic process (Darwin, 1859; Dobzhansky, 1937). As new species form (generally in allopatry), the cumulative impacts of adaptive divergence, genetic drift, and the sorting of ancestral variation can lead to the evolution of reproductive isolation, which limits gene flow between these species when they come into secondary contact (Dobzhansky, 1937; Mayr, 1942; Coyne & Orr, 2004). Nevertheless, gene flow between recognized species – at rates high enough to have substantial genomic consequences – is not uncommon, even when strong reproductive isolating barriers exist (Nolte *et al.*, 2009; Teeter *et al.*, 2010; Ellegren *et al.*, 2012; Renaut *et al.*, 2013; Larson *et al.*, 2014; Delmore *et al.*, 2015; Caeiro-Dias *et al.*, 2023). At the extremes, hybridization can break down established barriers causing previously isolated lineages to fuse (Taylor *et al.*, 2006) or to strengthen reproductive isolation through reinforcement (Servedio & Kirkpatrick, 1997; Jaenike et al., 2006; Hopkins & Rausher, 2012). On the other hand, theory suggests that hybridization might sometimes reflect partial reproductive isolation as a stable optimum(Servedio & Hermisson, 2020). Studies of naturally hybridizing species can provide a window into the causes of these alternative evolutionary outcomes, allowing us to identify and measure the impact of the genetic loci involved in reproductive isolation.

One powerful approach to this problem is experimental hybridization of incompletely isolated species that occur together in secondary sympatry. In particular, the use of late-generation hybrids such as recombinant inbred lines (RILs) can enable replication of wild, admixed genotypes and facilitate genetic mapping of barrier loci under controlled

environmental conditions. This approach should be especially fruitful for identifying loci involved in postzygotic isolation because strongly incompatible allele combinations are likely to be purged during RIL formation. Indeed, selection against hybrid incompatibilities can be a major source of transmission ratio distortion (TRD) in RIL populations (Colomé-Tatché & Johannes, 2016). Although there are often additional contributors to TRD in experimental hybrid populations (reviewed in Fishman & McIntosh, 2019), hybrid incompatibilities are expected to leave a particular signature of distortion, generating both local peaks and linkage disequilibrium between unlinked loci caused by underrepresented or absent multi-locus genotypes. This signature might be particularly apparent in RILs, which have the advantage of multiple generations of recombination, increasing power to detect and localize incompatibilities by amplifying their effects (and revealing recessive phenotypes) through inbreeding (Moyle & Nakazato, 2008).

Despite the clear value of experimental hybridization and RILs for illuminating the genetic causes of reproductive isolation, inferences to natural populations can be challenging because such studies are often based on initial crosses between only two individuals or inbred lines. This limitation might be serious for investigations of postzygotic isolation between species in the early stages of divergence, as hybrid incompatibilities are often polymorphic (Sweigart *et al.*, 2007; Good *et al.*, 2008; Cutter, 2012), particularly in populations with ongoing hybridization (Zuellig & Sweigart, 2018). Variation in chromosomal structure is also a common feature of natural populations (Hoffmann & Rieseberg, 2008), and polymorphic inversions are often associated with adaptive differences (Feder *et al.*, 2003; Lowry & Willis, 2010; Jones *et al.*, 2012) and reproductive isolation (Noor *et al.*, 2001; Sotola *et al.*, 2023). One way to capture a more

77 representative set of natural variation is to generate a multi-parent mapping population, for
78 instance by performing multiple biparental crosses to a common founder (Scott *et al.*, 2020).
79 Although this strategy is now routinely used in plant breeding programs (Scott *et al.*, 2020) and
80 to dissect the genetics of complex traits (Aylor *et al.*, 2011; Long *et al.*, 2014) it has rarely been
81 applied to studies of speciation.

82 In this study we investigate patterns and mechanisms of reproductive isolation in three
83 independent RIL populations constructed from crosses between *Mimulus guttatus* and *M.*
84 *nasutus* (also referred to as *Erythranthe guttata* and *E. nasuta*: see Lowry *et al.*, 2019 and
85 Nesom *et al.*, 2019). These two species are closely related (~200 KYA diverged: Brandvain *et al.*,
86 2014), and broadly allopatric across western North America, but they also occur in secondary
87 sympatry at many sites in their shared range. One such sympatric site occurs at Catherine Creek
88 (CAC) in Washington state, a system of ephemeral seeps and streams that flow into the
89 Columbia River. The two *Mimulus* species have diverged in mating system (*M. guttatus* is large
90 flowered and predominantly outcrossing, whereas *M. nasutus* is a small flowered and primarily
91 selfing), which acts as a strong premating barrier where the two species co-occur (Martin &
92 Willis, 2007). At Catherine Creek, divergent flowering phenology (Kenney & Sweigart, 2016) and
93 microhabitat adaptation (Mantel & Sweigart, 2019) are also important contributors to
94 premating isolation. Despite these substantial barriers to interspecific mating, studies of
95 population genomic variation at Catherine Creek have revealed clear signatures of historical and
96 contemporary hybridization (Kenney & Sweigart, 2016), resulting in largely unidirectional
97 introgression from *M. nasutus* into *M. guttatus* (Sweigart & Willis, 2003; Brandvain *et al.*, 2014;
98 Kenney & Sweigart, 2016). Even in the absence of interspecific gene flow, *M. guttatus*

populations are exceptionally genetically diverse (Flagel *et al.*, 2014; Puzey *et al.*, 2017) and maintain substantial variation for complex phenotypes (Troth et al., 2018).

Here, we attempt to capture and leverage this diversity at Catherine Creek to understand the patterns and mechanisms of hybrid breakdown in naturally hybridizing species. We generate three independent RIL populations by crossing distinct CAC *M. guttatus* progenitors to a common *M. nasutus* parent. Using this powerful crossing design, we discover that differences in admixture have cascading effects on structural variation and reproductive barriers. Moreover, even in this sample of three *M. guttatus* lines, we find segregating variation for hybrid incompatibilities with *M. nasutus*, suggesting this population harbors diverse contributors to postzygotic isolation. Finally, we discover that even with substantial admixture, hybrid incompatibilities between *Mimulus* species persist, suggesting postzygotic isolation might be a potent force in maintaining species barriers in the face of ongoing hybridization.

Materials and Methods

Plant Material and Crossing Design

The plants used in this study were derived from a collection of inbred lines (>10 generations inbred, single seed decent) produced from wild-collected seed from Catherine Creek (CAC). The CAC site consists of a system of gently sloping streams and seeps carrying snowmelt and spring rain out of the Cascade Mountains southward through a rocky meadow into the Columbia River Gorge. While *M. nasutus* and *M. guttatus* grow sympatrically at CAC, often within centimeters of each other, they occupy somewhat distinct microhabitats and flower asynchronously (Kenney & Sweigart, 2016). Still, reproductive isolation is incomplete between the species and ongoing introgression is detectable, mostly from *M. nasutus* into *M. guttatus* (Brandvain *et al.*, 2014; Kenney & Sweigart, 2016).

We produced three parallel RIL populations from crosses between CAC *M. guttatus* and *M. nasutus*. We selected three previously studied CAC *M. guttatus* inbred lines (CAC110, CAC162, and CAC415; TableS1; Mantel & Sweigart, 2019) with stereotypic *M. guttatus* morphological and phenological characteristics and which produced highly fertile F1s with *M. nasutus.* One *M. nasutus* inbred line (CAC9) served as a common maternal parent, which we emasculated before pollen development, and crossed by hand-pollination with pollen from each of the *M guttatus* inbred lines, producing three F1 hybrids. For each of these F1 hybrids, we self-fertilized a single plant to generate three corresponding F2 populations (*N* = 500 each). We planted seeds onto moist Fafard 3-B potting mix (Sun Gro Horticulture, Agawam, MA) in 2.5” pots, and cold stratified them for seven days at 4°C before moving them to a Conviron growth chamber (16-hr days; 23°C days/16°C nights) for germination. We transplanted seedlings into

133 individual cells of 96-cell plug trays filled with potting mix and moved them to the University of
134 Georgia greenhouses under 16-hr supplemental light, 23°C days/16°C nights. Under these
135 germination and growing conditions, we performed four additional rounds of self-fertilization
136 using single-seed-descent to produce three populations of F6 recombinant inbred lines (RILs;
137 Figure S1). We generated a total of 368 RILs (151 CAC110 RILs, 128 CAC162 RILs, and 89 CAC415
138 RILs), much lower than the initial 1500 due to line extinction during the inbreeding process.
139
140 *Library Preparation, Sequencing, and Processing*
141 We grew one individual of each of the 368 RILs (F6 generation or later) for tissue
142 collection and DNA extraction in the greenhouse at the University of Georgia under the
143 conditions described above. We collected bud and meristem tissue from each individual into 96-
144 well plates on dry ice, stored them at -80°C, and extracted genomic DNA using a modified CTAB
145 method in a 96-well format (dx.doi.org/10.17504/protocols.io.bgv6jw9e). We then constructed
146 ddRADseq libraries using a modified version of RAD Capture (Ali *et al.*, 2016), "BestRAD"
147 (dx.doi.org/10.17504/protocols.io.6awhafe). Briefly, we digested 50-100 ng of genomic DNA
148 with BfaI and PstI, and used the 'NEBNext Ultra II' library preparation kits for Illumina (New
149 England BioLabs, Ipswich, MA) to ligate 48 unique barcoded i5 adaptors to each sample, isolated
150 tagged fragments, and pooled samples into 8 pools of 48 or fewer samples each. We attached a
151 unique 'NEBNext Adaptor for Illumina' i7 adaptor to each pool of samples, and enriched the
152 samples with PCR. We size-selected the libraries to 300-900bp using BluePippin 2% agarose
153 cassettes (Sage Science, Beverly, MA) and pooled the libraries in equimolar concentrations
154 following quantification via qPCR. We prepared libraries for, and sequenced the same RILs

155 twice, each on two partial lanes of Illumina HiSeq4000 for paired end 150-bp reads at the
156 Genome Sequencing Facility at Duke University. We also extracted genomic DNA from bud and
157 leaf tissue of the three parental CAC *M. guttatus* lines using a modified CTAB method as above.
158 Whole genome sequence (WGS) libraries were prepared and sequenced on a partial lane of
159 Illumina HiSeq4000 for paired end 150-bp reads at the Genome Sequencing Facility at Duke
160 University.

161 After trimming Illumina adaptors from reads using Trimmomatic (v0.36; Bolger *et al.*,
162 2014), we aligned WGS reads to the *Mimulus guttatus* IM62v3 refence genome (phytozome.org)
163 using BWA-MEM (v0.7.17; Li & Durbin, 2009; Li, 2013). We then removed reads with alignment
164 qualities <Q29 with SAMtools view (v1.6; Li *et al.*, 2009) and added read groups, checked mate-
165 pair information, and removed PCR duplicates with Picard (v2.16.0;
166 broadinstitute.github.io/picard/). We then removed paired reads which had been mapped to
167 different contigs using SAMtools view (v0.7.17; Li *et al.*, 2009). Finally, using GATK
168 HaplotypeCaller (v3.8.1; Van der Auwera & O'Connor, 2020) in GVCF mode we called SNPs, and
169 filtered SNPs to remove heterozygous calls and retain sites with a minimum depth of 3x, and a
170 maximum depth of 2 standard deviations above the mean (calculated with Qualimap2 (v2.2.1;
171 Okonechnikov *et al.*, 2016)) for each line. To allow for genotyping of *M. guttatus* and *M. nasutus*
172 SNPs across the genome, we identified a full list of diagnostic SNPs (those homozygous for
173 different alleles in each of the parental pairs, CAC9 & CAC110, CAC9 & CAC162, and CAC9 &
174 CAC415). We joint genotyped each pair of parental lines using GATK GenotypeGVCFs (v3.8.1;
175 Van der Auwera & O'Connor, 2020). We quality filtered the called SNPs (QD < 2.0, FS > 60.0, MQ
176 < 40.0, MQRankSum < -12.5, ReadPosRankSum < -8.0) and retained only biallelic SNPs using

177 VariantFiltration and SelectVariants. From these three VCFs we extracted a list of high quality
178 diagnostic SNPs with VCFtools (v0.1.16; Danecek *et al.*, 2011).
179 We demultiplexed the ddRADseq data by i7 index following sequencing and removed
180 PCR duplicates from each library, using the unique molecular barcode of the i5 adaptor with a
181 custom Python script (dx.doi.org/10.17504/protocols.io.bjnbkman). We demultiplexed each
182 library to the individual sample level using Flip2BeRAD (github.com/tylerhether/Flip2BeRAD)
183 and Stacks process_radtags (v2.55; Catchen *et al.*, 2011, 2013). We removed Illumina adaptors
184 and aligned reads to the *Mimulus guttatus* IM62 v3 reference assembly (IM: Iron Mountain, an
185 allopatric *M. guttatus* population in Oregon, ~200km south of CAC). 6 samples were removed
186 from further analysis (4 from the CAC162 RILs, and 2 from the CAC415 RILs) due to low
187 similarity between duplicate BAMs produced from the two independent ddRAD library
188 preparations. We then merged the remaining duplicate BAMs with SAMtools merge (v0.7.17; Li
189 *et al.*, 2009), leaving a total of 362 RIL individuals (151 CAC110 RILs, 124 CAC162 RILs, and 87
190 CAC415 RILs). We then processed reads with Picard and SAMtools as above (with the exception
191 of MarkDuplicates, as PCR duplicates were already removed). We called SNPs, joint genotyped
192 each RIL population with the parental lines from which it was derived, and filtered called SNPs
193 as described above. We then removed sites with only parental coverage with VariantFiltration
194 and SelectVariants in GATK (v3.8.1; Van der Auwera & O'Connor, 2020). Finally, using the list of
195 diagnostic SNPs between each pair of parental lines, we removed non-diagnostic sites with
196 VCFtools (v0.1.16; Danecek *et al.*, 2011).
197 To assess levels of residual heterozygosity in the RIL populations and ensure its removal
198 would not skew our RIL genotypes, we filtered the VCFs of diagnostic SNPs to a minimum depth

199 of 10x (GATK VariantFiltration and SelectVariants as above). We then estimated genome wide
200 heterozygosity at the SNP level. Apart from a few very small regions of intermediate
201 heterozygote frequency which may warrant future investigation, heterozygosity was low and
202 uniform across the genome: CAC110 RILs: 1.95%, N=13,975; CAC162 RILs: 2.34%, N=33,340;
203 CAC415 RILs: 2.79%, N=23,178 and consistent with the Mendelian expectation (~1.5-3%, in
204 F6/F7 individuals).
205
206 *Assessment of Introgression in Parental Lines*
207 As previous studies have shown that admixture between *M. guttatus* and *M. nasutus* is
208 common at CAC (Brandvain *et al.*, 2014; Kenney & Sweigart, 2016) we first checked the selected
209 CAC *M. guttatus* parental lines for evidence of introgression from *M. nasutus*. To coarsely
210 identify putative regions of introgression between CAC *M. nasutus* and the CAC *M. guttatus*
211 parental lines, we used a custom perl script to calculate Dxy between CAC9 and the three
212 parental CAC *M. guttatus* lines in non-overlapping 50kb windows which contained 5000 or more
213 called sites.
214 To more concretely asses evidence of *M. nasutus* introgression in the parental CAC *M.*
215 *guttatus* lines we used the newly generated WGS data, plus WGS data from 12 other inbred
216 *Mimulus* accessions downloaded from the SRA (https://www.ncbi.nlm.nih.gov/sra): the parental
217 *M. nasutus* line CAC9, 3 non-CAC *M. nasutus* lines, 5 additional non-parental *M. guttatus* lines
218 from CAC, 2 non-CAC *M. guttatus* lines, and 1 *M. dentilobus* line as an outgroup) (Table S1). We
219 processed reads from additional (non-parental) lines as above and joint genotyped all lines
220 together using GATK GenotypeGVCFs (v3.8.1; Van der Auwera & O'Connor, 2020). We used

221 GATK to filter called SNPs based on quality as above, and retained only biallelic SNPs with
222 VariantFiltration and SelectVariants, producing a high-quality set of called SNPs.
223 We identified putative regions of introgression using a Hidden Markov Model (HMM,
224 modified from (Durbin *et al.*, 1998) developed in (Brandvain *et al.*, 2014)). As an input for the
225 model, we identified fourfold degenerate sites in the IM62 v3 reference assembly using the
226 associated gene annotations extracted with a Perl script developed by Tim Sackton
227 (https://github.com/tsackton/linked-selection/tree/master/misc_scripts), and identified non-
228 degenerate sites in the same way using modified versions of the script. With these lists and the
229 VCF of high-quality filtered SNPs in parental and non-parental *Mimulus* lines described above,
230 we used custom Perl scripts to count the total number of sites, as well as the number of non-
231 degenerate and fourfold degenerate sites, with genotype calls in each 1kb window across the
232 genome of each sequenced line. We then counted the number of those sites which differed in
233 their SNP call between each pairwise comparison of lines. With these counts and the HMM, we
234 calculated posterior probabilities of *M. nasutus* and *M. guttatus* ancestry across the genomes of
235 the parental CAC *M. guttatus* lines. We considered 1kb windows with a calculated posterior
236 probability of *M. nasutus* ancestry >0.95 to be windows showing evidence of introgression.
237
238 *RIL Genotyping and Linkage Mapping*
239 To genotype the RILs we first used custom python scripts to count the number of reads
240 supporting reference and alternate SNP calls at each site, in each RIL individual. We then
241 assigned parental ancestry to these calls, with a custom R script leveraging the parental SNP
242 information to convert ref/alt calls to *M. guttatus* or *M. nasutus* allele calls. We then used a

243 custom python script to average SNP calls across non-overlapping 50kb windows, producing a
244 consensus call leveraging the read depth at each called SNP. We called windows with >75% *M.*
245 *guttatus* calls as homozygous *M. guttatus*, and vice versa, and called windows with between 25
246 and 75% of either genotype heterozygous. This produced windowed genotype calls for many
247 50kb windows across the genome, but left gaps where windows containing no sequencing reads
248 could not be genotyped. To fill these gaps we used Python scripts from the processing steps of
249 the program GOOGA (Flagel *et al.*, 2019) to calculate genotype probabilities for each window in
250 each RIL individual. We first used the windowed genotypes to estimate genotype error rates and
251 recombination rates for each RIL sample, using the advanced generation RIL expectation of 1:1
252 homozygous genotype frequencies. During this process we dropped 39 samples from further
253 analysis due to a low number of called genotypes (from low original coverage) leading to high
254 (e1 or e2 > 0.2) estimated error rates (8 from the CAC110 RILs, 26 from the CAC162 RILs, and 5
255 from the CAC415 RILs). We used an HMM (Flagel *et al.*, 2019) leveraging this error and
256 recombination information to estimate genotype probabilities at each 50kb window across the
257 genome in each RIL individual. We converted genotype probabilities to hard genotype calls by
258 excluding calls with an estimated genotype probability of <0.75. Of the original 368 RILs, we
259 generated genotype data for 323 of them (143 of the original 151 from the CAC110 RILs, 98/128
260 from the CAC162 RILs, and 82/89 from the CAC415 RILs).
261 We used LepMAP3 (Rastas, 2017) to construct a high density linkage map for each of
262 the three RIL families using the genotype matrices produced above. We used the affx2post.awk
263 script to calculate posterior genotype probabilities, and then ran ParentCall2 with default
264 parameters. We ran SeparateChromosomes2 to group markers from the same chromosome,

265 followed by OrderMarkers2 (grandparentPhase=1, useKosambi=1, sexAveraged=1, 10
266 iterations/per chromosome) to create a linkage map for each chromosome of the reference
267 genome (details in Table S2). Of the 10 iterations of OrderMarkers2, (or using the physical order
268 of markers in the reference genome if marker order was poorly resolved), we selected the order
269 with the highest likelihood for each chromosome (Table S2). We then manually removed
270 standalone markers whose physical position differed greatly with their calculated genetic
271 position on the chromosome. This procedure produced three linkage maps containing 3,828,
272 4,389 and 4,379 markers respectively. Of these markers, we retained 794, 606, and 690 which
273 mapped to recombination-informative sites.
274
275 *Assessment of Transmission Ratio Distortion and Linkage Disequilibrium*
276 Following linkage mapping, we calculated genotype frequencies at each marker in each
277 map and identified regions of transmission ratio distortion (TRD) by testing for deviations from
278 Mendelian 1:1 expectation with χ^2 tests. We used both an uncorrected $\alpha = 0.01$ and a more
279 stringent Bonferonni-corrected α (unique α for each chromosome in each RIL population
280 depending on the number of markers tested). Because the linkage maps for the three RIL
281 populations varied both in size and marker order, we investigated TRD colocalization among the
282 three papulations on a marker-by-marker basis. To investigate whether peaks of TRD were
283 associated with major two-locus hybrid incompatibilities we used the package pegas (Paradis,
284 2010) to characterize pairwise linkage disequilibrium (LD) between all markers with unique map
285 positions in the three RIL populations. To minimize false positives driven by the large number of
286 pairwise comparisons, we first identified putative interacting loci associated with inter-

287 chromosomal LD based on r values greater than the 95% percentile (CAC110 RILs: $r > 0.37$,
288 CAC162 RILs: $r > 0.41$, CAC415 RILs: $r > 0.39$). At these interacting loci we then performed
289 likelihood ratio tests comparing observed genotype ratios to expected ratios (calculated by cross
290 tabulation of observed single locus allele frequencies). We describe only the most significant
291 epistatic interactions where $p<0.0001$.
292
293 *Assessment of Hybrid Male and Female Sterility*
294 To measure male fertility, we collected pollen from three flowers (second flower pair or
295 later) of each RIL individual. We suspended the pollen of each flower separately in lactophenol-
296 aniline blue stain (Kearns & Inouye, 1993) and inspected the pollen grains using a compound
297 microscope. For each flower, we estimated pollen fertility by calculating the proportion of darkly
298 stained (viable) pollen grains from a haphazardly selected group of >100 pollen grains within a
299 field of view in of the microscope. When fertility estimates from flowers of the same plant
300 differed by more than 0.2, pollen from up to 3 more flowers was collected and counted. We
301 then calculated the average pollen viability from the collected flowers for each RIL individual.
302 Because the distribution of pollen viability in each RIL population was left-skewed, we logit
303 transformed the data. We also collected pollen from and estimated viability in each parental
304 line, and the three F1s between them.
305 To estimate hybrid female sterility, we intercrossed random pairs of RILs in at least
306 duplicate, and collected all recombinant inbred intercrossed (RIX) seeds produced. We counted
307 the number of seeds produced per fruit for each cross made and ran a linear mixed model
308 (LMM, using the lmer command in the 'lme4' package). In addition to maternal parent genotype

309 (fixed effect), the model included average viable pollen proportion of the paternal parent (as
310 calculated above, fixed effect), a unique RIX identifier nested within RIX cross type (CAC110 RIL x
311 CAC162 RIL, CAC162 RIL x CAC415 RIL, etc.; random effect) and the year that the cross was
312 made (crosses were made during two separate grow-outs in separate years; random effect). We
313 then calculated least square means (LSMs) of female viability (using seeds per fruit as a proxy)
314 for each RIL genotype using the emmeans function in the 'emmeans' package. For each of the
315 three RIL families this produced distributions with a long right tail, so we used a square root
316 transformation to more closely match a normal distribution.
317
318 *QTL Mapping*
319 Given the small sample sizes of each RIL population, we took a multistep approach to
320 genetically mapping hybrid male and female sterility. For each trait in each RIL population, we
321 first used r/QTL (Broman & Sen, 2009; Arends *et al.*, 2010) to perform 10 iterations of composite
322 interval mapping (CIM; Zeng, 1993, 1994; Jansen & Stam, 1994). Because CIM requires no
323 missing data, missing genotypes are imputed before the scan is run, leading to potential
324 differences between iterations. We set lenient LOD thresholds ($\alpha = 0.15$) for QTL significance, by
325 performing 5,000 permutations, and calculated 1.5-LOD intervals ('lodint' command) for each
326 significant peak position in any of the 10 iterations. We then performed single-QTL scans using
327 each QTL identified with CIM as an interactive covariate ('intcovar' option) in separate runs. We
328 again we set LOD thresholds ($\alpha = 0.15$, 10,000 permutations) for interacting QTL significance,
329 and calculated 1.5-LOD intervals for each significant peak position. With these identified peaks,
330 we then fit a multiple-QTL model ('fitqtl' command; HK method) and directly estimated additive

331 QTL effects (at each peak position) and identified epistatic effects. We then removed any

332 nonsignificant ($p > 0.05$) effects, and re-fit the model.

333 **Results**

334 *Admixture in M. guttatus parental lines*

335 All three *M. guttatus* parents show clear evidence of admixture from *M. nasutus*, but the
336 genomic location and proportion of introgression vary considerably across lines (Figure 1, Figure
337 S2). Of the three parents, CAC110 is the most admixed with ~24% of its genome showing very
338 low genetic divergence (*Dxy*) and a high posterior probability of recent coalescence with *M.*
339 *nasutus* via probabilistic inference (HMM, see Methods; Brandvain *et al.*, 2014). At least some
340 of this introgression in CAC110 appears to be recent, with large portions of entire chromosome
341 arms showing evidence of introgression (Figure S2). Although the largest inferred contiguous
342 blocks in CAC110 are only ~1.1Mb (Figure S3B), the HMM may sometimes break up true
343 contiguous blocks of introgression (or incorrectly identify short regions with low *Dxy* as
344 admixture blocks – see Brandvain et al. 2014). Given the improbability of inheriting a large
345 number of small introgressions immediately adjacent to one another, we think it likely that
346 several regions in CAC110 (on Chromosomes 1, 4, 8, 11, and 13 – Figure 1 and Figure S2)
347 represent true contiguous blocks of admixture. In both CAC162 and CAC415, the overall
348 proportion of admixture is lower (~9% in each) and blocks are generally smaller and more
349 evenly dispersed throughout the genome (Figure S2; Figure S3B), consistent with introgression
350 events that occurred in the more distant past. Even in CAC110, however, there are many very
351 small regions of inferred introgression (Figure S3), suggesting *M. guttatus* genomes at Catherine
352 Creek (CAC) are shaped by a long history of introgression from *M. nasutus*.

353

354

355 *Comparative linkage mapping*

356 Across most of the genome, the three RIL linkage maps are colinear with similar lengths
357 (Table 1), and marker order generally follows the physical order of the *M. guttatus* IM62 v3
358 reference assembly (Figure 2, Figure S4). However, we identified three clear exceptions to this
359 pattern, where the maps differ due to parental variation in putative inversions, characterized by
360 a large number of physically dispersed markers mapping to the same genetic position. Two of
361 these putative inversions are on LG1 (*inv1.1* and *inv1.2*) and are potentially unique to Catherine
362 Creek (or locally distributed), having not been reported in other crosses with these *Mimulus*
363 species (Fishman *et al.*, 2014; Flagel *et al.*, 2019). In both cases, the CAC9 *M. nasutus* parent
364 carries the ancestral orientation and the *M. guttatus* parents segregate for the derived variant.
365 At *inv1.1*, recombination is suppressed in the CAC110 and CAC415 RILs, but not in the CAC162
366 RIL, indicating collinearity between the CAC9 *M. nasutus* and CAC162 *M. guttatus* parents. At
367 *inv1.2*, on the other hand, the genetic maps suggest CAC9 is collinear only with CAC110.
368 Remarkably, this *M. guttatus* parent also carries a large block of introgression spanning this
369 entire region (Figure 1; Figure S2), suggesting that gene flow from *M. nasutus* has re-introduced
370 the ancestral variant into CAC110. We discovered a similar situation on LG13, where
371 introgression from *M. nasutus* accounts for collinearity between CAC9 and CAC110 at *inv13*
372 (recombination rates in the CAC110 RIL are much higher in this region than in the CAC162 and
373 CAC415 RILs; Figure S4). Additionally, *inv13* might have arisen in *M. nasutus*, as it is also appears
374 to be present in the reference genome assembly of *M. nasutus* SF5 (an accession derived from
375 Shear's Falls, an allopatric *M. nasutus* population ~70 km from CAC), but not in other recently
376 assembled *M. guttatus* genomes (phytozome.org). Taken together, these mapping results point

377 to introgression from *M. nasutus* as a major source of large-scale structural variation at
378 Catherine Creek, responsible both for restoring ancestral variants and for introducing new
379 derived inversions into *M. guttatus*.
380 In addition to the effects of structural variation, we observed some instances of map
381 length variation that appear to be associated only with parental differences in introgression. In
382 the CAC110 RILs, introgressed regions on LGs 1, 11, 12, and 13 have elevated genetic distances
383 relative the same (non-introgressed) regions in the other two RIL populations (Table 1, Figure 2,
384 Figure S4). Rather than reflecting a biological difference in recombination frequency between
385 introgressed and non-introgressed regions, we attribute this effect to technical differences
386 arising from the much lower marker densities in introgressed regions, which are highly similar
387 to the CAC9 parent (Table 1, Figure 2, Figure S4).
388
389 *Genome-wide patterns of transmission ratio distortion (TRD)*
390 With the exception of LG9, we observed strong TRD in at least one RIL population on all
391 linkage groups (Figure 3, Figure S6, Table S3). Globally, patterns of TRD are highly variable across
392 RIL populations. In the CAC110 and CAC415 RILs, the majority of distorted markers show an
393 excess of *M. guttatus* genotypes (59% in CAC110 and 80% in CAC162), whereas in the CAC162
394 RILs, there is a strong deficit of *M. guttatus* across the genome (80% of distorted markers show
395 an excess of *M. nasutus*). In a few cases, the same region is even distorted in opposite directions
396 (e.g., on the end of LG4: toward *M. guttatus* in CAC110 RILs and *M. nasutus* in CAC162 RILs;
397 Figure 3, Figure S6). Despite this general variability, there are a few instances of shared
398 distortion in multiple RIL populations, potentially implying the same causal mechanisms. Most

399 notably, the proximal end of LG14 shows an excess of *M. guttatus* alleles in all three
400 populations. There is also an excess of *M. guttatus* alleles on LGs 1 and 4 and an excess of *M.*
401 *nasutus* alleles on LGs 8, 12, and 13 in two of the three RIL populations (CAC110 and CAC162).
402 These regions of shared distortion are largely confined to segments of the genome that are non-
403 introgressed in parental lines. In addition to local peaks of TRD among homozygous marker
404 genotypes, we also investigated levels of residual heterozygosity in the three RIL populations. At
405 the SNP level we observed low levels of heterozygosity consistent with Mendelian expectation.
406 Residual heterozygosity was broadly uniform across the genome, with no clear regions enriched
407 for heterozygous SNP calls.
408
409 *Hybrid incompatibilities as a source of TRD*
410 In each RIL population, we identified several instances of two-locus epistasis (10 in the
411 CAC110 RILs, 4 in the CAC162 RILs, 9 in the CAC415 RILs: Table S4, Table 2). All but one of these
412 23 cases are due to a deficit of heterospecific allele combinations, consistent with the action of
413 hybrid incompatibilities reducing viability or fertility during RIL formation. In 16 of these cases,
414 the underlying mechanism seems to be epistatic selection favoring parental genotypes – that is,
415 we observed an excess of *M. guttatus* genotypes or *M. nasutus* genotypes at *both* loci. In six
416 cases, however, there are clear deficits of only one of the two heterospecific genotype
417 combinations *and* the expected distortion stemming from selection against the incompatible
418 genotype at each locus (Table 2). This asymmetry is a hallmark of Dobzhansky-Muller
419 incompatibilities. In four of the six cases, loci involved in these incompatibilities occur
420 exclusively in non-introgressed regions. However, in two of the pairs, one or both loci reside in

421 introgressed blocks, suggesting there may also be segregating incompatibilities within CAC *M.*
422 *nasutus*. As with overall patterns of TRD, regions involved in two-locus epistasis are largely
423 population specific (although in some cases, we likely have limited power to detect shared
424 epistasis due to small sample sizes and genetic background effects).
425
426 *Genetics of hybrid fertility traits*
427 Despite six generations of selfing, all three RIL populations exhibited substantial
428 variation in male fertility. Some of this variation might be due to inbreeding depression in *M.*
429 *guttatus* parental lines, which showed lower pollen viability than the *M. nasutus* parent (Figure
430 S13). However, heterospecific interactions are likely also involved, as all three RIL populations
431 included a considerable fraction of individuals (~10-22%) with pollen viability <50% (well below
432 the *M. guttatus* average of 72%). In the CAC110 RIL population, we mapped five pollen viability
433 QTLs accounting for ~36% of variance, including two separate epistatic pairs (Table 3, Figure 4).
434 One of these epistatic pairs leads to reduced male fertility in RILs with *M. nasutus* alleles on LG4
435 and *M. guttatus* alleles on LG14 (Figure S14A). The pattern of TRD at these same loci (excess of
436 *M. guttatus* on LG4 and *M. nasutus* alleles on LG14, Figure 3) might suggest the action of a
437 gametic incompatibility that reduces pollen viability, but other genetic mechanisms are also
438 possible (e.g., a sporophytic incompatibility that reduces pollen viability to the point of
439 preventing effective self-fertilization/seed production). The second epistatic pair in the CAC110
440 RIL population – between QTLs on LG12 and LG14 – also arises due to a negative heterospecific
441 interaction (RILs homozygous for *M. nasutus* alleles on LG12 and *M. guttatus* on LG14 have the
442 lowest fertility: Figure S14A), although *M. nasutus* genotypes have higher pollen fertility at each

443 QTL individually (Table 3). At the remaining QTL for male fertility on LG11, *M. nasutus* alleles
444 result in lower pollen viabilities (opposite to parental values), suggesting there could be
445 additional unmapped loci that interact with this QTL to decrease male fertility. In the CAC162
446 RIL population, we mapped two QTLs for pollen viability (accounting for ~28% of the variance),
447 but because we detected no epistasis between them and *M. nasutus* alleles increased fertility at
448 both, these effects might be due to inbreeding depression or to incompatibilities with additional
449 loci below our detection thresholds. We mapped no QTLs for male fertility in the CAC415 RIL
450 population.

451 For female fertility, all three *M. guttatus* parents had much lower fruit production than
452 the *M. nasutus* parent, suggesting substantial inbreeding depression affecting this trait (Figure
453 S13). Accordingly, all QTLs we identified – three in the CAC110 RIL and one in the CAC415 RIL –
454 were additive with *M. nasutus* alleles increasing fertility (Table 3).

455 **Discussion**

456 Closely related species living in secondary sympatry, especially those displaying
457 incomplete reproductive isolation and still experiencing gene flow, are an excellent opportunity
458 to investigate the evolution and maintenance of reproductive barriers in nature. Here we
459 construct three RIL populations from crosses in such a system, sister species *Mimulus guttatus*
460 and *M. nasutus,* from the sympatric site Catherine Creek. This multi-parent design allows for a
461 uniquely powerful assessment of the hybrid incompatibilities maintaining species boundaries in
462 a naturally admixed and highly genetically diverse population, assessing the effects of genetic
463 variation in *M. guttatus* on the outcomes of hybridization. Overall, patterns of transmission ratio
464 distortion and long-range linkage disequilibrium, paired with mapping of fertility in the
465 experimental hybrid populations reveal the hallmarks of substantial segregating hybrid
466 incompatibilities, as well as structural variation between this pair of naturally hybridizing taxa.
467 Additionally, these RILs are now a permanent resource to be used in research on adaptation and
468 speciation at CAC, allowing for continued investigations into the genetic basis of hybrid
469 incompatibilities, and hybrid fitness in replicate, genetically identical individuals across
470 environmental conditions.

471

472 *Introgression in sympatry: M. nasutus ancestry in CAC M. guttatus*

473 Suggestive of a long history of admixture, including recent hybridization events at
474 Catherine Creek, and consistent with previous analyses (Brandvain *et al.*, 2014; Kenney &
475 Sweigart, 2016) we identified substantial introgression from *M. nasutus* across the genomes of
476 three CAC *M. guttatus* inbred lines. Both the amount and location of introgression varies greatly

477 among the *M. guttatus* lines. Although variable, introgression within the genome does appear
478 non-random, with some consistent loci showing evidence of introgression in all three lines
479 (Figure S2). This is consistent with previous findings, which identified frequent introgression in a
480 large sample of wild individuals, with some loci more commonly introgressed than expected by
481 chance (Kenney & Sweigart, 2016). These overrepresented areas of introgression may indicate
482 adaptive introgression (Suarez-Gonzalez *et al.*, 2018) and therefore warrant further
483 investigation of additional sequenced *M. guttatus* lines from CAC, especially wild collected
484 individuals (as the process of creating inbred lines will likely influence observed levels of
485 admixture in lab created lines). While our data suggest adaptive introgression is likely not
486 ubiquitous, there may be small regions of *M. nasutus* variation (most notably, the distal regions
487 of Chr03 Chr04; Figure S2) that are being preferentially retained in *M. guttatus* genomes.
488
489 *M. nasutus as a source of structural variation in sympatric M. guttatus*
490 The ongoing and prevalent hybridization occurring at CAC also appears to have strong
491 impacts on segregating variation in genome architecture in CAC *M. guttatus*. Genome wide, the
492 three linkage maps produced are largely colinear, and have similar lengths (Table 1), following
493 the physical order of the reference genome. However, there are notable local differences
494 associated with segregating structural variation in CAC *M. guttatus* (Figure 2, Figure S4). We
495 identified three previously unidentified structural variants segregating within *M. guttatus* at CAC
496 with high confidence. Incredibly, two of these variants appear to have been introduced into *M.*
497 *guttatus* through admixture with *M. nasutus* (Figure S5). The most admixed *M. guttatus* line,
498 CAC110, carries the *M. nasutus* orientation of inv1.2 and inv13 in regions which show a high

499 probability of recent introgression (Figure S4, Figure S5, Figure S2). As inversions can help to
500 prevent the breakup of coevolved alleles, such as in the known inversion distinguishing
501 perennial and annual ecotypes of *M. guttatus* (Lowry & Willis, 2010; Twyford & Friedman,
502 2015), these inverted regions, will be worth comparing to past and future QTL mapping studies,
503 as introgression of these loci may be expected to have profound effects on species boundaries
504 and fitness.
505
506 *Variation in transmission ratio distortion across experimental hybrid populations*
507 TRD is frequently variable across the RIL populations, with the *M. guttatus* parent greatly
508 influencing patterns of distortion. In many instances, one *M. guttatus* allele is favored over the
509 *M. nasutus* allele in one population, while others are highly disfavored, or inherited in a
510 Mendelian fashion. Similar patterns, in which distinct crosses show vastly different patterns of
511 TRD, is consistent with previous crosses between species/ecotypes in *Mimulus* (Hall & Willis,
512 2005), however, such large scale differences have rarely been investigated within populations.
513 Of particular interest, however, are the small number of consistently distorted regions across
514 the RIL populations, which may point to a conserved mechanism of TRD in these instances. For
515 example, across all three maps, a ~2Mb region on the proximal arm of chromosome 14 shows
516 an excess of *M. guttatus* alleles. Interestingly, this same region shows evidence of distortion in
517 one previous analyses of TRD between *M. guttatus* ecotypes, but *not* between allopatric *M.*
518 *nasutus* and *M. guttatus* populations in that study (Hall & Willis, 2005). It therefore, may be an
519 especially good candidate for further investigations of loci contributing to distortion specifically
520 at CAC.

521 Further analysis will be needed to begin to determine likely agents causing the pervasive
522 TRD observed in this experiment. Distortion may arise for a number of reasons, each of which
523 have potentially important implications for species maintenance. Among others, meiotic drive
524 (Fishman & Saunders, 2008), gamete killers (Koide *et al.*, 2008), pollen competition (Fishman *et*
525 *al.*, 2008), and Dobzhansky-Muller incompatibilities which effect the viability of gametes or
526 zygotes (Leppälä *et al.*, 2013; Kerwin & Sweigart, 2017) can all effect genomic patterns of
527 distortion. Additionally, cytonuclear incompatibilities, which we are unable to identify given our
528 unidirectional crossing design, may impact patterns of TRD if the three *M. guttatus* genomes
529 interact differently with CAC9 cytoplasmic factors. Reciprocal crosses in these same CAC
530 individuals would allow for the investigation of this possibility. Here we focus on instances
531 where transmission patterns at individual loci suggest selection against epistatic incompatible
532 alleles, indicative of DMI loci, but these other causes certainly influence variation in distortion
533 across the genome.
534
535 *Evidence for multiple epistatic hybrid incompatibility loci*
536 Overall, patterns of observed TRD and linkage disequilibrium in the three RIL
537 populations, paired with QTL mapping of fertility, reveal highly complex epistatic relationships
538 between alleles across the genome. It is likely that more complicated multi-locus
539 incompatibilities, that we don't have the sample size or power to full detect, are present,
540 contributing to the observed discordance between two-locus epistasis and patterns of single
541 locus TRD. Further explaining these patterns, many regions of high interchromosomal LD display
542 patterns of TRD consistent with epistatic selection for one parental genotype. Such patterns can

543 be explained by diverse mechanisms including selection against trait mismatches (Thompson *et*
544 *al.*, 2022), in the case of selection for *M. nasutus* alleles, avoidance of inbreeding depression, or
545 environmental selection during greenhouse growth. These factors are all likely to influence
546 patterns of distortion, further complicating the interpretation of trends. The patterns we
547 identified of LD and distortion, caused by putative DMIs, could be the result of negative
548 epistasis occurring at either the gametic or zygotic stage. Although we are not able to
549 definitively distinguish between these different potential mechanisms leading to incompatible
550 epistatic interactions, because incompatibilities acting at the gametic stage would require both
551 a strong effect on both pollen genotype *and* pollen number to effectively purge incompatibility
552 loci, this option seems more in line with our observation of significant distortion without
553 complete purging.

554 Of the *M. guttatus* lines we crossed, CAC110 had the greatest proportion of *M. nasutus*
555 ancestry. We may have expected that this pervasive introgression might limit the potential
556 effects of hybrid incompatibilities, as *M. nasutus* alleles, entirely compatible with each other,
557 increase in frequency. However, we do not observe this trend. Even with nearly ¼ of its genome
558 introgressed from *M. nasutus,* multiple postzygotic barriers are still present in the CAC110 RIL
559 population. As such, long term hybrid persistence at CAC does not seem likely, as the
560 maintenance of a high proportion of *M. nasutus* ancestry following hybridization (through self-
561 fertilization, or mating with other admixed individuals) is likely to retain a substantial load of
562 hybrid incompatibilities. Rather, backcrossing to *M. guttatus* and purging *M. nasutus* ancestry
563 would seem to be most stable. This finding, along with the relatively small effect sizes of the
564 identified fertility QTLs, supports previous evidence for broad genome wide selection against *M.*

565 *nasutus* ancestry in an *M. guttatus* background (Brandvain *et al.*, 2014), supporting a complex
566 and dynamic genetic basis of hybrid incompatibility at CAC, with many small effect loci across
567 the genome decreasing hybrid fitness in concert.

568 Despite six generations of selfing, which is expected to purge deleterious heterospecific
569 combinations, the CAC110 RILs retained at least two hybrid incompatibilities with effects on
570 pollen viability, both of which lie in non-introgressed regions as expected. Despite their
571 maintenance in the CAC110 RILs, likely due to supplemental pollination and our concerted effort
572 to retain lines, these genotypes are likely to be under strong selection in nature, where pollen
573 limitation is more likely. Interestingly, these interacting loci did not appear in our tests for two-
574 locus epistasis. Although these loci are associated with pollen viability, and may be expected to
575 cause two-locus distortion, in these cases even the incompatible genotype class retained
576 intermediate pollen viability (~55-70% viable), and therefore was maintained in the RIL
577 population during the selfing process. If this strong, but incomplete sterility is the norm, it may
578 also explain why seemingly incompatible genotypes have not been entirely purged from the
579 population during RIL construction. Additionally, incompatibilities acting in gametes rather than
580 zygotes wouldn't necessarily lead to complete purging of incompatible genotypes even if
581 selection is strong.

582 Although we found no significant epistatic loci interacting with the remainder of the
583 QTLs we identified, they did frequently show some evidence of epistasis among them, although
584 it did not reach significance. This seems to be evidence of other subtle epistatic interactions
585 influencing hybrid fertility that warrant further investigation with larger sample sizes.
586 Additionally, the fact that we still see DMI-like epistasis in areas of introgression suggests that

587 there may also be segregating incompatibilities within CAC *M. nasutus*. Variation in
588 incompatibility loci has been identified previously between populations of *M. nasutus* (Sweigart
589 *et al.*, 2007), but this may be unlikely within this highly inbred population. Alternatively, there
590 may be small blocks of true *M. guttatus* variation within these diagnosed blocks of introgression
591 which are harboring incompatible alleles.

592 Together, these results provide a wealth of evidence for the maintenance of substantial
593 postzygotic reproductive isolation between *M. nasutus* and *M. guttatus* in sympatry. Despite a
594 long history of admixture, these intrinsic barriers remain pervasive, limiting the homogenizing
595 effects of geneflow between species, and are likely integral to the maintenance of these species.

596 **Author Contributions**

597 Research conceived and designed by SJM and ALS. Data collected and analyzed by SJM.

598 Manuscript written by SJM and ALS.

599

600 **Data Accessibility**

601 All whole genome sequence data and RADseq data will be deposited at the NCBI Sequence Read

602 Archive upon acceptance. Other data and scripts will be made available from the Dryad Digital

603 Repository.

604

605 **Acknowledgements**

606 We thank Amanda Kenney for seed collection at Catherine Creek. Jill Anderson, Lisa Donovan,

607 Bob Schmitz, Mike White provided helpful discussions and guidance. This work was supported

608 by a National Science Foundation grant [IOS-1827645 to ALS]; [Rules of Life]; funds from the

609 University of Georgia Research Foundation [to ALS]; the National Institute of General Medical

610 Sciences of the National Institute of Health [T32GM007103 to SJM]; and the UGA Genetics Jan

611 and Kirby Alton Graduate Fellowship [to SJM].

612

613 **Conflict of Interest**

614 The authors declare no conflicts of interest.

615

616 **ORCID**

617 *Samuel J. Mantel* https://orcid.org/0000-0001-6392-4022

References

Ali OA, O'Rourke SM, Amish SJ, Meek MH, Luikart G, Jeffres C, Miller MR. **2016**. RAD Capture (Rapture): Flexible and Efficient Sequence-Based Genotyping. *Genetics* **202**: 389–400.

Arends D, Prins P, Jansen RC, Broman KW. **2010**. R/qtl: high-throughput multiple QTL mapping. *Bioinformatics* **26**: 2990–2992.

Aylor DL, Valdar W, Foulds-Mathes W, Buus RJ, Verdugo RA, Baric RS, Ferris MT, Frelinger JA, Heise M, Frieman MB, *et al.* 2011. Genetic analysis of complex traits in the emerging Collaborative Cross. *Genome Research* **21**: 1213–1222.

Barker WR, Nesom GL, Beardsley PM, Fraga NS. **2012**. A taxonomic conspectus of Phrymaceae: A narrowed circumscription for Mimulus, new and resurrected genera, and new names and combinations. *Phytoneuron* **2012–39**: 1–60.

Bolger AM, Lohse M, Usadel B. **2014**. Trimmomatic: a flexible trimmer for Illumina sequence data. *Bioinformatics* **30**: 2114–2120.

Brandvain Y, Kenney AM, Flagel L, Coop G, Sweigart AL. **2014**. Speciation and Introgression between Mimulus nasutus and Mimulus guttatus. *PLOS Genetics* **10**: e1004410.

Broman KW, Sen S. **2009**. *A Guide to QTL Mapping with R/qtl*. New York, NY: Springer New York.

Caeiro-Dias G, Brelsford A, Meneses-Ribeiro M, Crochet P-A, Pinho C. **2023**. Hybridization in late stages of speciation: Strong but incomplete genome-wide reproductive isolation and 'large Z-effect' in a moving hybrid zone. *Molecular Ecology* **32**: 4362–4380.

Catchen JM, Amores A, Hohenlohe P, Cresko W, Postlethwait JH. **2011**. Stacks: Building and Genotyping Loci De Novo From Short-Read Sequences. *G3 Genes|Genomes|Genetics* **1**: 171–182.

Catchen J, Hohenlohe PA, Bassham S, Amores A, Cresko WA. **2013**. Stacks: an analysis tool set for population genomics. *Molecular Ecology* **22**: 3124–3140.

Colomé-Tatché M, Johannes F. **2016**. Signatures of Dobzhansky–Muller Incompatibilities in the Genomes of Recombinant Inbred Lines. *Genetics* **202**: 825–841.

Coyne JA, Orr HA. **2004**. *Speciation*. Oxford, New York: Oxford University Press.

Cutter AD. **2012**. The polymorphic prelude to Bateson–Dobzhansky–Muller incompatibilities. *Trends in Ecology & Evolution* **27**: 209–218.

Danecek P, Auton A, Abecasis G, Albers CA, Banks E, DePristo MA, Handsaker RE, Lunter G, Marth GT, Sherry ST, *et al.* 2011. The variant call format and VCFtools. *Bioinformatics* **27**: 2156–2158.

Darwin C. **1859**. *On the Origin of Species*.

Delmore KE, Hübner S, Kane NC, Schuster R, Andrew RL, Câmara F, Guigó R, Irwin DE. **2015**. Genomic analysis of a migratory divide reveals candidate genes for migration and implicates selective sweeps in generating islands of differentiation. *Molecular Ecology* **24**: 1873–1888.

Dobzhansky T. **1937**. *Genetics and the Origin of Species*. New York, NY: Columbia University Press.

Durbin R, Eddy SR, Krogh A, Mitchison G. **1998**. *Biological Sequence Analysis: Probabilistic Models of Proteins and Nucleic Acids*. Cambridge: Cambridge University Press.

Ellegren H, Smeds L, Burri R, Olason PI, Backström N, Kawakami T, Künstner A, Mäkinen H, Nadachowska-Brzyska K, Qvarnström A, *et al.* 2012. The genomic landscape of species divergence in Ficedula flycatchers. *Nature* **491**: 756–760.

Feder JL, Roethele JB, Filchak K, Niedbalski J, Romero-Severson J. **2003**. Evidence for Inversion Polymorphism Related to Sympatric Host Race Formation in the Apple Maggot Fly, Rhagoletis pomonella. *Genetics* **163**: 939–953.

Fishman L, Aagaard J, Tuthill JC. **2008**. TOWARD THE EVOLUTIONARY GENOMICS OF GAMETOPHYTIC DIVERGENCE: PATTERNS OF TRANSMISSION RATIO DISTORTION IN MONKEYFLOWER (MIMULUS) HYBRIDS REVEAL A COMPLEX GENETIC BASIS FOR CONSPECIFIC POLLEN PRECEDENCE. *Evolution* **62**: 2958–2970.

Fishman L, McIntosh M. **2019**. Standard Deviations: The Biological Bases of Transmission Ratio Distortion. *Annual Review of Genetics* **53**: 347–372.

Fishman L, Saunders A. **2008**. Centromere-Associated Female Meiotic Drive Entails Male Fitness Costs in Monkeyflowers. *Science* **322**: 1559–1562.

Fishman L, Willis JH, Wu CA, Lee Y-W. **2014**. Comparative linkage maps suggest that fission, not polyploidy, underlies near-doubling of chromosome number within monkeyflowers (Mimulus; Phrymaceae). *Heredity* **112**: 562–568.

Flagel LE, Blackman BK, Fishman L, Monnahan PJ, Sweigart A, Kelly JK. **2019**. GOOGA: A platform to synthesize mapping experiments and identify genomic structural diversity. *PLOS Computational Biology* **15**: e1006949.

Flagel LE, Willis JH, Vision TJ. **2014**. The Standing Pool of Genomic Structural Variation in a Natural Population of Mimulus guttatus. *Genome Biology and Evolution* **6**: 53–64.

Good JM, Handel MA, Nachman MW. **2008**. ASYMMETRY AND POLYMORPHISM OF HYBRID MALE STERILITY DURING THE EARLY STAGES OF SPECIATION IN HOUSE MICE. *Evolution* **62**: 50–65.

683 **Hall MC, Willis JH**. **2005**. Transmission Ratio Distortion in Intraspecific Hybrids of *Mimulus*
684 *guttatus*: Implications for Genomic Divergence. *Genetics* **170**: 375–386.

685 **Hoffmann AA, Rieseberg LH**. **2008**. Revisiting the Impact of Inversions in Evolution: From
686 Population Genetic Markers to Drivers of Adaptive Shifts and Speciation? *Annual Review of*
687 *Ecology, Evolution, and Systematics* **39**: 21–42.

688 **Jansen RC, Stam P**. **1994**. High resolution of quantitative traits into multiple loci via interval
689 mapping. *Genetics* **136**: 1447–1455.

690 **Jones FC, Grabherr MG, Chan YF, Russell P, Mauceli E, Johnson J, Swofford R, Pirun M, Zody**
691 **MC, White S, *et al.* 2012**. The genomic basis of adaptive evolution in threespine sticklebacks.
692 *Nature* **484**: 55–61.

693 **Kearns C, Inouye D**. **1993**. *Techniques for Pollination Biologists*. Niwot, CO: University of
694 Colorado Press.

695 **Kenney AM, Sweigart AL**. **2016**. Reproductive isolation and introgression between sympatric
696 Mimulus species. *Molecular Ecology* **25**: 2499–2517.

697 **Kerwin RE, Sweigart AL**. **2017**. Mechanisms of Transmission Ratio Distortion at Hybrid Sterility
698 Loci Within and Between Mimulus Species. *G3 Genes|Genomes|Genetics* **7**: 3719–3730.

699 **Koide Y, Ikenaga M, Sawamura N, Nishimoto D, Matsubara K, Onishi K, Kanazawa A, Sano Y**.
700 **2008**. The Evolution of Sex-Independent Transmission Ratio Distortion Involving Multiple Allelic
701 Interactions at a Single Locus in Rice. *Genetics* **180**: 409–420.

702 **Larson EL, White TA, Ross CL, Harrison RG**. **2014**. Gene flow and the maintenance of species
703 boundaries. *Molecular Ecology* **23**: 1668–1678.

704 **Leppälä J, Bokma F, Savolainen O**. **2013**. Investigating Incipient Speciation in Arabidopsis lyrata
705 from Patterns of Transmission Ratio Distortion. *Genetics* **194**: 697–708.

706 **Li H**. **2013**. Aligning sequence reads, clone sequences and assembly contigs with BWA-MEM.
707 *arXiv:1303.3997 [q-bio]*.

708 **Li H, Durbin R**. **2009**. Fast and accurate short read alignment with Burrows–Wheeler transform.
709 *Bioinformatics* **25**: 1754–1760.

710 **Li H, Handsaker B, Wysoker A, Fennell T, Ruan J, Homer N, Marth G, Abecasis G, Durbin R,**
711 **1000 Genome Project Data Processing Subgroup**. **2009**. The Sequence Alignment/Map format
712 and SAMtools. *Bioinformatics* **25**: 2078–2079.

713 **Long AD, Macdonald SJ, King EG**. **2014**. Dissecting complex traits using the Drosophila Synthetic
714 Population Resource. *Trends in Genetics* **30**: 488–495.

Lowry DB, Sobel JM, Angert AL, Ashman T-L, Baker RL, Blackman BK, Brandvain Y, Byers KJRP, Cooley AM, Coughlan JM, *et al.* 2019. The case for the continued use of the genus name Mimulus for all monkeyflowers. *TAXON* **68**: 617–623.

Lowry DB, Willis JH. **2010**. A Widespread Chromosomal Inversion Polymorphism Contributes to a Major Life-History Transition, Local Adaptation, and Reproductive Isolation. *PLOS Biology* **8**: e1000500.

Mantel SJ, Sweigart AL. **2019**. Divergence in drought-response traits between sympatric species of Mimulus. *Ecology and Evolution* **9**: 10291–10304.

Martin NH, Willis JH. **2007**. Ecological Divergence Associated with Mating System Causes Nearly Complete Reproductive Isolation between Sympatric Mimulus Species. *Evolution* **61**: 68–82.

Mayr E. **1942**. *Systematics And The Origin Of Species*.

Mojica JP, Lee YW, Willis JH, Kelly JK. **2012**. Spatially and temporally varying selection on intrapopulation quantitative trait loci for a life history trade-off in Mimulus guttatus. *Molecular Ecology* **21**: 3718–3728.

Monnahan PJ, Kelly JK. **2015**. Naturally segregating loci exhibit epistasis for fitness. *Biology Letters* **11**: 20150498.

Monnahan PJ, Kelly JK. **2017**. The Genomic Architecture of Flowering Time Varies Across Space and Time in Mimulus guttatus. *Genetics* **206**: 1621–1635.

Moyle LC, Nakazato T. **2008**. Comparative Genetics of Hybrid Incompatibility: Sterility in Two Solanum Species Crosses. *Genetics* **179**: 1437–1453.

Nesom GL, Fraga NS, Barker WR, Beardsley PM, Tank DC, Baldwin BG, Olmstead RG. **2019**. Response to "The case for the continued use of the genus name Mimulus for all monkeyflowers". *TAXON* **68**: 624–627.

Nolte AW, Gompert Z, Buerkle CA. **2009**. Variable patterns of introgression in two sculpin hybrid zones suggest that genomic isolation differs among populations. *Molecular Ecology* **18**: 2615–2627.

Noor MAF, Grams KL, Bertucci LA, Reiland J. **2001**. Chromosomal inversions and the reproductive isolation of species. *Proceedings of the National Academy of Sciences* **98**: 12084–12088.

Okonechnikov K, Conesa A, García-Alcalde F. **2016**. Qualimap 2: advanced multi-sample quality control for high-throughput sequencing data. *Bioinformatics* **32**: 292–294.

Paradis E. **2010**. pegas: an R package for population genetics with an integrated–modular approach. *Bioinformatics* **26**: 419–420.

Puzey JR, Willis JH, Kelly JK. **2017**. Population structure and local selection yield high genomic variation in Mimulus guttatus. *Molecular Ecology* **26**: 519–535.

Rastas P. **2017**. Lep-MAP3: robust linkage mapping even for low-coverage whole genome sequencing data. *Bioinformatics* **33**: 3726–3732.

Renaut S, Grassa CJ, Yeaman S, Moyers BT, Lai Z, Kane NC, Bowers JE, Burke JM, Rieseberg LH. **2013**. Genomic islands of divergence are not affected by geography of speciation in sunflowers. *Nature Communications* **4**: 1827.

Scott MF, Ladejobi O, Amer S, Bentley AR, Biernaskie J, Boden SA, Clark M, Dell'Acqua M, Dixon LE, Filippi CV, *et al.* 2020. Multi-parent populations in crops: a toolbox integrating genomics and genetic mapping with breeding. *Heredity* **125**: 396–416.

Servedio MR, Hermisson J. **2020**. The evolution of partial reproductive isolation as an adaptive optimum. *Evolution* **74**: 4–14.

Servedio MR, Kirkpatrick M. **1997**. The Effects of Gene Flow on Reinforcement. *Evolution* **51**: 1764–1772.

Sotola VA, Berg CS, Samuli M, Chen H, Mantel SJ, Beardsley PA, Yuan Y-W, Sweigart AL, Fishman L. **2023**. Genomic mechanisms and consequences of diverse postzygotic barriers between monkeyflower species. : 2023.04.21.537885.

Suarez-Gonzalez A, Lexer C, Cronk QCB. **2018**. Adaptive introgression: a plant perspective. *Biology Letters* **14**: 20170688.

Sweigart AL, Mason AR, Willis JH. **2007**. NATURAL VARIATION FOR A HYBRID INCOMPATIBILITY BETWEEN TWO SPECIES OF MIMULUS. *Evolution* **61**: 141–151.

Sweigart AL, Willis JH. **2003**. Patterns of Nucleotide Diversity in Two Species of Mimulus Are Affected by Mating System and Asymmetric Introgression. *Evolution* **57**: 2490–2506.

Taylor EB, Boughman JW, Groenenboom M, Sniatynski M, Schluter D, Gow JL. **2006**. Speciation in reverse: morphological and genetic evidence of the collapse of a three-spined stickleback (Gasterosteus aculeatus) species pair. *Molecular Ecology* **15**: 343–355.

Teeter KC, Thibodeau LM, Gompert Z, Buerkle CA, Nachman MW, Tucker PK. **2010**. The Variable Genomic Architecture of Isolation Between Hybridizing Species of House Mice. *Evolution* **64**: 472–485.

Thompson KA, Peichel CL, Rennison DJ, McGee MD, Albert AYK, Vines TH, Greenwood AK, Wark AR, Brandvain Y, Schumer M, *et al.* 2022. Analysis of ancestry heterozygosity suggests that hybrid incompatibilities in threespine stickleback are environment dependent. *PLOS Biology* **20**: e3001469.

Twyford AD, Friedman J. **2015**. Adaptive divergence in the monkey flower Mimulus guttatus is maintained by a chromosomal inversion. *Evolution; International Journal of Organic Evolution* **69**: 1476–1486.

Van der Auwera G, O'Connor B. **2020**. *Genomics in the Cloud: Using Docker, GATK, and WDL in Terra (1st Edition)*. O'Reilly Media.

Zeng ZB. **1993**. Theoretical basis for separation of multiple linked gene effects in mapping quantitative trait loci. *Proceedings of the National Academy of Sciences* **90**: 10972–10976.

Zeng ZB. **1994**. Precision mapping of quantitative trait loci. *Genetics* **136**: 1457–1468.

Zuellig MP, Sweigart AL. **2018**. A two-locus hybrid incompatibility is widespread, polymorphic, and active in natural populations of Mimulus*. *Evolution* **72**: 2394–2405.

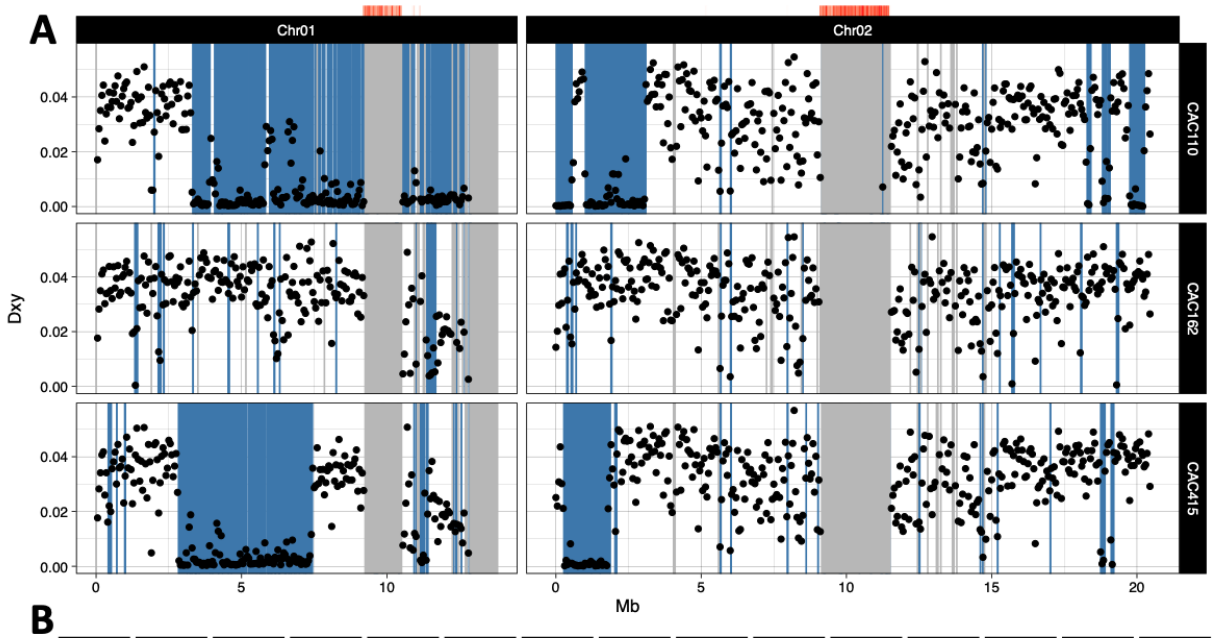

B

	Chr01	Chr02	Chr03	Chr04	Chr05	Chr06	Chr07	Chr08	Chr09	Chr10	Chr11	Chr12	Chr13	Chr14	Genome
CAC110	46.18%	18.90%	11.93%	32.88%	14.65%	5.31%	7.92%	32.65%	14.82%	17.93%	54.44%	15.10%	40.03%	10.13%	23.83%
CAC162	4.68%	3.25%	6.33%	8.73%	6.41%	13.48%	23.40%	18.54%	6.07%	12.56%	9.89%	4.78%	1.94%	9.15%	9.24%
CAC415	32.17%	10.67%	11.46%	8.78%	5.86%	8.15%	9.72%	4.82%	5.03%	8.55%	14.22%	7.05%	2.54%	2.94%	8.61%

Figure 1. Introgression from *M. nasutus* into sympatric *M. guttatus.* A) *Dxy* calculated in 50kb windows across the first two chromosomes of the IM62 v3 *Mimulus guttatus* reference genome, between the parental lines of the three RIL populations (CAC9 v. CAC110, CAC9 v. CAC162, and CAC9 v. CAC415). Blue shaded regions indicate putatively admixed regions in the three focal CAC *M. guttatus* lines tested, diagnosed by a greater than a 95% posterior probability of *M. nasutus* ancestry (in 1kb windows) as inferred via the HMM (i.e. more recent coalescence with included *M. nasutus* samples than with included *M. guttatus* samples). Grey shaded regions indicate missing data (fewer than 5000 genotyped sites within any 50kb window). Red heatmaps above each chromosome indicate the density of centromeric repeats in the same 50kb windows. All chromosomes are shown in Figure S2. **B)** Heatmap showing the proportion of *M. nasutus* ancestry in each chromosome, and across the genome, of each of the three CAC *M. guttatus* lines used as parents of the RIL populations, as estimated as the proportion of 1kb windows with a greater than a 95% posterior probability of *M. nasutus* ancestry as inferred via the HMM. Darker blue shading indicates a higher proportion of *M. nasutus* ancestry.

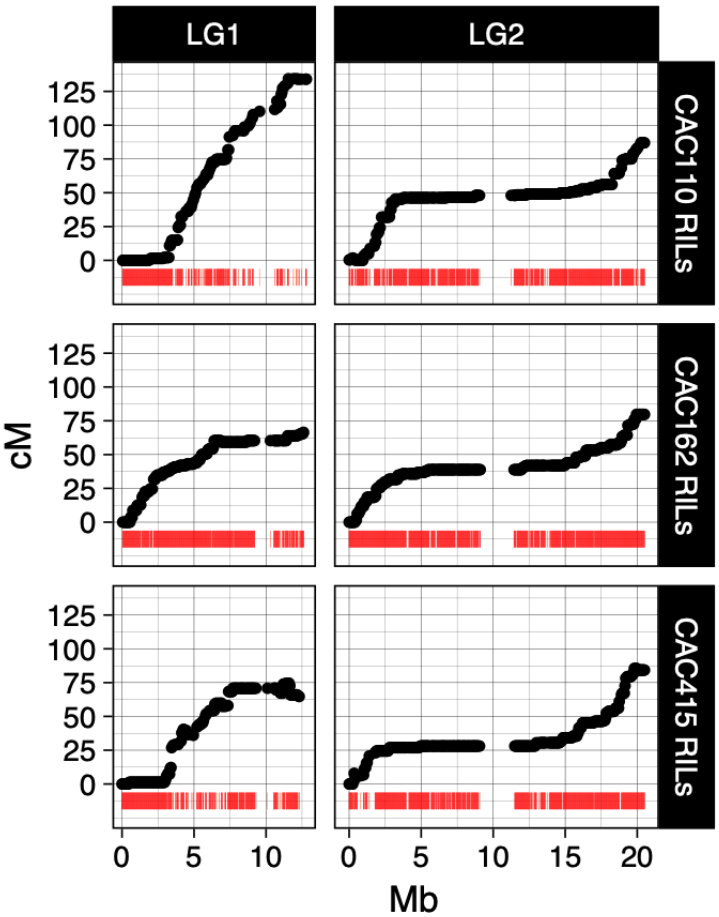

Figure 2. Map position (cM) versus physical marker positions (Mb) for the first two chromosomes of the IM62 v3 *Mimulus guttatus* reference genome in the three RIL populations. Red heatmaps below each curve indicate the density of markers, measured as the distance in Mb to the nearest neighboring marker. Low SNP density, and the subsequent inability to genotype markers in areas of the *M. guttatus* parental genomes showing evidence of introgression from *M. nasutus* manifests as regions of low marker density on some chromosomes.

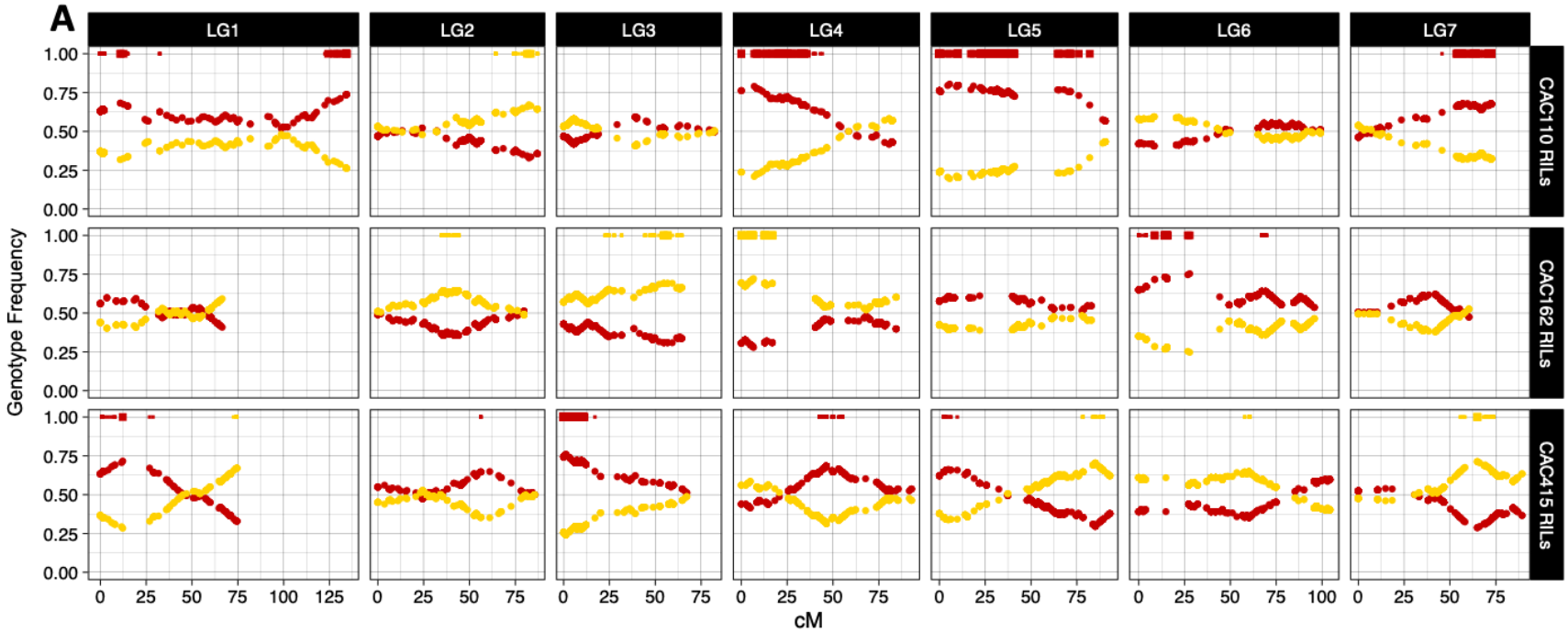
A
LG1
LG2
LG3
LG4
LG5
LG6
LG7
CAC110 RILs
CAC162 RILs
CAC415 RILs
Genotype Frequency
1.00
0.75
0.50
0.25
0.00
0
25
50
75
100
125
cM

815

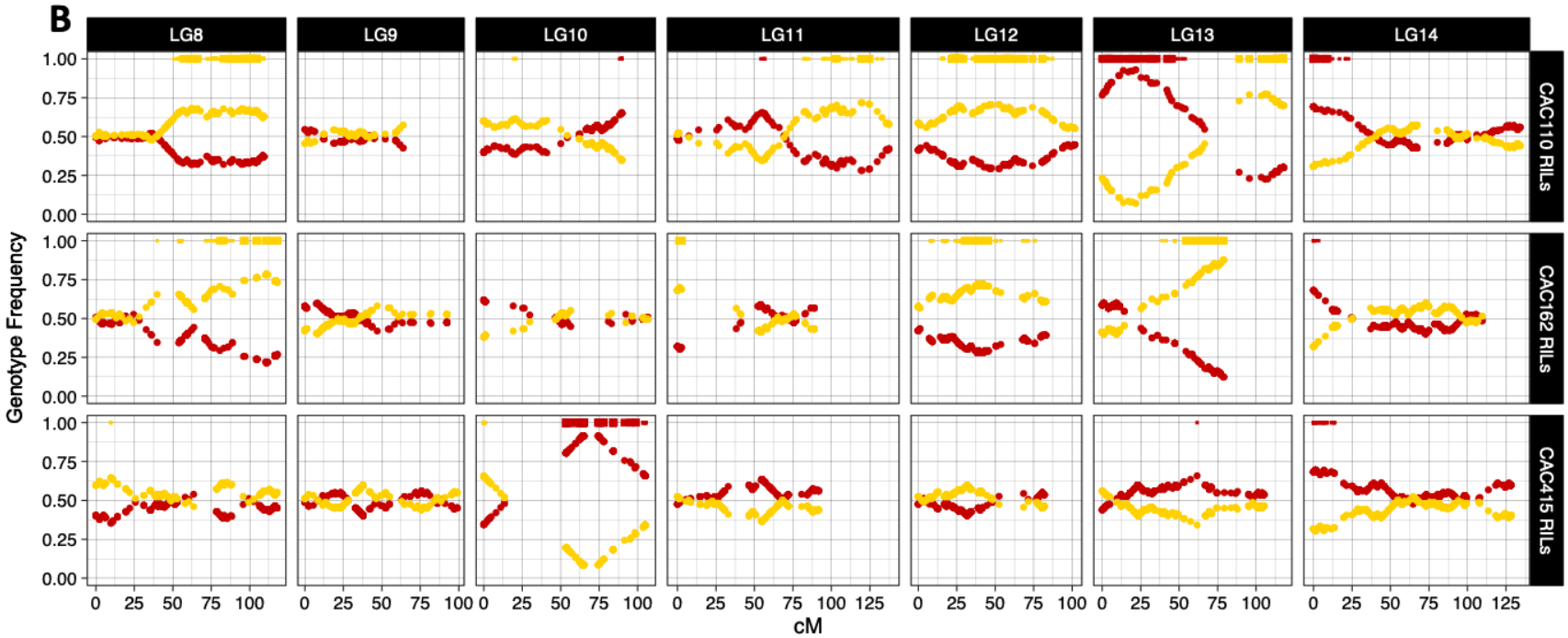

Figure 3. Transmission Ratio Distortion, cM, A) LG1 – LG7, B) LG8 – LG14. Genotype frequencies across the 14 linkage groups of the three RIL populations. Red dots indicate homozygous *M. guttatus* genotypes, yellow dots, homozygous *M. nasutus* genotypes. Bars at the top of each plot indicate regions showing significant transmission ratio distortion from the Mendelian 1:1 expectation by χ^2 tests at $\alpha = 0.01$ (thin bars), and a more stringent Bonferonni-corrected α (thick bars, unique α for each chromosome in each RIL population depending on the number of markers tested, see Table S3 for values). Bar color indicates an excess of *M. guttatus* (red), or *M. nasutus* (yellow) genotypes. Markers are ordered by genetic position within each map (cM).

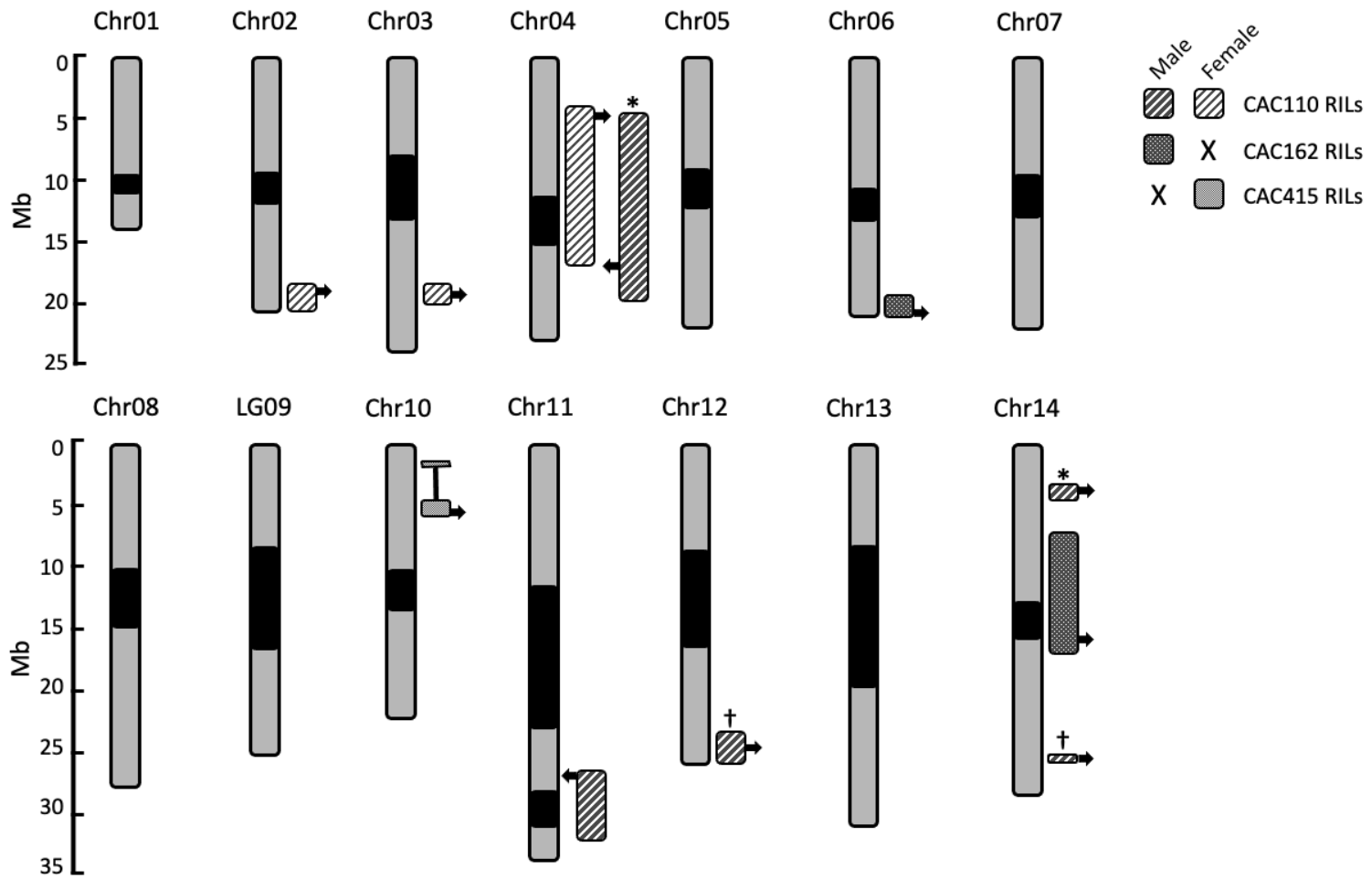

Figure 4. Male and female fertility QTL locations in each mapping population. Physical position (Mb) of the 1.5-LOD interval of each significant QTL is shown. Centromeres are indicated in black. Phenotype and RIL population indicated in key. Arrows indicate the position of peak marker(s). Arrows pointing left indicate the *M. guttatus* allele has the lower value, arrows pointing right indicate the *M. nasutus* allele has the lower value. QTLs with significant epistatic effects are indicated with shared symbols. The 1.5-LOD interval of the QTL underlying female fertility on Chr10 in the CAC415 RILs spans a breakpoint of the known derived inversion in the reference *M. guttatus* line IM62, leading to a disjunct interval.

830 **Table 1. Summary of linkage map length and intrascaffold recombination rate estimates.** Total
831 map length and intrascaffold recombination rate estimates for each chromosome, plus total
832 map length and average recombination rate in each of the three RIL populations.

		CAC110 RILs		CAC162 RILs		CAC415 RILs	
Chromosome	Reference Length (Mb)	Map Length (cM)	cM/Mb	Map Length (cM)	cM/Mb	Map Length (cM)	cM/Mb
1	13.88	134.368	9.68	66.451	4.79	74.470	5.37
2	20.54	86.970	4.23	79.725	3.88	85.500	4.16
3	23.80	82.263	3.46	64.360	2.70	67.161	2.82
4	22.81	82.362	3.61	84.446	3.70	92.822	4.07
5	21.77	90.440	4.15	82.863	3.81	92.963	4.27
6	20.89	99.115	4.74	95.776	4.58	104.195	4.99
7	21.88	72.643	3.32	60.311	2.76	89.304	4.08
8	27.69	109.184	3.94	117.963	4.26	117.700	4.25
9	25.15	63.801	2.54	92.286	3.67	98.934	3.93
10	22.12	89.656	4.05	106.661	4.82	104.910	4.74
11	33.60	137.499	4.09	88.907	2.65	91.633	2.73
12	25.84	101.548	3.93	82.763	3.20	81.868	3.17
13	30.77	117.730	3.83	78.866	2.56	105.060	3.41
14	28.29	134.029	4.74	109.580	3.87	128.236	4.53
Global	339.04	1401.608	4.13	1210.958	3.57	1334.756	3.94

833

Table 2. Positions of two-locus epistasis. Physical (Mb) positions of pairs of loci on each linkage group (LG) in the three RIL populations that show LD (r) in the 95th percentile, as well as Chi-Square statistics from likelihood ratio tests with p<0.0001. Counts of each genotypic class in the population are shown. Loci marked with an asterisk have peak r and χ^2 values at adjacent markers. Single locus proportions of *M. guttatus* alleles (G Prop.) were used to determine if the pattern of TRD at each epistatic locus could be explained by a two locus hybrid incompatibility (NG- or GN-), or if single locus distortion in the same direction better explains the pattern (GG++, GG+, NN++, or NN+). The best candidates for two locus hybrid incompatibilities are shaded grey. See Table S5 for full list of epistatic loci in LD 95th percentile.

	Locus 1		Locus 2										Locus 1	Locus 2	
Population	LG	Mb	LG	Mb	r	GG	GN	NG	NN	N	χ2	p	G Prop.	G Prop.	Pattern
CAC110	03	20.40 - 22.65	13	3.05 - 5.20	0.56	64	3	17	19	103	32.552	<0.0001	0.65	0.79	GG++
	05	3.10 - 20.75	11	2.55 - 4.90	0.54	39	21	1	22	83	29.035	<0.0001	0.72	0.48	NG-
	01	11.15 - 12.85	04	1.20 - 19.65	0.46	73	13	12	19	117	22.858	<0.0001	0.74	0.73	GG++
	02	2.85 - 18.95	13	21.75 - 23.65	0.45	54	1	26	14	95	21.079	<0.0001	0.58	0.84	GG++
	09	0.80 - 0.90	11	26.30 - 26.60	0.38	29	37	6	54	126	19.359	<0.0001	0.52	0.28	NG-
	05	2.40 - 20.90	11	5.05 - 10.20*	0.50	43	14	5	17	79	18.697	<0.0001	0.72	0.61	GG++
	03	0.15 - 18.95	11	24.35 - 25.30	0.40	29	24	12	56	121	18.567	<0.0001	0.44	0.34	NN++
	11	8.80 - 24.40	12	1.00 - 19.2	0.44	18	12	12	59	101	17.988	<0.0001	0.30	0.30	NN++
	01	3.30 - 5.50	11	4.00 - 5.75	0.47	29	9	10	24	72	16.515	<0.0001	0.53	0.54	GG+
	05	2.25 - 3.50	13	24.00 - 25.00	0.44	54	13	7	14	88	15.846	<0.0001	0.76	0.69	GG++
CAC162	04	19.90 - 22.80	14	2.35 - 18.15	0.50	29	10	14	44	97	24.708	<0.0001	0.40	0.44	NN+
	01	1.40 - 5.55	10	19.65 - 19.95	0.54	27	9	8	31	75	23.571	<0.0001	0.48	0.47	NN+
	06	6.30 - 15.10	12	6.20 - 7.75	0.47	9	50	23	15	97	21.637	<0.0001	0.61	0.33	HV
	01	2.35 - 5.45	03	0.00 - 20.65	0.45	28	21	7	42	98	20.628	<0.0001	0.50	0.36	NG-
CAC415	04	1.90 - 22.30	14	2.15 - 25.60	0.61	34	9	7	31	81	31.85	<0.0001	0.53	0.51	GG+
	06	17.00 - 19.25	10	19.50 - 20.25	0.43	38	0	22	13	73	22.217	<0.0001	0.52	0.82	GG+
	05	3.50 - 20.40	14	16.50 - 23.00	0.49	26	5	17	32	80	19.799	<0.0001	0.39	0.54	GN-
	07	13.20 - 21.80	08	22.30 - 27.70	0.48	23	7	14	38	82	19.719	<0.0001	0.37	0.45	NN+
	13	22.05 - 25.55	14	0.00 - 3.00	0.47	41	6	15	20	82	18.738	<0.0001	0.57	0.68	GG+
	06	9.65 - 16.00	08	23.60 - 25.55	0.44	22	10	12	37	81	15.892	<0.0001	0.40	0.42	NN+
	01	5.85 - 7.40	04	4.10 - 16.55	0.43	32	6	18	24	80	15.338	<0.0001	0.48	0.63	GN-
	01	7.70 - 11.70	13	24.20 - 25.15	0.42	24	4	22	30	80	15.279	<0.0001	0.35	0.58	GN-
	05	20.85 - 21.75	06	7.10 - 16.05	0.43	20	11	11	40	82	15.242	<0.0001	0.38	0.38	NN++

842 **Table 3. Male and female fertility QTL locations and effects in each mapping population.** Linkage group (LG), map (cM) and physical
843 (Mb) position of each significant QTL is shown. Additive effects (a) are negative when the *M. guttatus* allele has the lower value,
844 indicated in the summary column. QTLs with significant epistatic effects are shaded together. Percentage of RIL population variance
845 (PVE) is shown for each additive and epistatic effect. The 1.5-LOD interval of the QTLs underlying female fertility on LG10 in the
846 CAC415 RILs, marked with an asterisk, spans a breakpoint of the known derived inversion in the reference *M. guttatus* line IM62,
847 leading to a disjunct interval.

					Additive effect				Epistatic effect			
Population	Trait	LG	cM Position (1.5 LOD)	Mb Position (1.5 LOD)	a	PVE (%)	p	Summary	a x a	PVE (%)	p	Summary
CAC110 RILs	Male Fertility	4	26.975 (21.030 - 36.595)	16.70 - 16.75 (4.50 - 19.65)	-0.145	7.746	0.0008	G+	0.347	6.786	0.0004	NN+ (NG-)
		14	42.717 (37.467 - 48.317)	3.40 - 3.85 (3.05 - 4.30)	0.474	13.876	<0.0001	N+				
		11	132.951 (131.376 - 137.499)	26.65 - 26.70 (26.60 - 32.20)	-0.278	4.054	0.0059	G+				
		12	87.711 (80.538 - 101.548)	24.45 - 24.55 (23.25 - 25.80)	0.080	5.620	0.0055	N+	0.302	5.037	0.0022	NN+ (NG-)
		14	114.441 (112.343 - 116.889)	25.20 - 25.40 (25.00 - 25.60)	0.230	10.317	<0.0001	N+				
	Female Fertility	2	71.214 (62.399 - 86.970)	18.90 - 18.95 (18.40 - 20.55)	0.991	9.736	0.0001	N+				
		3	15.741 (11.890 - 20.758)	18.95 - 19.10 (18.40 - 19.95)	0.747	6.820	0.0012	N+				
		4	21.030 (16.833 - 26.101)	4.50 - 4.75 (3.85 - 16.70)	0.968	10.245	<0.0001	N+				
CAC162 RILs	Male Fertility	6	95.776 (90.673 - 95.776)	20.70 - 20.90 (19.25 - 20.90)	0.490	10.010	0.0011	N+				
		14	57.509 (54.192 - 61.594)	15.90 - 16.20 (7.05 - 16.80)	0.680	19.320	<0.0001	N+				
	Female Fertility	NA										
CAC415 RILs	Male Fertility	NA										
	Female Fertility	10	51.596 (48.660 - 53.554)	5.70 - 5.75 (4.50 - 5.75, 1.40 - 1.80)*	1.473	12.439	0.0022	N+				

848

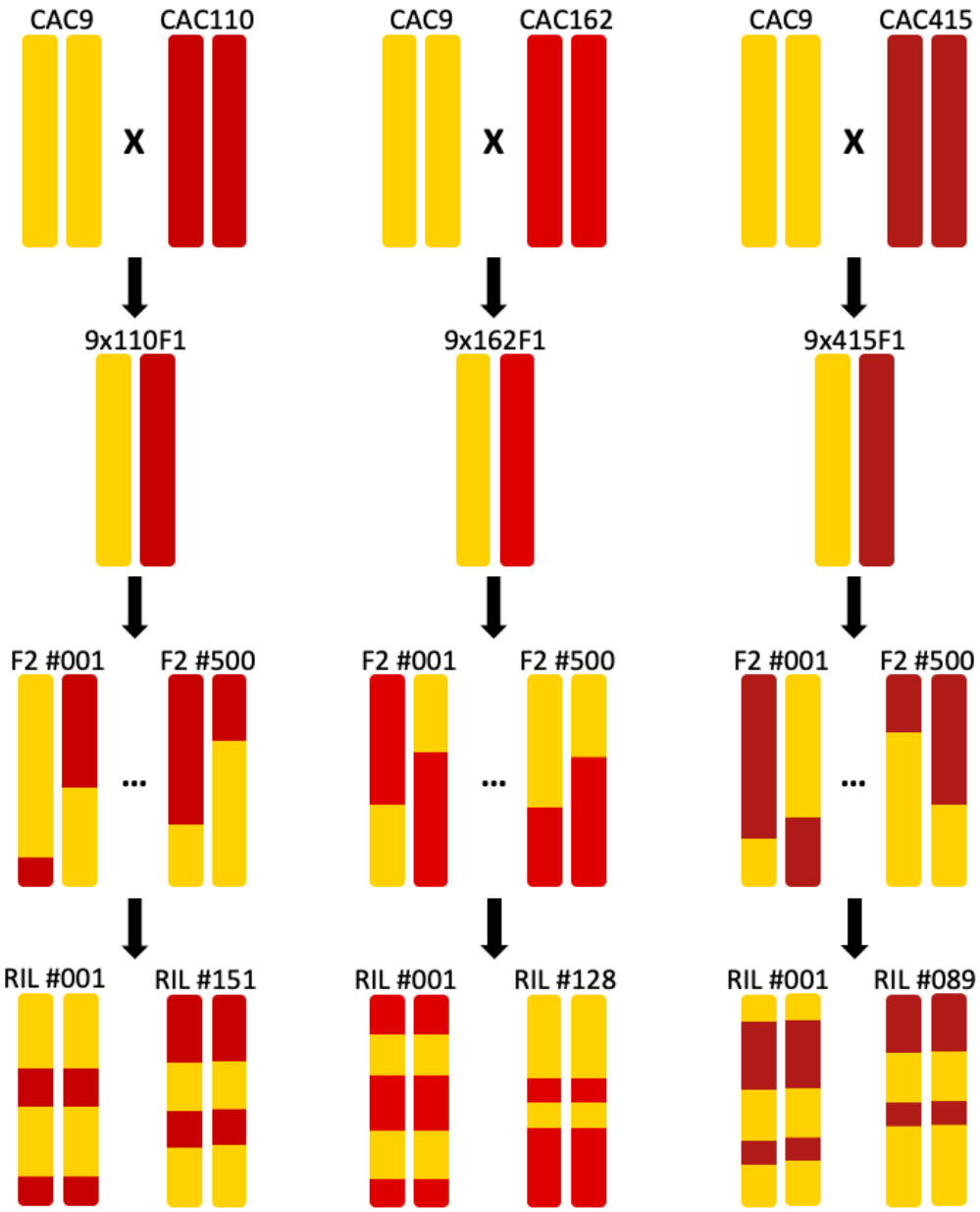

Figure S1. Recombinant inbred line (RIL) population crossing designs. We constructed three parallel RIL populations by crossing maternal *M. nasutus* line CAC9 to three paternal *M. guttatus* lines: CAC110, CAC162, and CAC415. We self-pollinated one F1 from each cross, producing a population of 500 F2s. We self-pollinated each F2 for at least 4 more generations with single seed decent to produce three RIL populations of F6 (or later generation) inbred individuals.

855

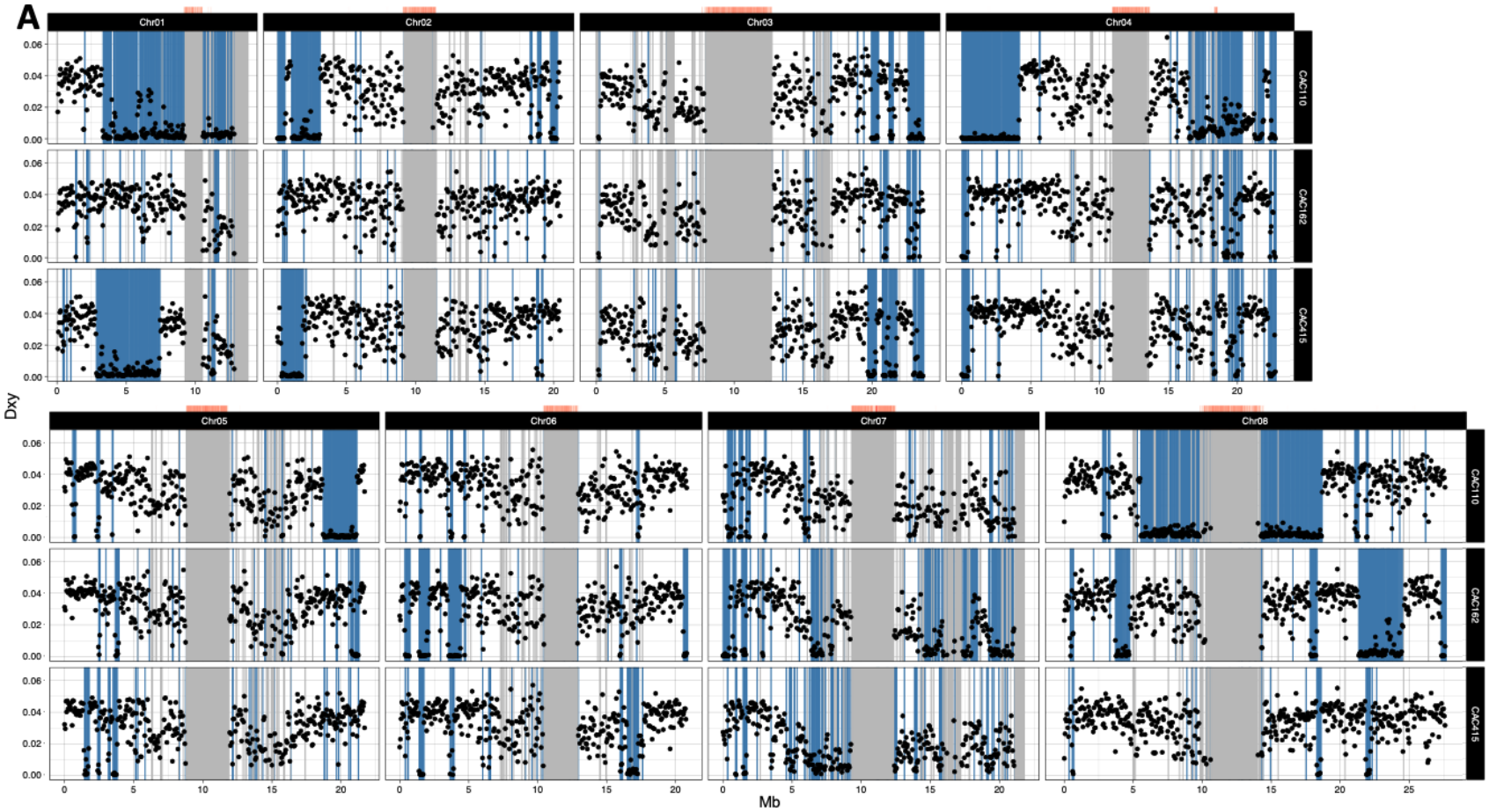
A
Chr01
Chr02
Chr03
Chr04
Chr05
Chr06
Chr07
Chr08
CAC110
CAC182
CAC415
Dxy
Mb

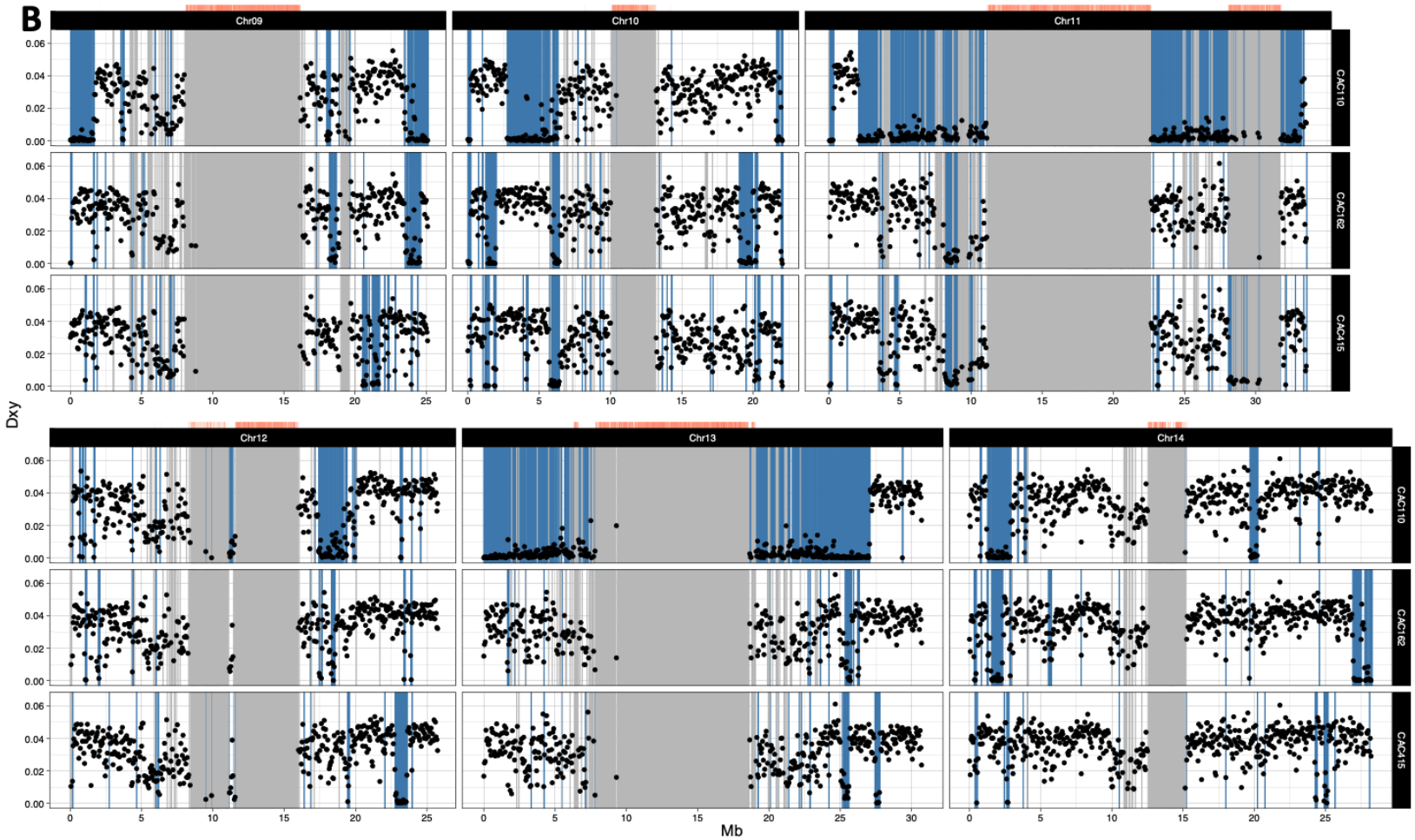

Figure S2. Introgression from *M. nasutus* into sympatric *M. guttatus.* A) Chr01-Chr08, B) Chr09-Chr14. Dxy calculated in 50kb windows across each chromosome of the IM62 v3 *Mimulus guttatus* reference genome, between the parental lines of the three RIL populations (CAC9 v. CAC110, CAC9 v. CAC162, and CAC9 v. CAC415). Blue shaded regions indicate putatively admixed regions of the three focal CAC *M. guttatus* lines tested, diagnosed by a greater than a 95% posterior probability of *M. nasutus* ancestry (in 1kb windows) as inferred via the HMM (i.e. more recent coalescence with included *M. nasutus* samples than with included *M. guttatus* samples). Grey shaded regions indicate missing data (fewer than 5000 genotyped sites within any 50kb window). Red heatmaps above each chromosome indicate the density of centromeric repeats in the same 50kb windows.

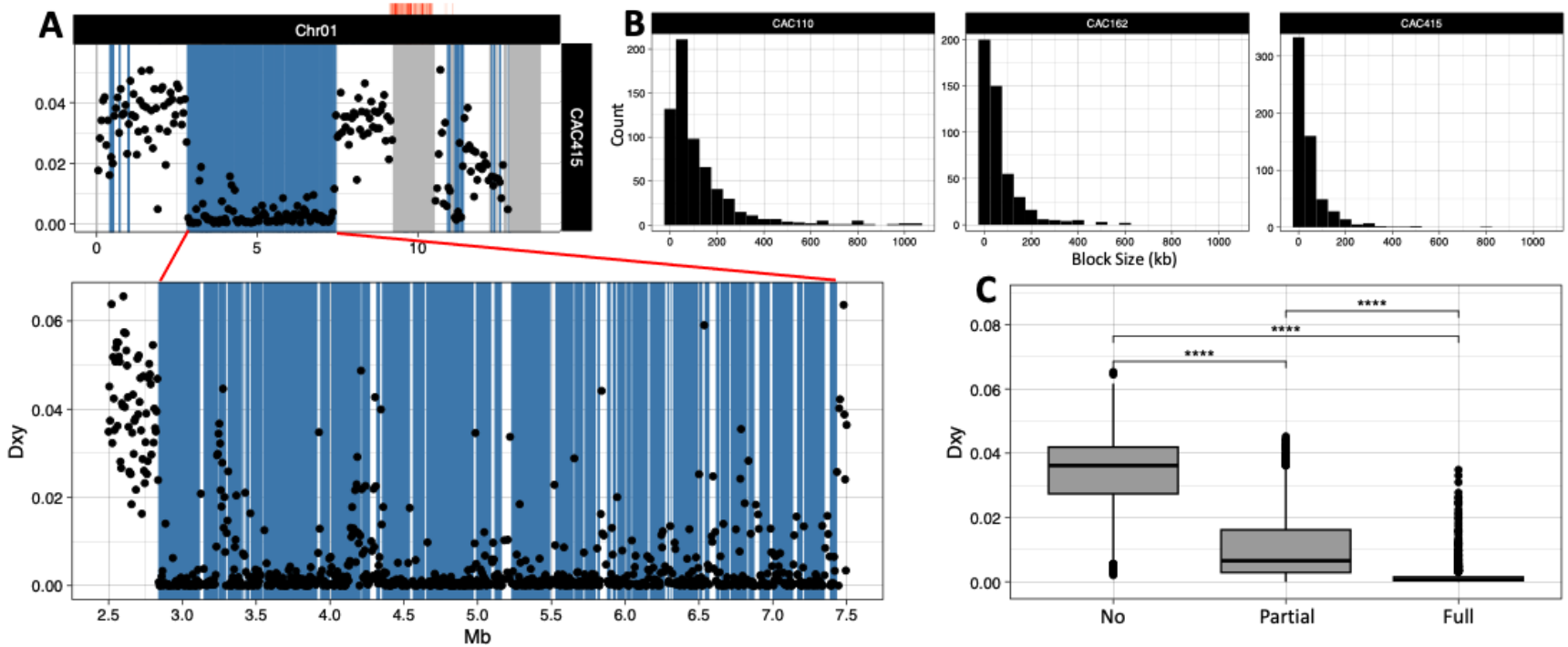

Figure S3. Block size and characteristics of introgression from *M. nasutus* into sympatric *M. guttatus.* A) A fine scale look at diagnosed blocks of introgression on the first chromosome in sympatric *M. guttatus* line CAC415. Blue shaded regions indicate putatively admixed regions diagnosed by a greater than a 95% posterior probability of *M. nasutus* ancestry (in 1kb windows) as inferred via the HMM (i.e. more recent coalescence with included *M. nasutus* samples than with included *M. guttatus* samples). Grey shaded regions indicate missing data (fewer than 5000 genotyped sites within any 50kb window). Red heatmaps above the chromosome indicate the density of centromeric repeats in the same 50kb windows. The shaded region between ~3 and 7.5 Mb is shown in finer detail, with Dxy calculated in 5kb windows across this region. **B)** Histograms showing the length of each inferred block of *M. nasutus* introgression in each of the sympatric *M. guttatus* lines used as parents for the three RIL populations. CAC110 average block length: ~125kb, n=645 blocks, CAC162: ~66kb, n=476, CAC415: ~48bk, n=603. **C)** Dxy in each 50kb window in the three sympatric *M. guttatus* lines used as parents for the three RIL populations binned by if that window has no inferred *M. nasutus* introgression within it (No), part of the window contains inferred introgression (Partial), or the entire window is covered by an inferred block of introgression (Full). Wilcox test, **** $p<0.0001$

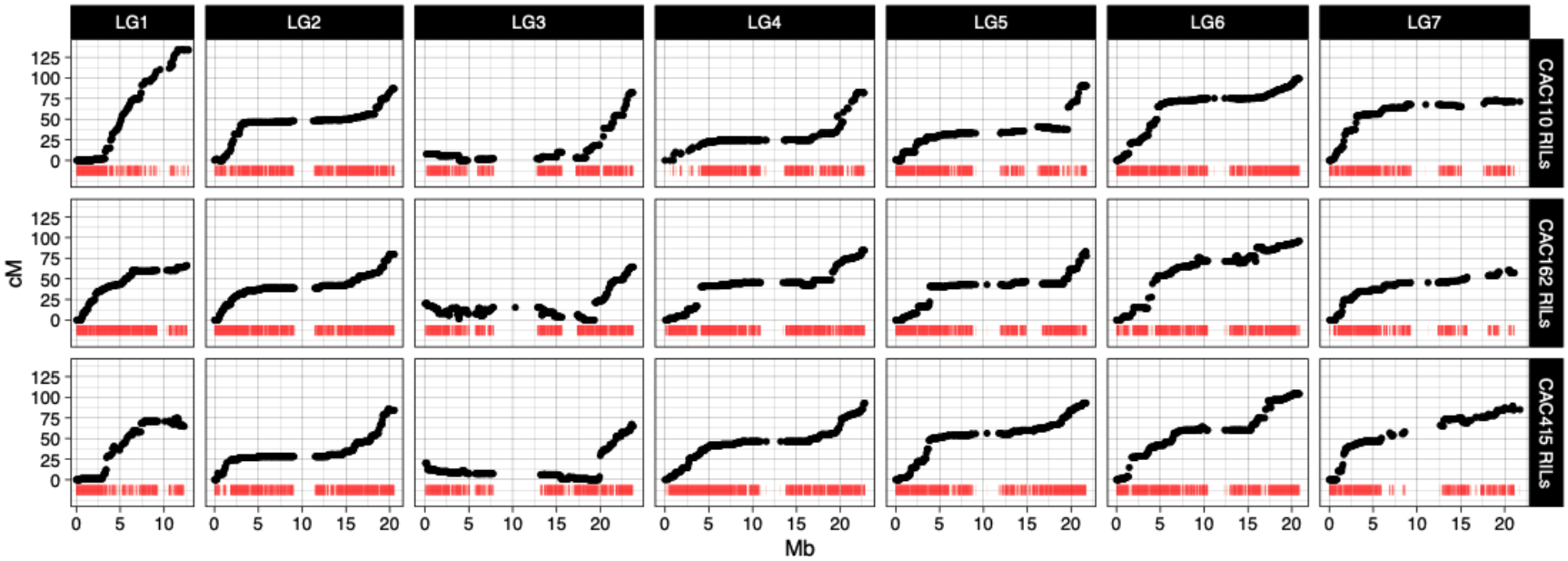
LG1
LG2
LG3
LG4
LG5
LG6
LG7
CAC110 RILs
CAC162 RILs
CAC415 RILs
cM
Mb
125
100
75
50
25
0
0
5
10
15
20

877

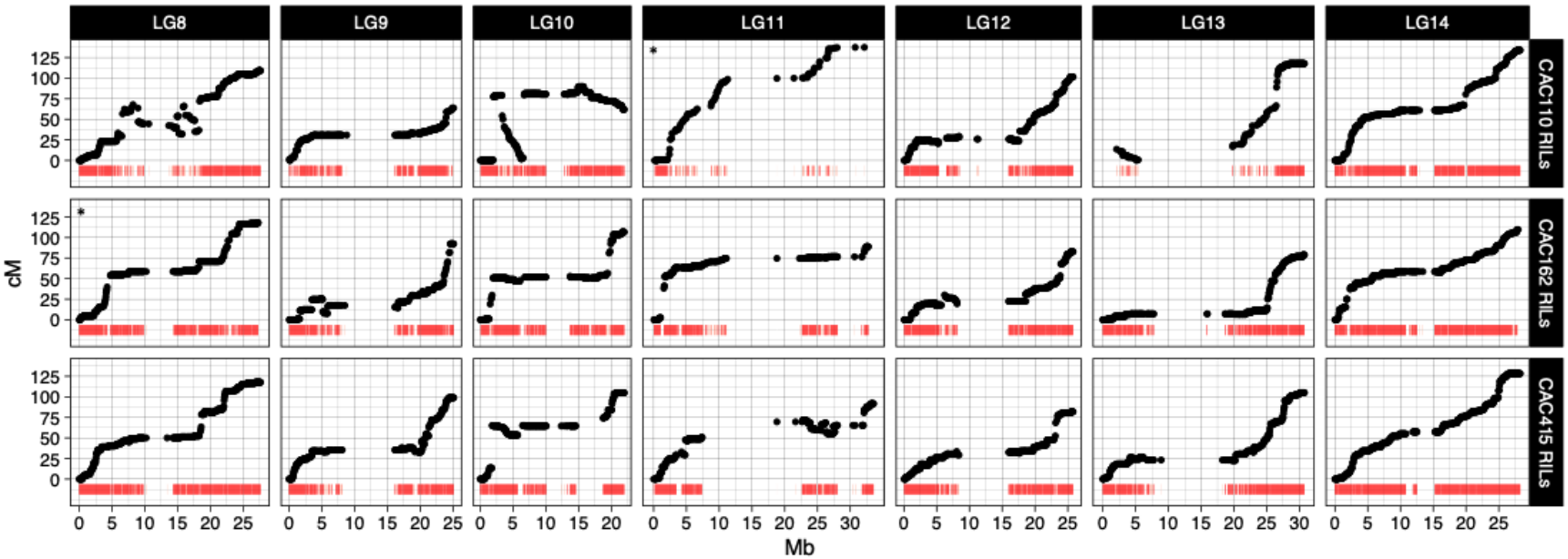

Figure S4. Map position (cM) versus physical marker positions (Mb) of the IM62 v3 *Mimulus guttatus* reference genome in the three RIL populations. A) LG1-7, B) LG8-14. Red heatmaps below each curve indicate the density of markers, measured as the distance in Mb to the nearest neighboring marker. Low SNP density, and the subsequent inability to genotype markers in areas of the *M. guttatus* parental genomes showing evidence of introgression from *M. nasutus* manifests as regions of low marker density on some chromosomes. Recombination rate is substantially lower across the center of each chromosome, with a gap in genotyped markers that colocalize with a metacentric (dicentric in the case of Chr11) chromosomal structure, identified via a high density of centromeric repeats. Negative slope suggests inverted marker order relative to the IM62 v3 *M. guttatus* reference genome in both the *M. nasutus* and *M. guttatus* parents. Blocks of markers spanning large physical distances but that map to nearly the same genetic position suggest inversions between the *M. guttatus* and *M. nasutus* parents used to produce that RIL population.

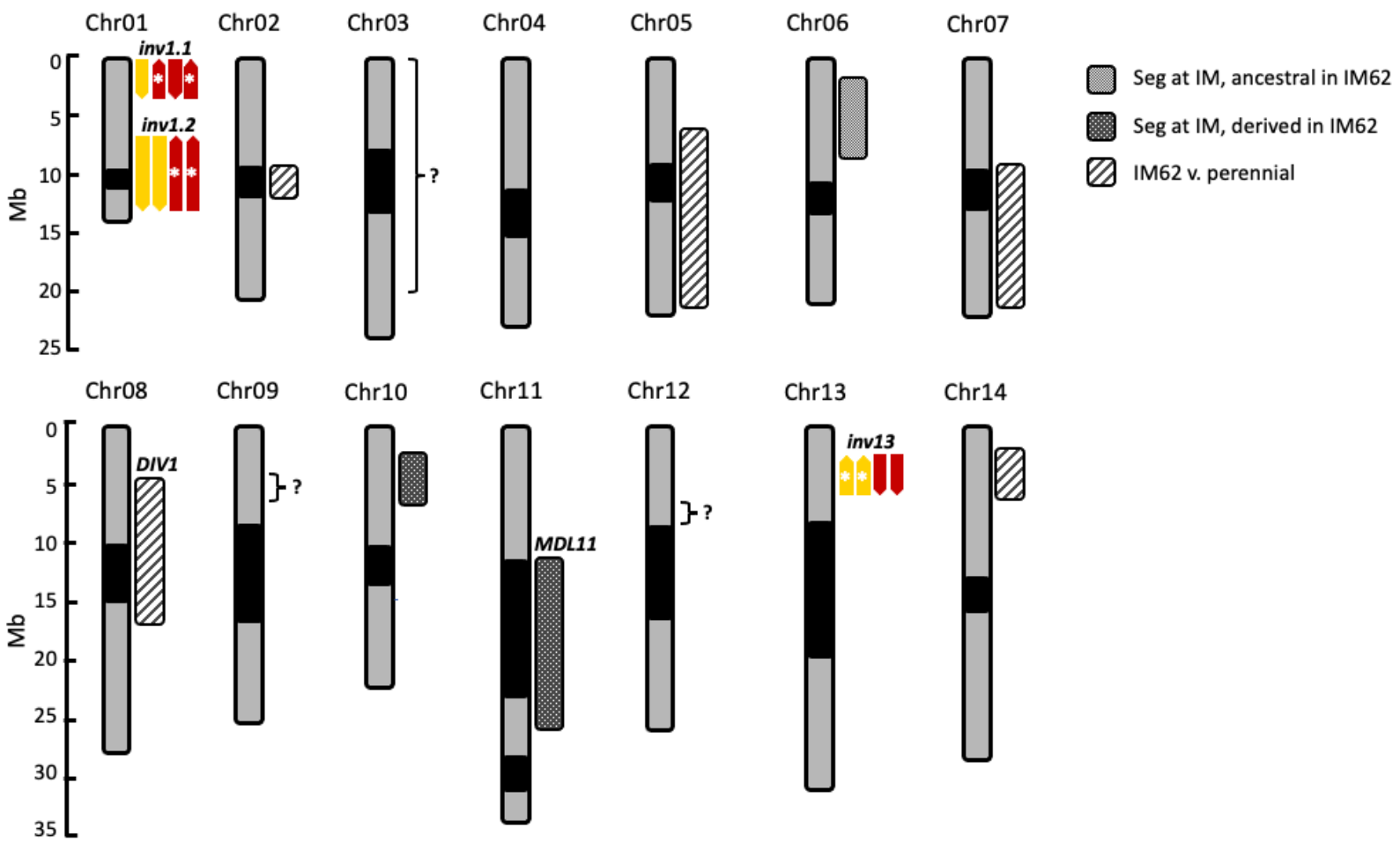

Figure S5. Locations of newly identified and known inversions in *M. guttatus*. Physical positions (Mb) of each of the identified putative chromosomal inversions among the CAC *M. nasutus* and *M. guttatus* lines crossed. Centromeres are indicated in black. Arrows to the right of each chromosome indicate the observed orientation of each inversion in CAC9, CAC110, CAC162, and CAC415 from left to right. Arrows in yellow show evidence of *M. nasutus* ancestry, arrows in red show evidence of *M. guttatus* ancestry. The locations of previously identified inversions in *M. guttatus* are shown to the right of each chromosome. Brackets marked with question marks indicate further areas of interest, due to unique marker order, but which could not be confidently identified as inversions.

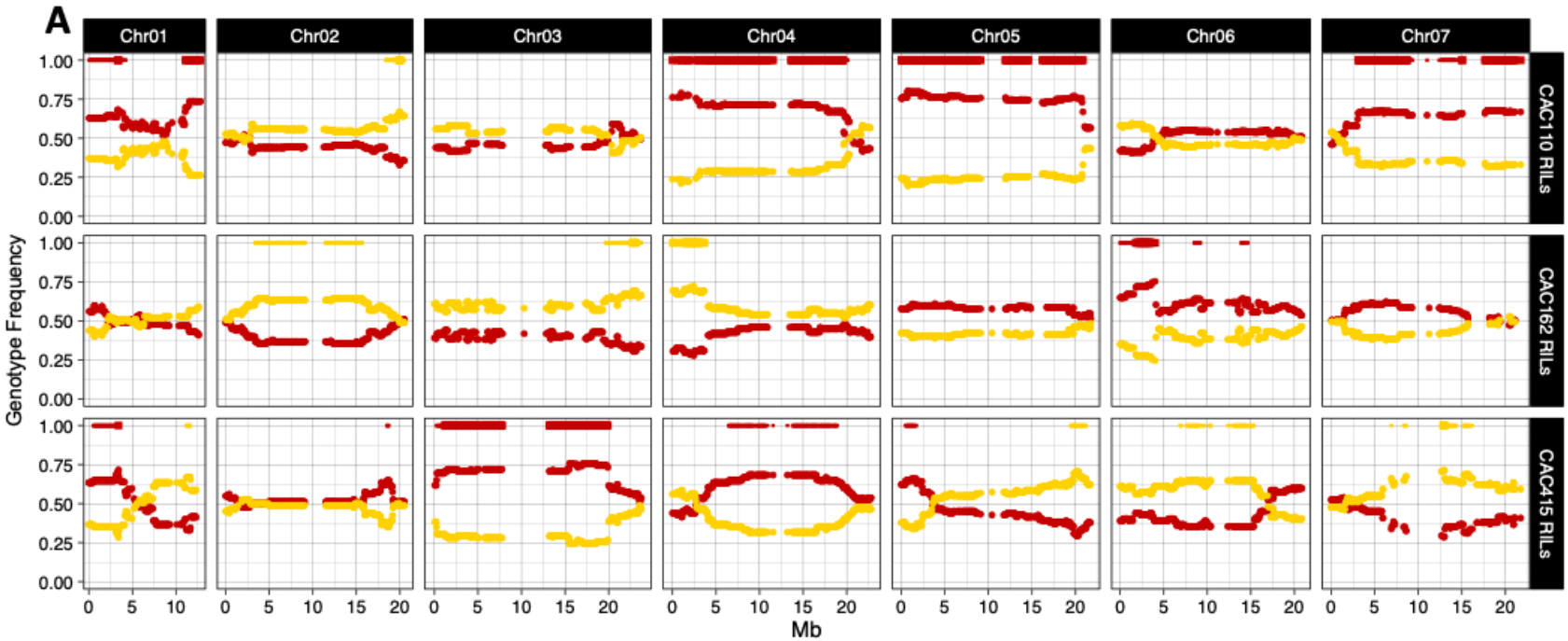
A
Chr01
Chr02
Chr03
Chr04
Chr05
Chr06
Chr07
CAC110 RILs
CAC162 RILs
CAC415 RILs
Genotype Frequency
1.00
0.75
0.50
0.25
0.00
0
5
10
15
20
Mb

896

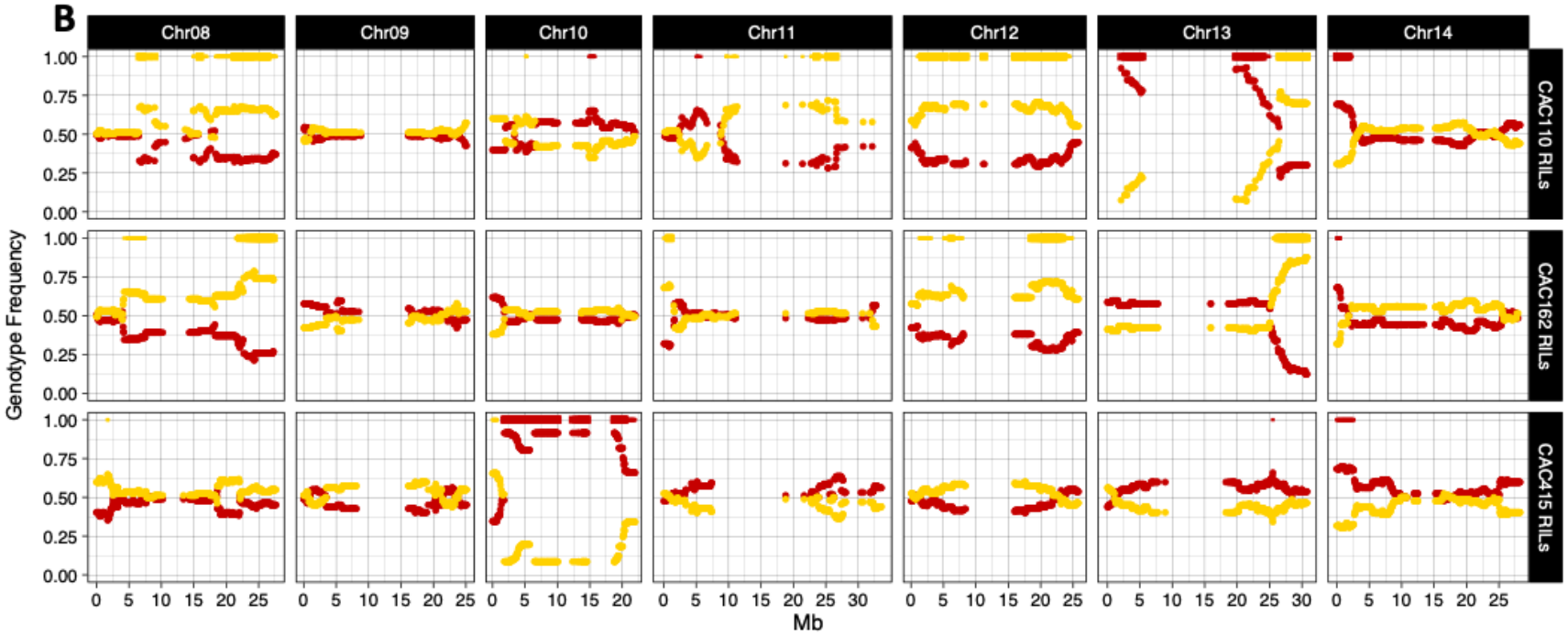

Figure S6. Transmission Ratio Distortion, Mb, A) Chr01-Chr07, B) Chr07-Chr14. Genotype frequencies across the first seven chromosomes of the three RIL populations. Red dots indicate homozygous *M. guttatus* genotypes, yellow dots, homozygous *M. nasutus* genotypes. Bars at the top of each plot indicate regions showing significant transmission ratio distortion from the Mendelian 1:1 expectation by χ^2 tests at $\alpha = 0.01$ (thin bars), and a more stringent Bonferonni-corrected α (thick bars, unique α for each chromosome in each RIL population depending on the number of markers tested, see Table S3 for values). Bar color indicates and excess of *M. guttatus* (red), or *M. nasutus* (yellow) genotypes. Markers are ordered by physical position (Mb) within the IM62 v3 *Mimulus guttatus* reference genome.

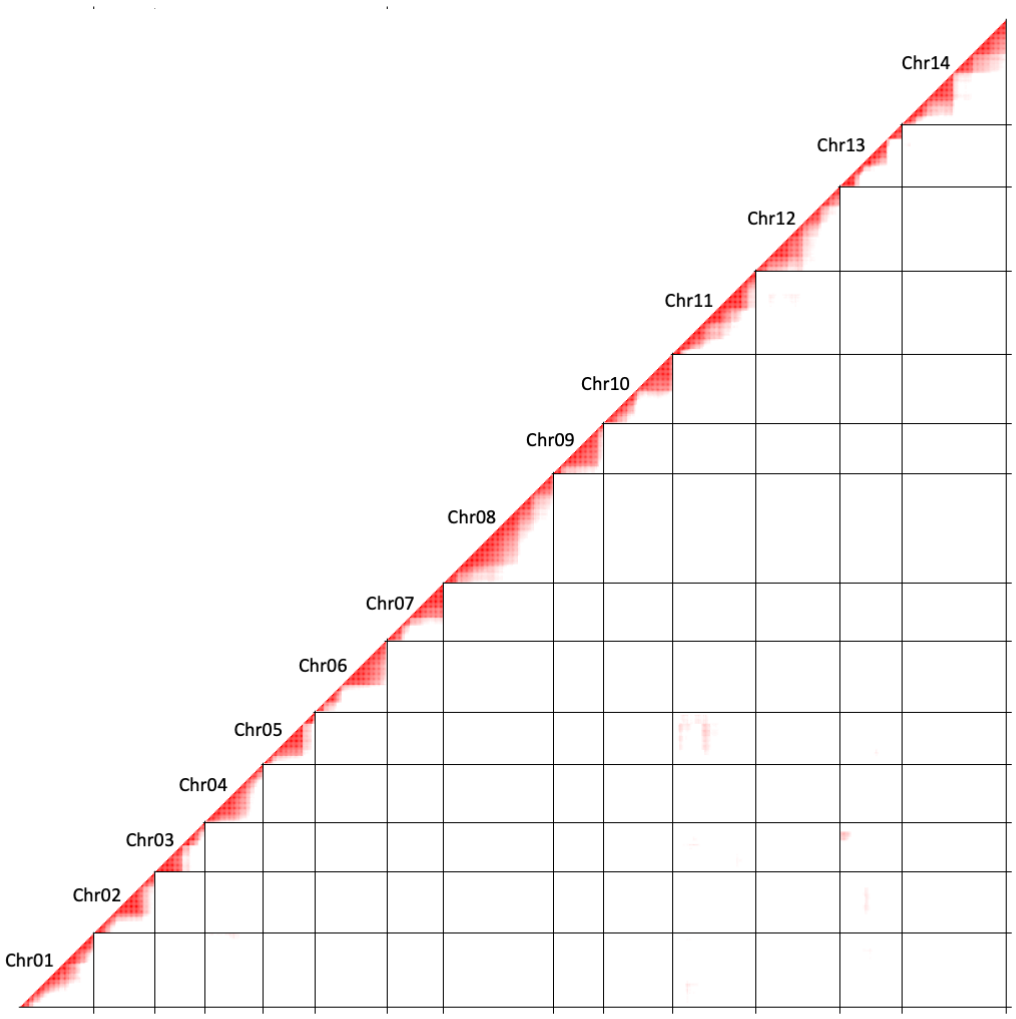

Figure S7. CAC110 RILs linkage disequilibrium heatmap. LD heatmap for each pairwise marker comparison across all 14 chromosomes, showing r values greater than the 95% quantile (>0.37) in the first RIL population. Values range from 0 (white) to 1 (red).

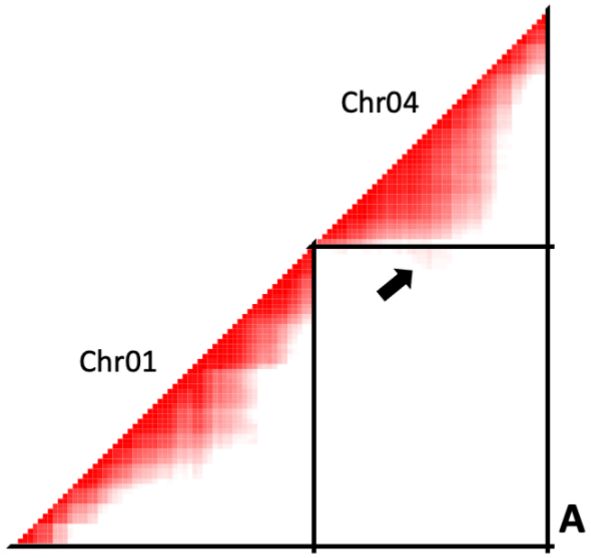

909

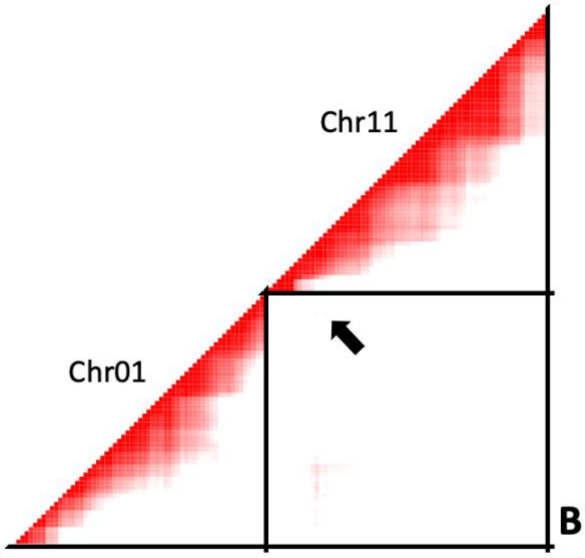

910

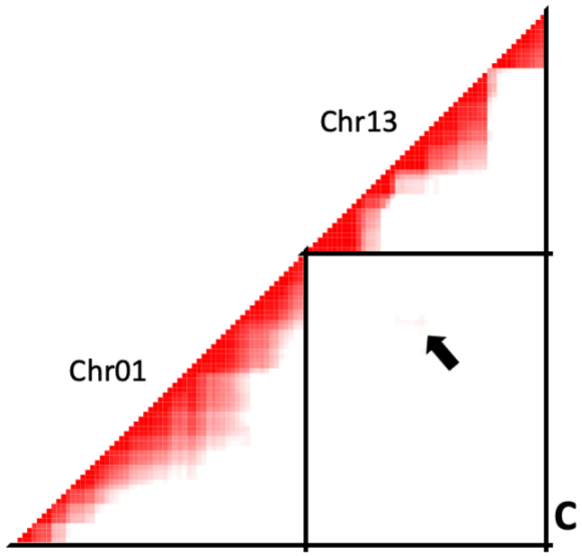

911

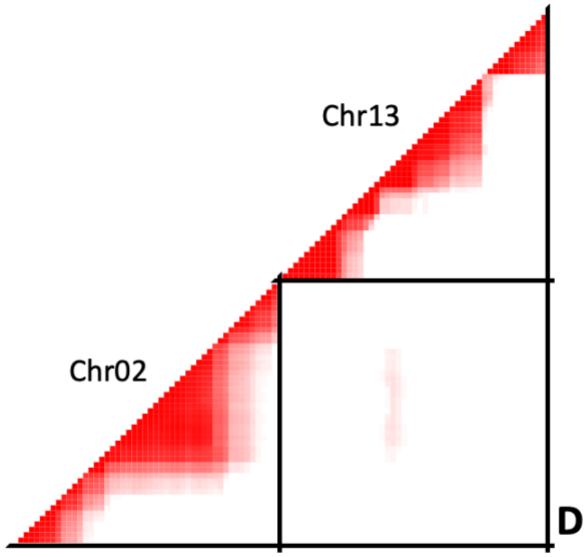

912

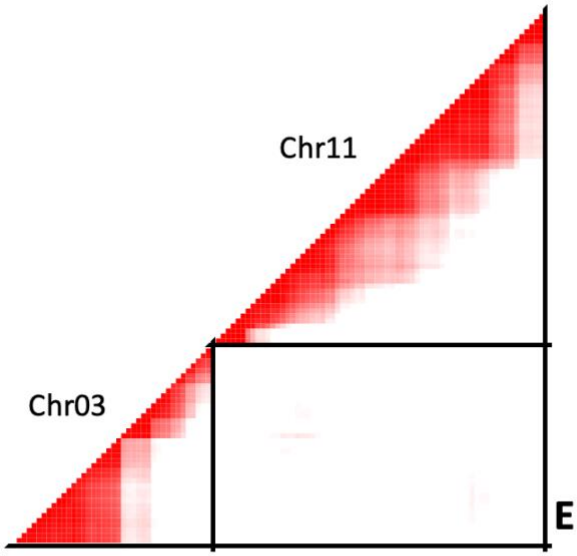

913

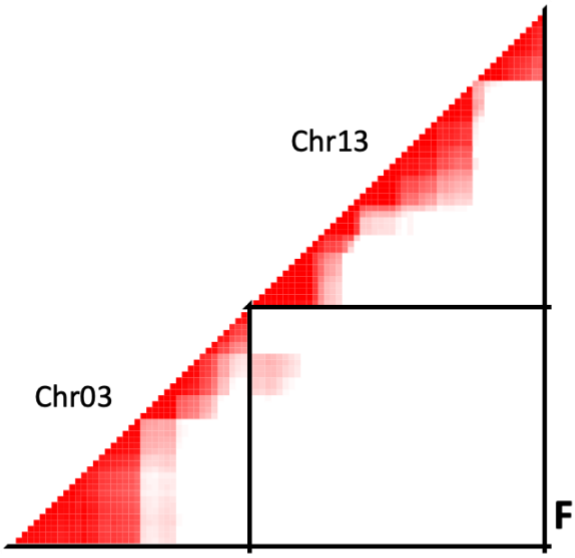

914

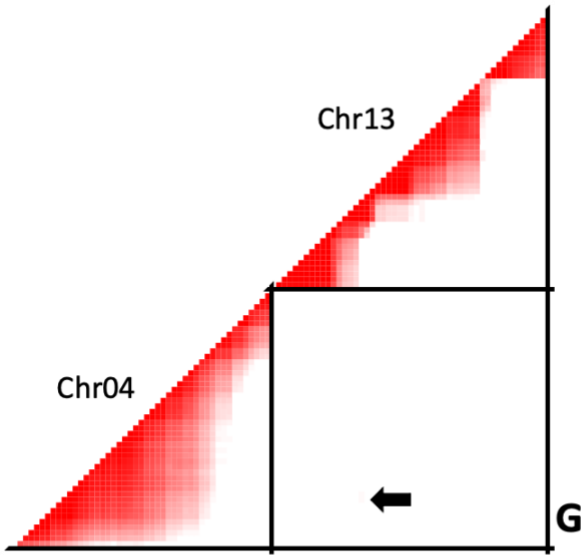

915

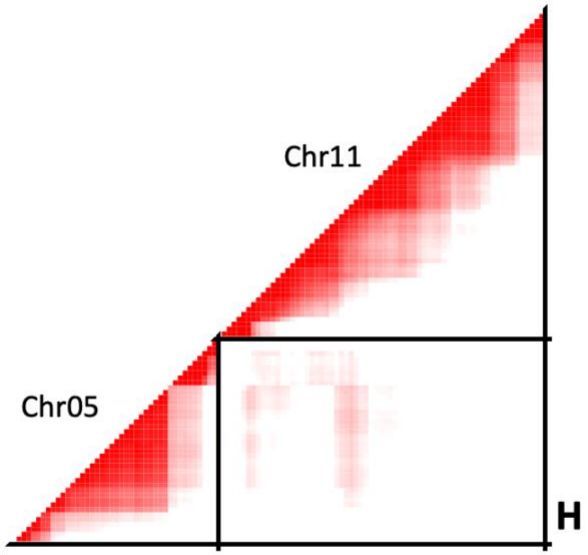

916

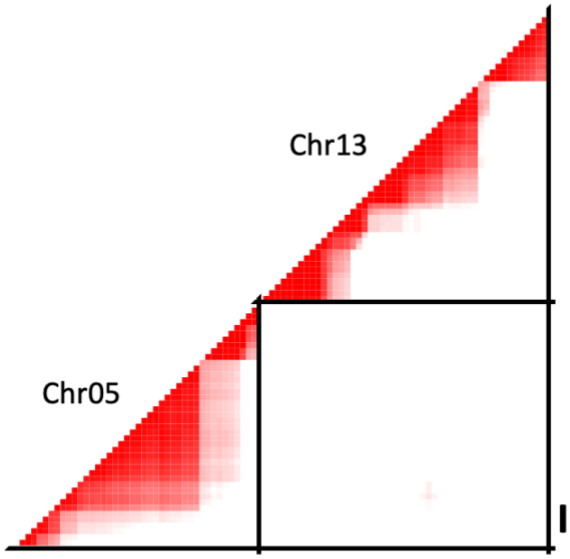

917

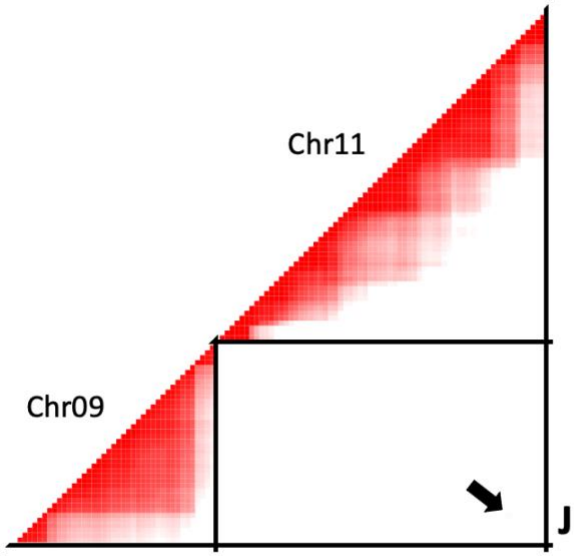

918

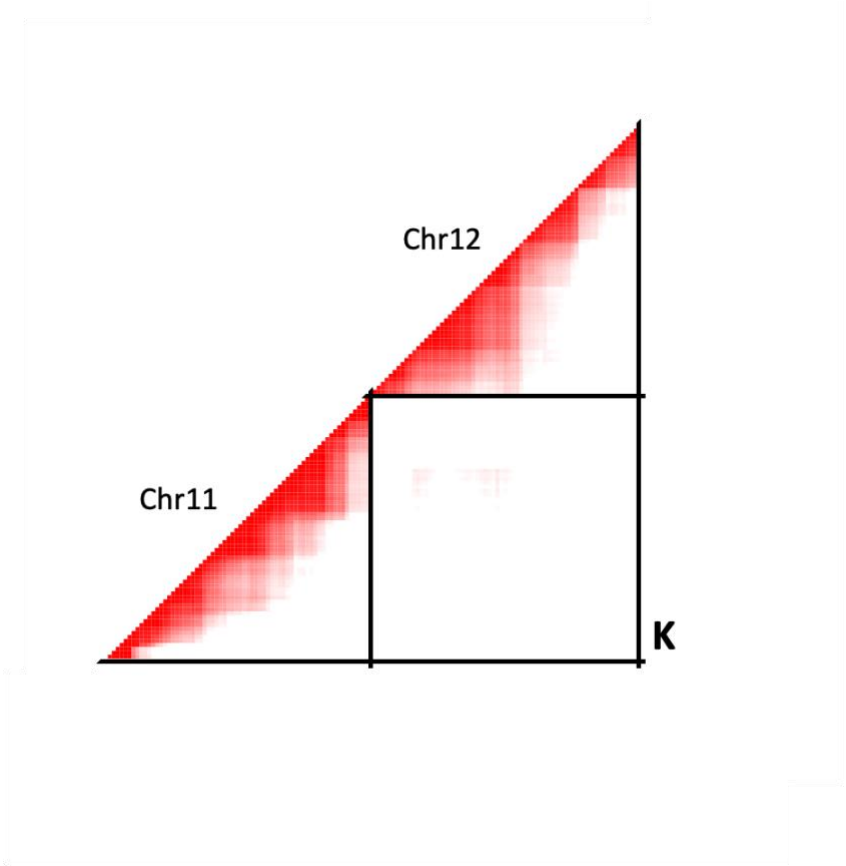

Figure S8. CAC110 RILs linkage disequilibrium heatmap. LD heatmaps for each pairwise marker comparison, showing r values greater than the 95% quantile (>0.37) in chromosome comparisons with at least 1 marker above the cutoff in the first RIL population. Values range from 0 (white) to 1 (red). Arrows indicates significant marker comparisons, when distorted regions are small. **A)** Chr01 and Chr04 **B)** Chr01 and Chr11 **C)** Chr01 and Chr13 **D)** Chr02 and Chr13 **E)** Chr03 and Chr11 **F)** Chr03 and Chr13 **G)** Chr04 and Chr13 **H)** Chr05 and Chr11 **I)** Chr05 and Chr13 **J)** Chr09 and Chr11 **K)** Chr11 and Chr12.

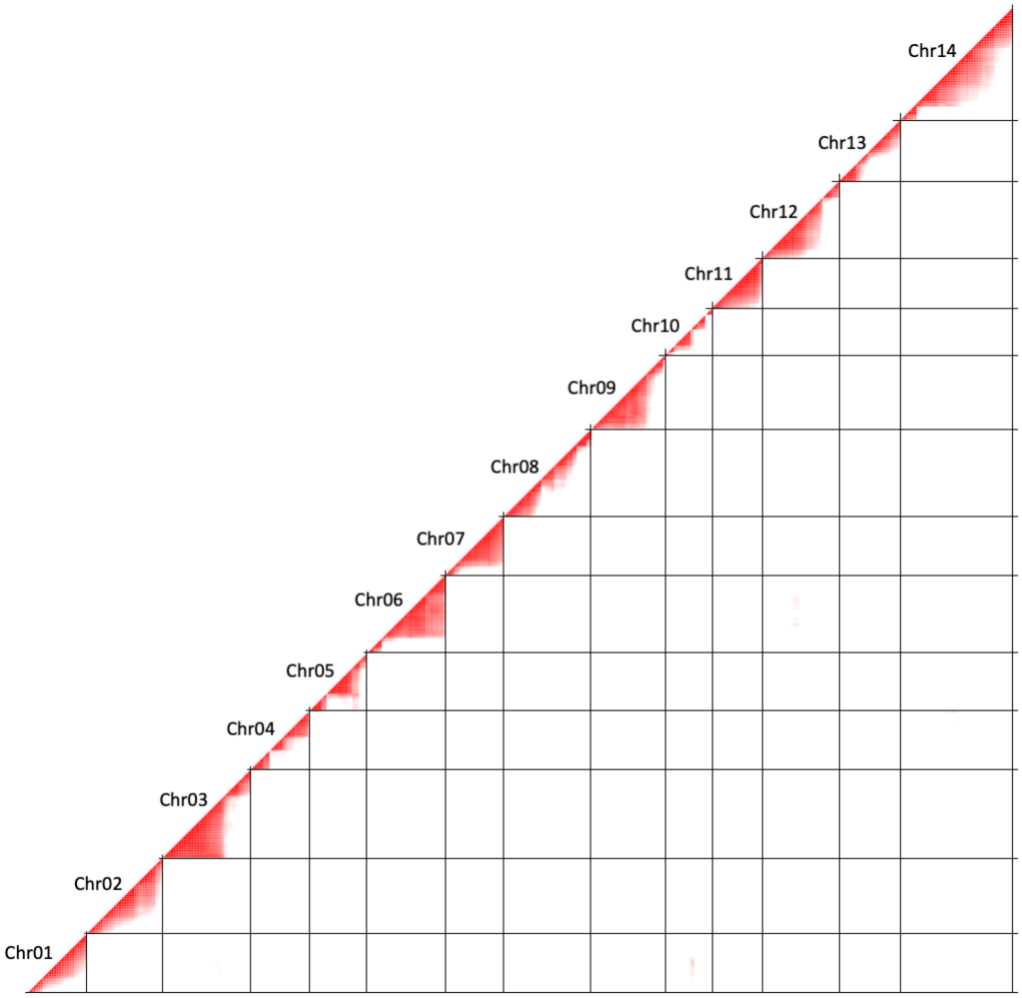

Figure S9. CAC162 RILs linkage disequilibrium heatmap. LD heatmap for each pairwise marker comparison across all 14 chromosomes, showing r values greater than the 95% quantile (>0.41) in the second RIL population. Values range from 0 (white) to 1 (red).

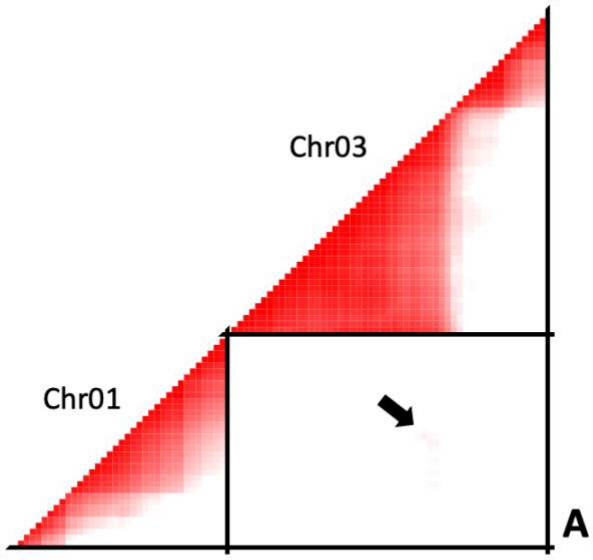

931

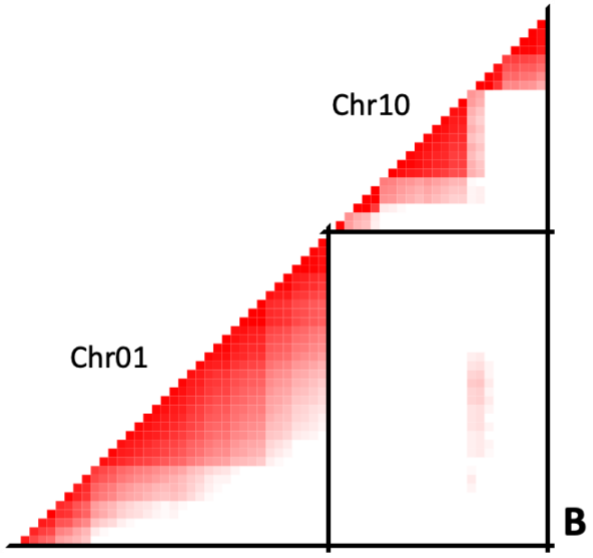

932

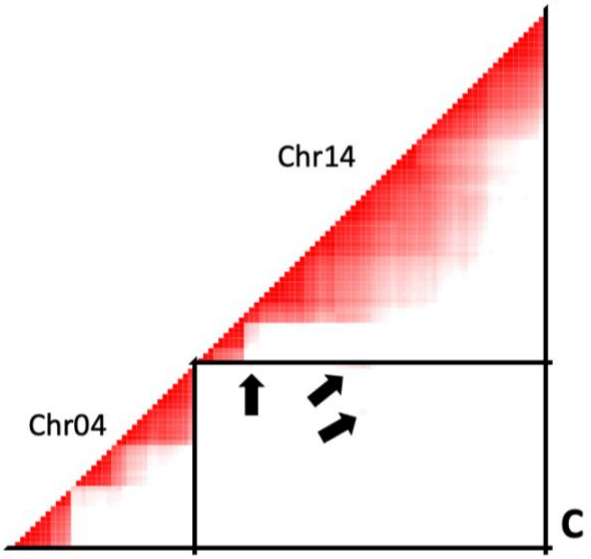

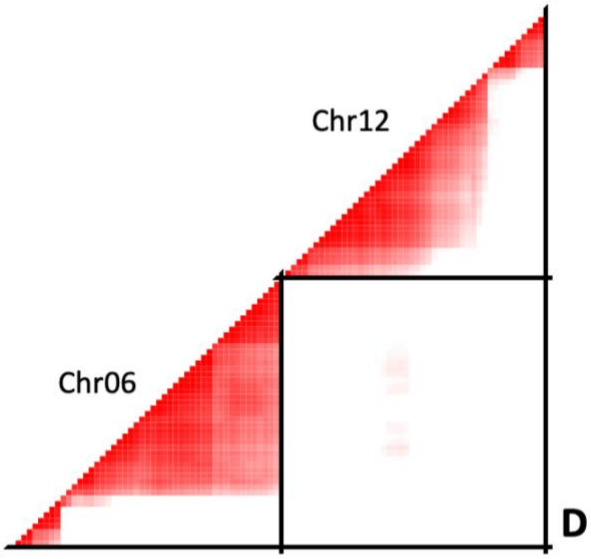

Figure S10. CAC162 RILs linkage disequilibrium heatmap. LD heatmaps for each pairwise marker comparison, showing r values greater than the 95% quantile (>0.41) in chromosome comparisons with at least 1 marker above the cutoff in the second RIL population. Values range from 0 (white) to 1 (red). Arrows indicates significant marker comparisons, when distorted regions are small. **A)** Chr01 and Chr03 **B)** Chr01 and Chr10 **C)** Chr04 and Chr14 **D)** Chr06 and Chr12.

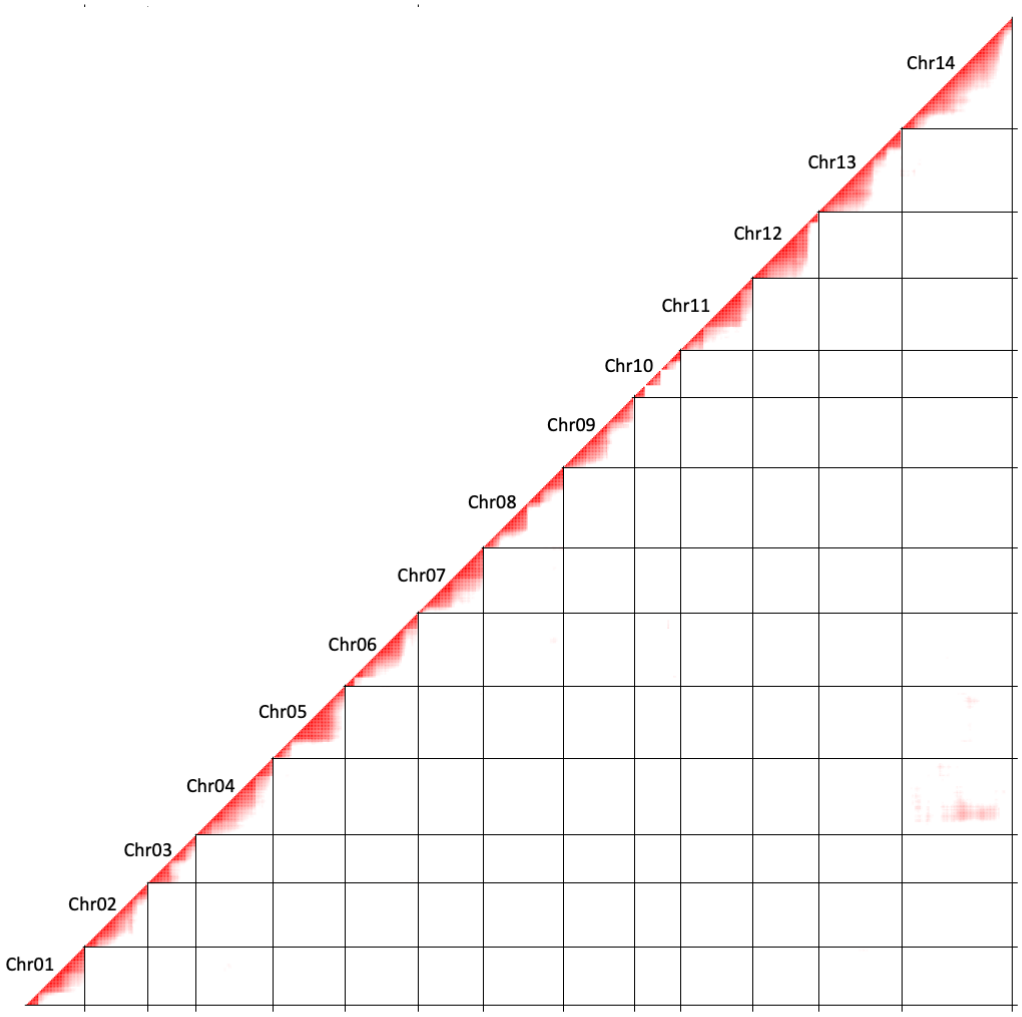

Figure S11. CAC415 RILs linkage disequilibrium heatmap. LD heatmap for each pairwise marker comparison across all 14 chromosomes, showing r values greater than the 95% quantile (>0.39) in the third RIL population. Values range from 0 (white) to 1 (red).

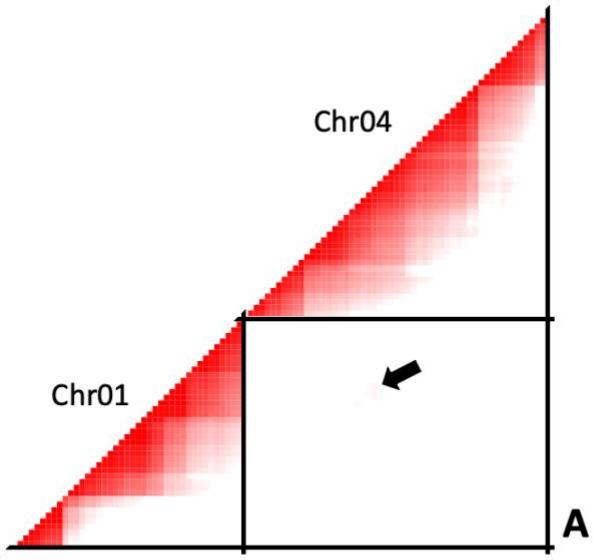

945

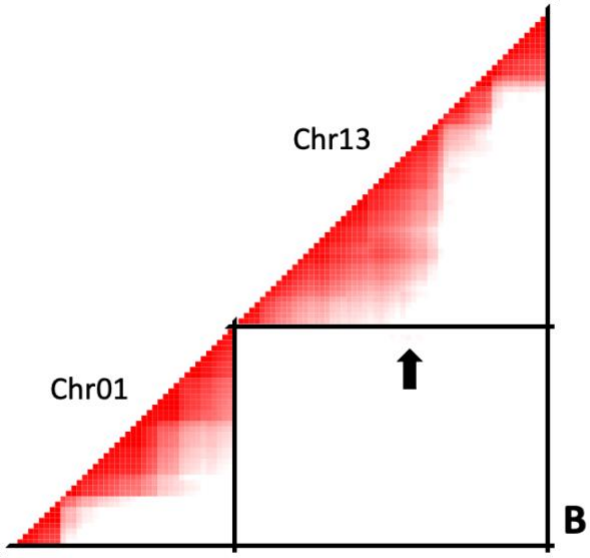

946

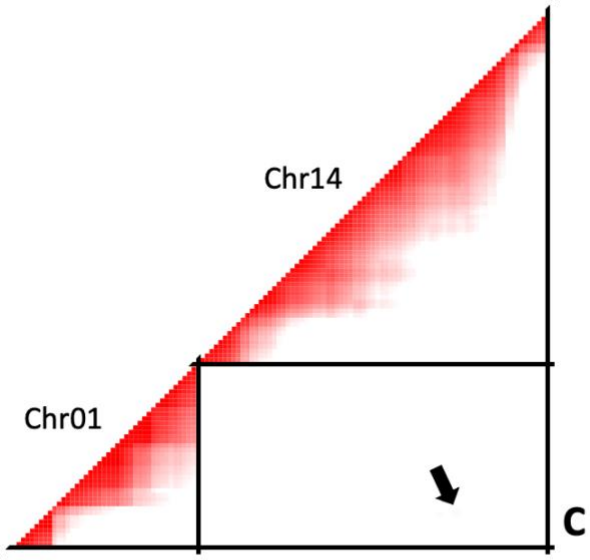

947

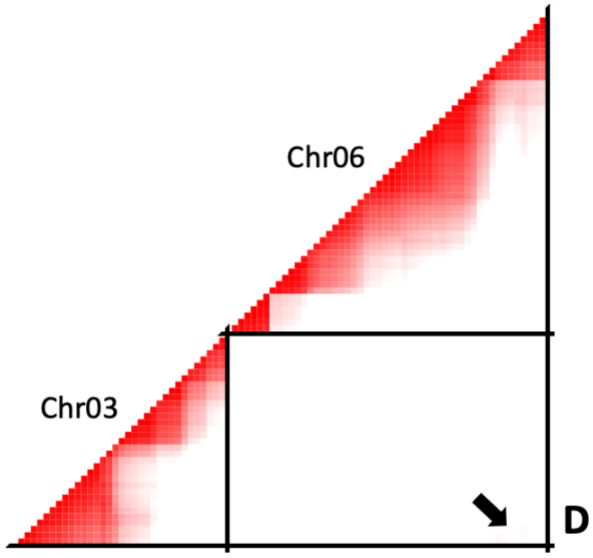

948

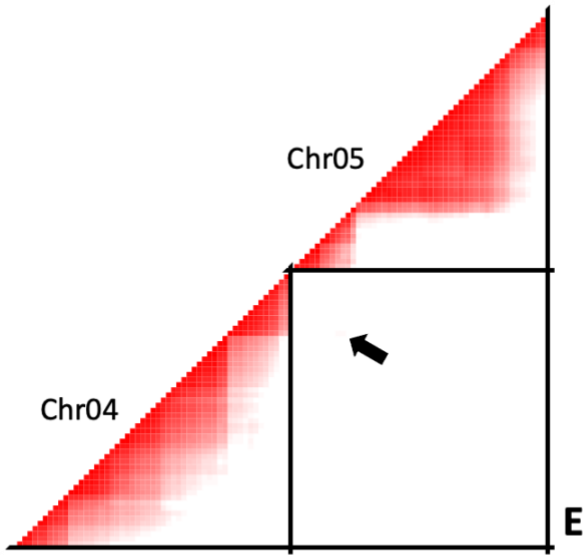
Chr05
Chr04
E

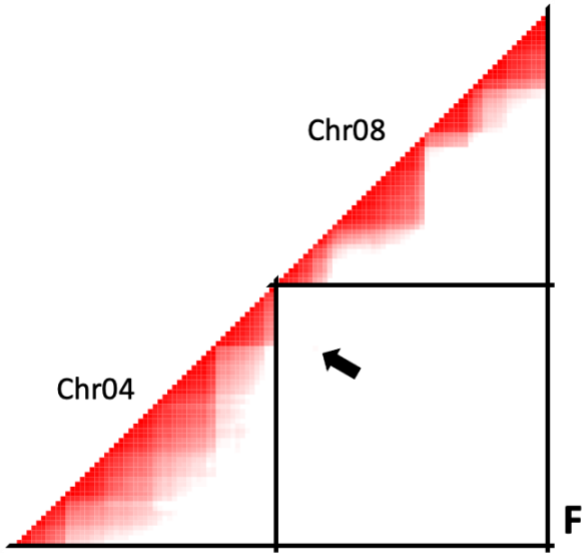
Chr08
Chr04
F

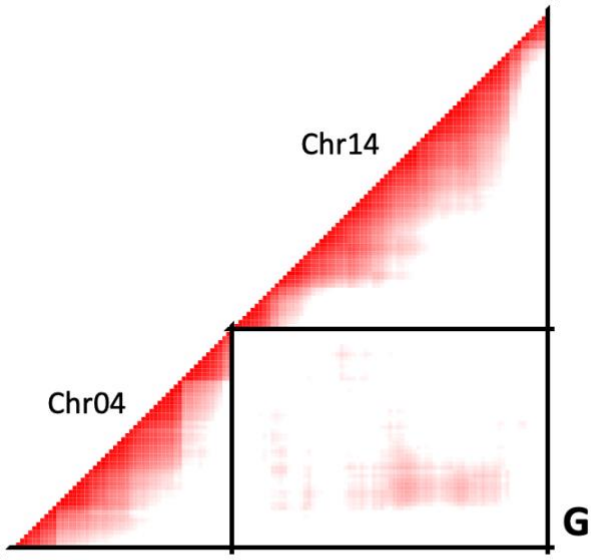

951

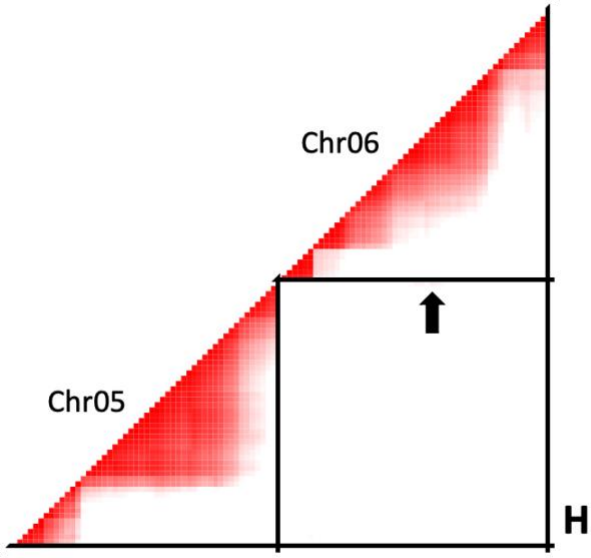

952

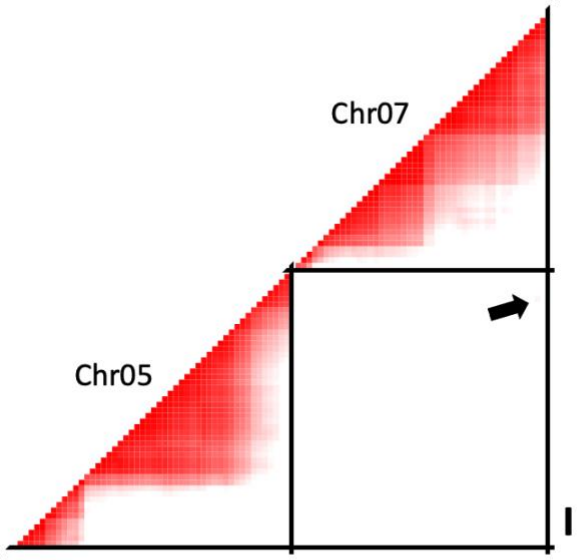

953

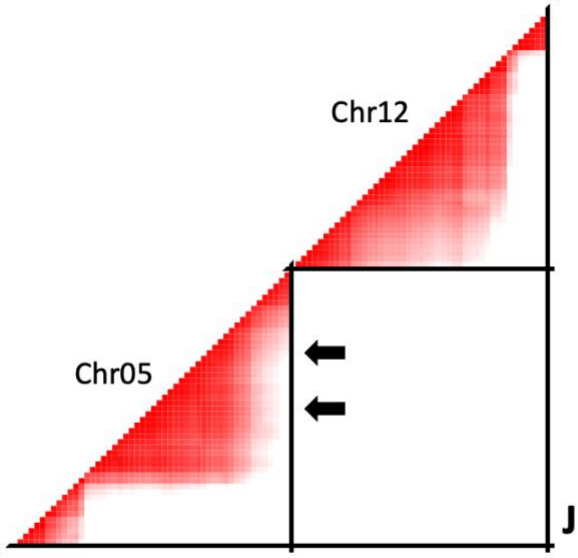

954

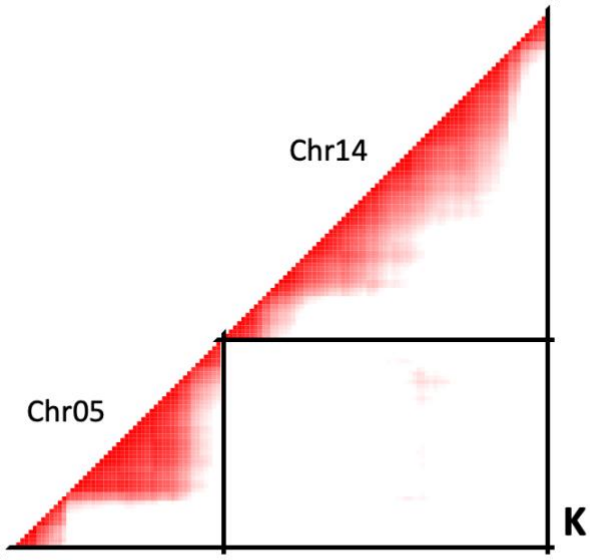

955

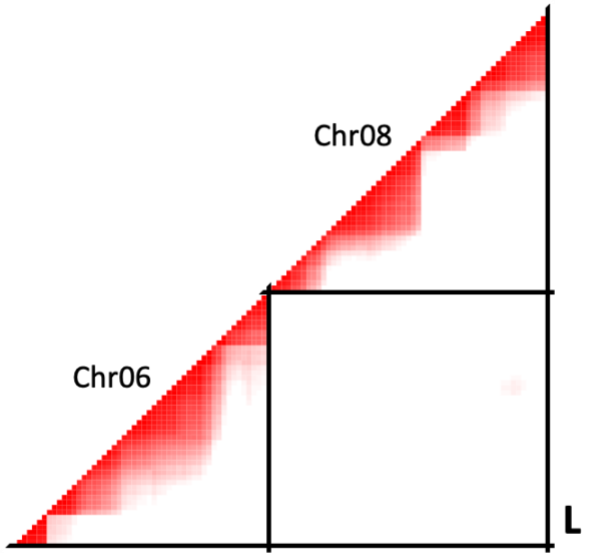

956

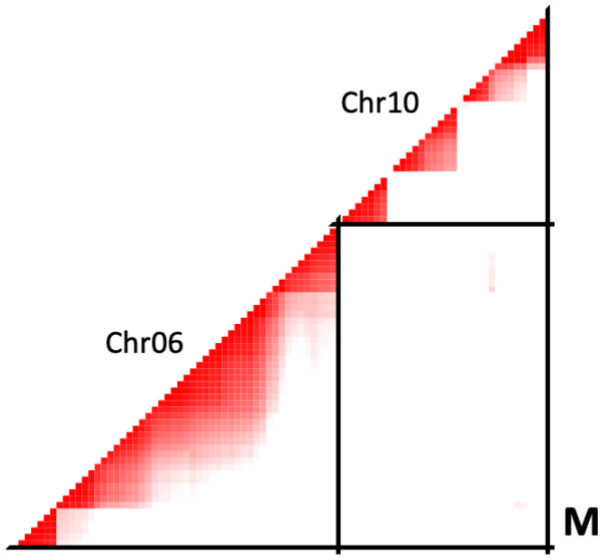

957

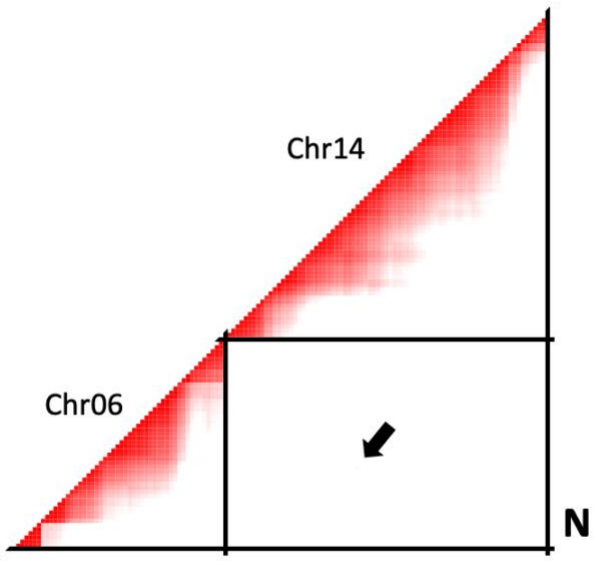

958

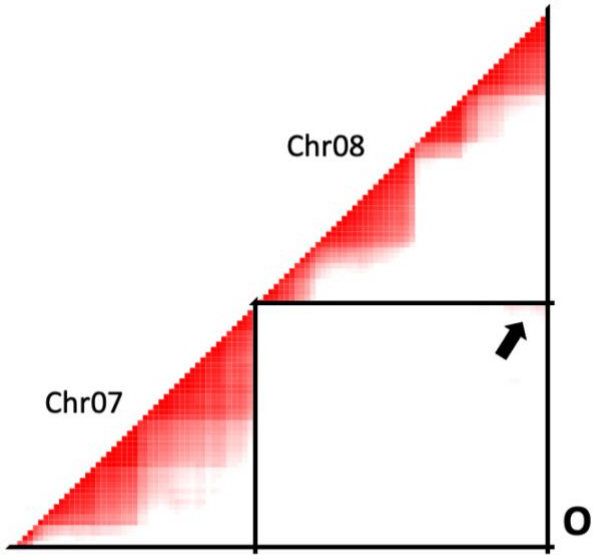

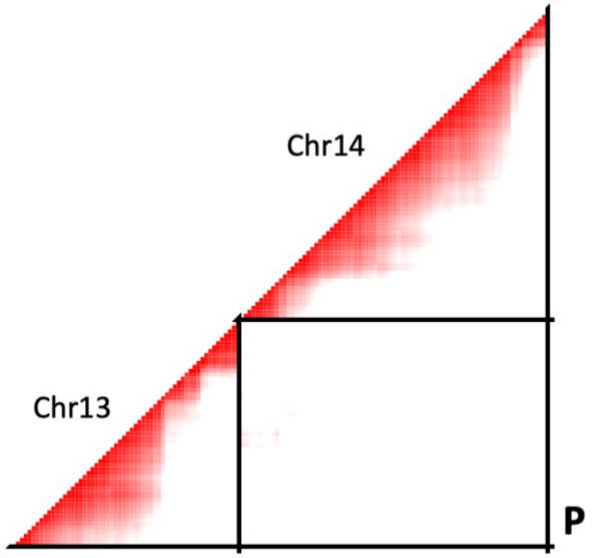

Figure S12. CAC415 RILs linkage disequilibrium heatmap.
LD heatmaps for each pairwise marker comparison, showing r values greater than the 95% quantile (>0.39) in chromosome comparisons with at least 1 marker above the cutoff in the third RIL population. Values range from 0 (white) to 1 (red). Arrows indicates significant marker comparisons, when distorted regions are small. A) Chr01 and Chr04 B) Chr01 and Chr13 C) Chr01 and Chr14 D) Chr03 and Chr06 E) Chr04 and Chr05 F) Chr04 and Chr08 G) Chr04 and Chr14 H) Chr05 and Chr06 I) Chr05 and Chr07 J) Chr05 and Chr12 K) Chr05 and Chr14 L) Chr06 and Chr08 M) Chr06 and Chr10 N) Chr06 and Chr14 O) Chr07 and Chr08 P) Chr13 and Chr14.

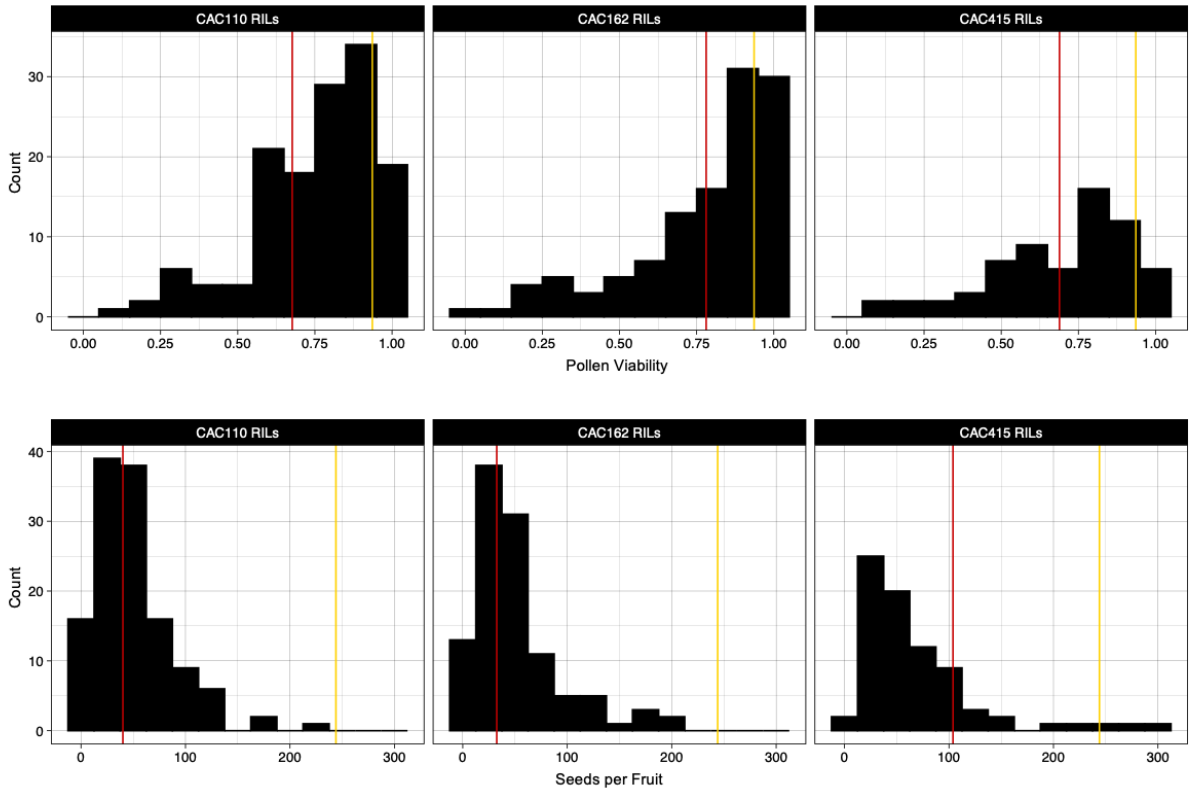

Figure S13. Male and female viability distributions in the three RIL populations. Yellow lines indicate *M. nasutus* average values, red lines indicate *M. guttatus* average values.

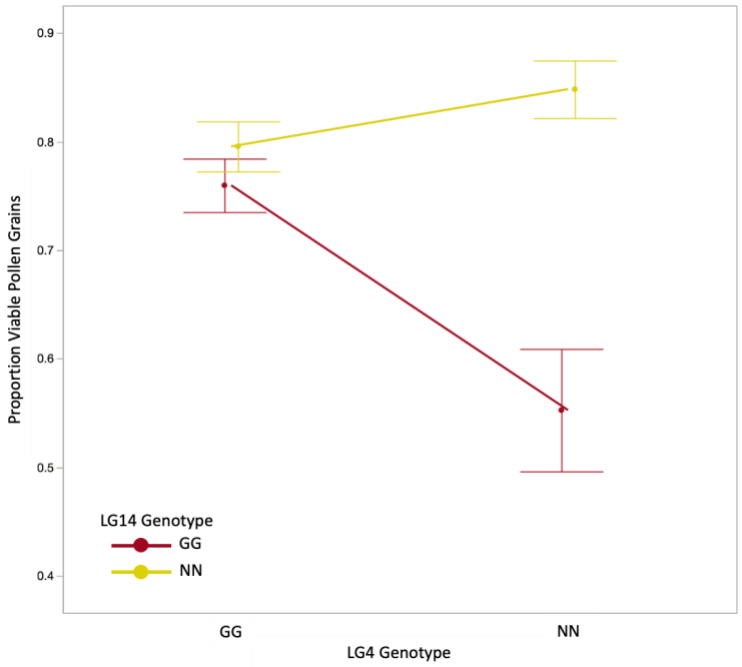
0.9
0.8
0.7
0.6
0.5
0.4
Proportion Viable Pollen Grains
LG14 Genotype
GG
NN
GG
NN
LG4 Genotype

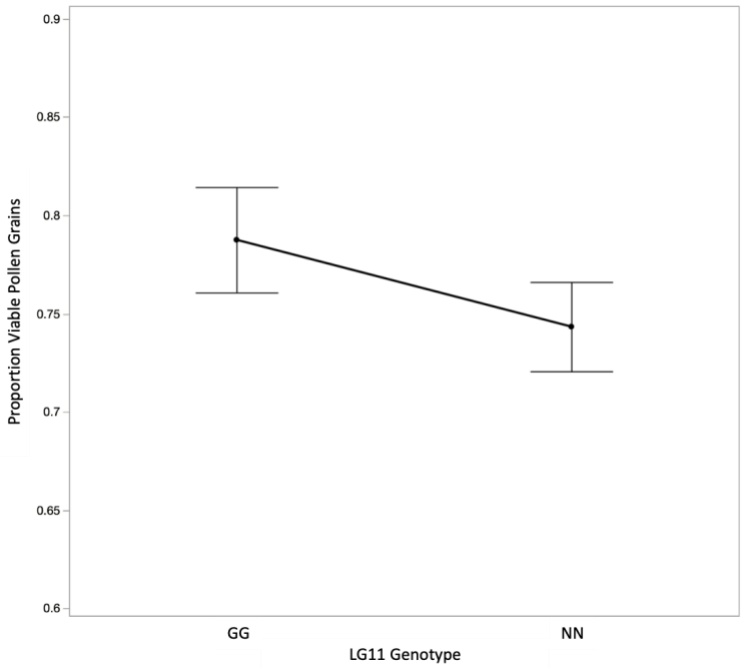
0.9
0.85
0.8
0.75
0.7
0.65
0.6
Proportion Viable Pollen Grains
GG
NN
LG11 Genotype

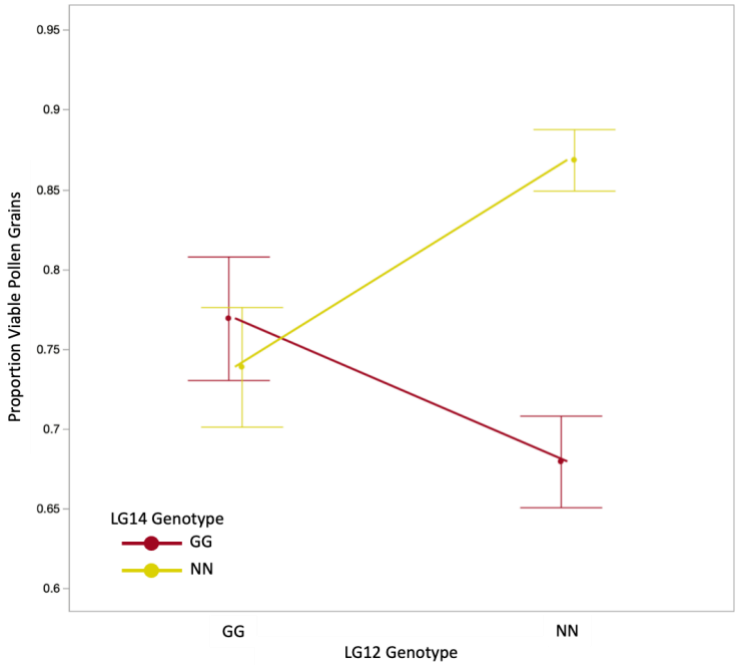

Figure S14. CAC110 RILs male fertility effect plots. Average proportion viable pollen grains of each genotypic class for each significant additive and epistatic QTL.

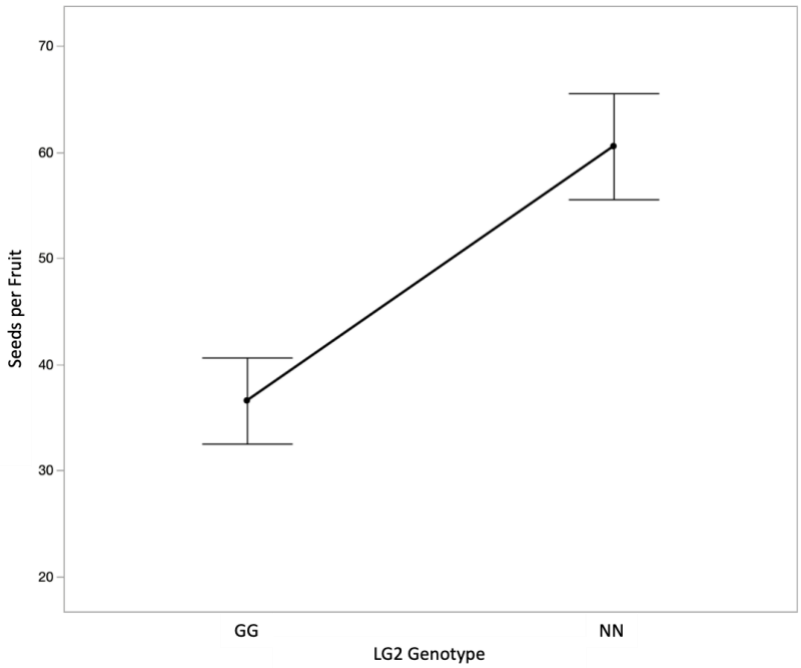
70
60
50
40
30
20
Seeds per Fruit
GG
NN
LG2 Genotype

977

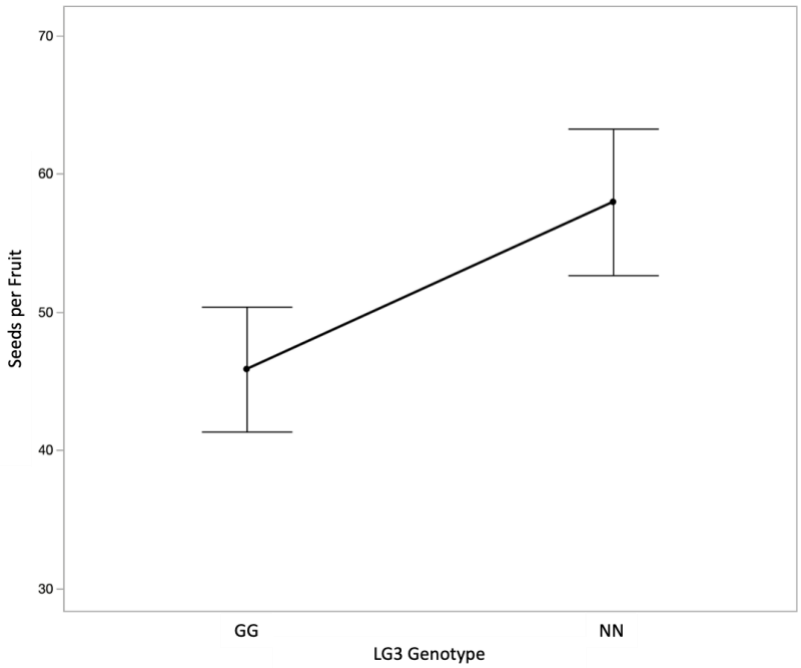
70
60
50
40
30
Seeds per Fruit
GG
NN
LG3 Genotype

978

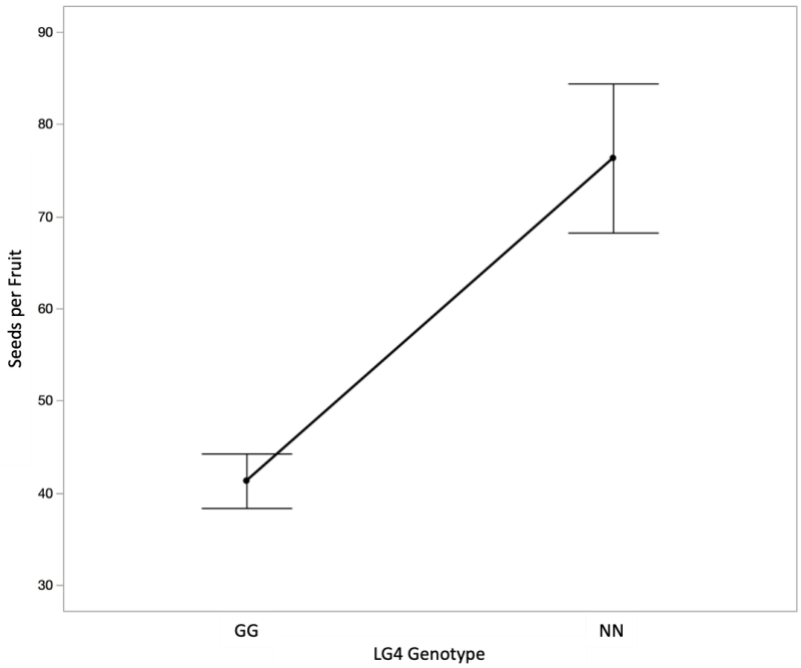

Figure S15. CAC110 RILs female fertility effect plots. Average seeds per fruit of each genotypic class for each significant additive QTL.

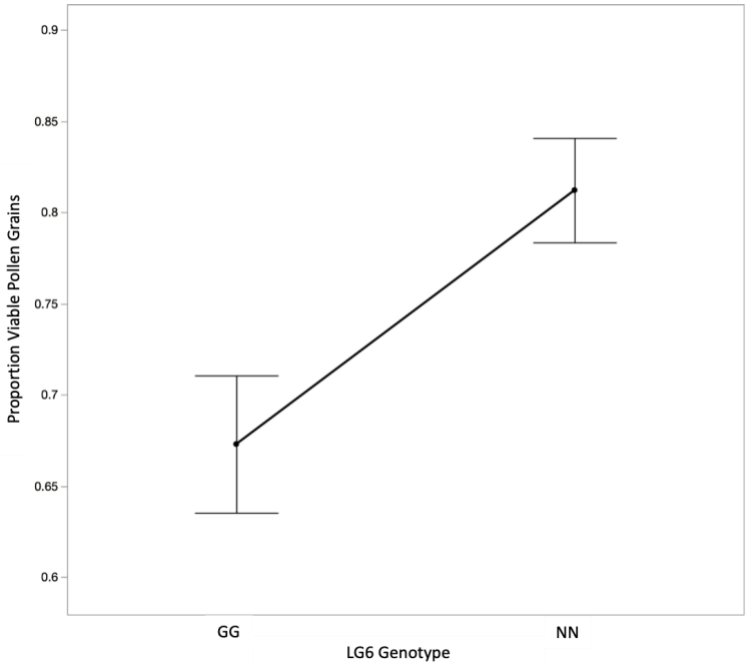

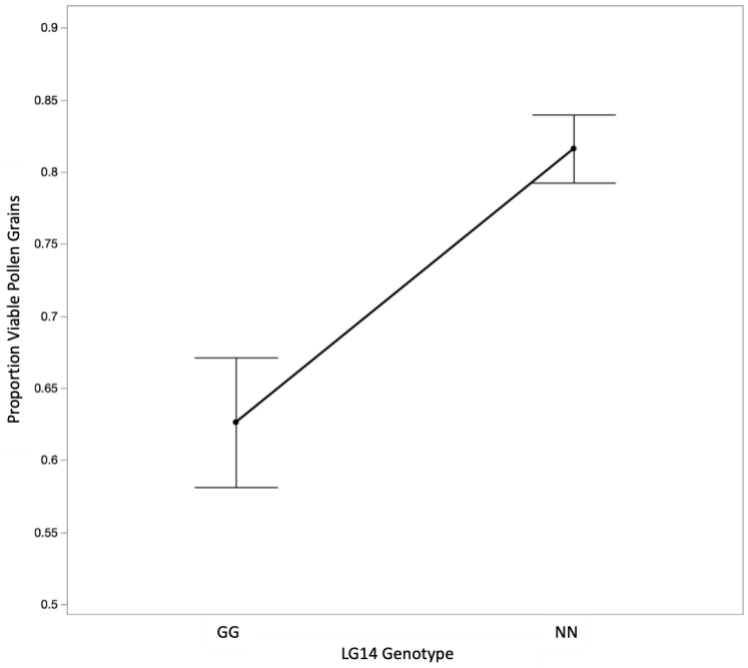

Figure S16. CAC162 RILs male fertility effect plots. Average proportion viable pollen grains of each genotypic class for each significant additive QTL.

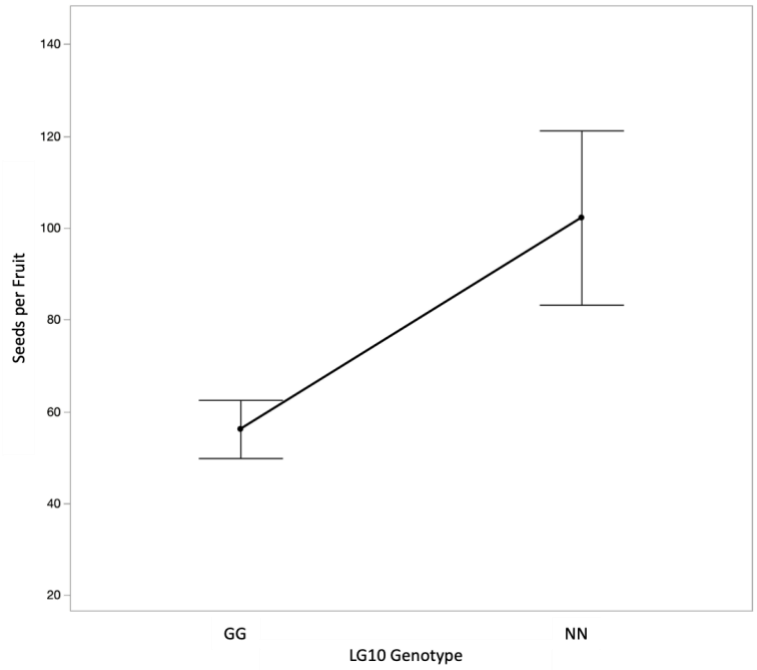

Figure S17. CAC415 RILs female fertility effect plots. Average seeds per fruit of each genotypic class for each significant additive QTL.

Table S1. Geographic locations of *Mimulus* populations used.
Information about the biology, geography, and sequencing of each sample used in this manuscript.

Line abbreviation	Species/Patry	Population	Latitude (N)	Longitude (W)	NCBI SRA Accession No.
CAC110	sympatric *M. guttatus*	Catherine Creek, Washington side of the Columbia River Gorge off of Hwy. 14	45°42′42′′	121°21′55′′	
CAC112					
CAC134					
CAC141					
CAC162					
CAC262					
CAC415					
CAC6					SRX525044
CAC9	sympatric *M. nasutus*	Catherine Creek, Washington side of the Columbia River Gorge off of Hwy. 14			SRX525048
IM62	allopatric *M. guttatus*	Iron Mountain, Hwy. 20, Linn County, Oregon	44°24'03"	122°08'16"	SRX115898
DPRG102	sympatric *M. guttatus*	Don Pedro Reservoir, Stanislaus National Forest, junction of Hwy. 120 and Jacksonville Road, Tuolumne County, California	37°49'44"	120°20'38"	
SF5	allopatric *M. nasutus*	Sherar's Falls, Tygh Valley, Wasco County, Oregon	45°15′52′′	121°01′21′′	SRX116529
KOOT	allopatric *M. nasutus*	West of Kootenai National Forest, off MT 200, north of Cabinet Gorge Reservoir	48°06'14"	115°58'59"	SRX525049
NHN26	sympatric *M. nasutus*	Notch Hill, north of Nanoose Harbour, Vancouver Island, BC	49°16'23'	124°09'36"	SRX525051
DENT13007	*M. dentilobus*	Arizona	unknown	unknown	SRX030541

Table S2. Linkage map construction. Information regarding the number of markers, and program options in LepMAP3 used to construct each of the three linkage maps featured in this manuscript. Each chromosome was either run through SeparateChromosomes2 on its own (independently) or as a group with other chromosomes in the same family (together). Physical orders with better higher likelihoods when run through OrderMarkers2 are shown in bold. The three linkage maps contain as total of 4,967 unique markers among them, 3,141 (~63%) of which are present in all three maps. 513 markers (~10%) are unique to a single map, leaving 1,330 markers (~27%) shared between two of the three maps.

			SeparateChromosomes2			OrderMarkers2			
	LG	Number of markers	Run conditions	LodLimit	Theta	Highest Likelihood 10 iterations	Physical Order Likelihood	Retained positions	Unique positions
CAC110 RILs	1	156	independently	0.1	0.15	-7,008.42	-	156	60
	2	314	independently	0.1	0.15	-6,946.23	-	314	49
	3	292	together	20	0.3	-6,326.90	-	271	40
	4	279	independently	0.1	0.15	-6,730.64	-	279	47
	5	305	together	20	0.3	-10,574.70	-	277	42
	6	335	together	20	0.3	-7,543.75	-	332	57
	7	279	together	20	0.3	-4,606.16	-	252	46
	8	352	independently	0.1	0.15	-15,013.73	-15,514.09	349	88
	9	255	together	20	0.3	-4,355.72	-	255	41
	10	322	together	20	0.3	-8,102.44	-16,185.25	319	55
	11	115	independently	0.1	0.15	-9,735.51	**-8,846.31**	115	67
	12	317	independently	0.1	0.15	-11,752.58	-	304	68
	13	166	independently	0.1	0.15	-6,879.29	-7,732.36	138	50
	14	467	together	20	0.3	-14,236.16	-	467	84
	Global	3954	-	-	-	-	-	3828	794
CAC162 RILs	1	218	together	15	0.25	-3,311.21	-	213	36
	2	340	together	15	0.25	-5,011.07	-	340	47
	3	309	together	15	0.25	-8,771.58	-	291	54
	4	359	independently	0.1	0.15	-6,319.86	-	359	36
	5	331	together	15	0.25	-7,611.04	-	307	36
	6	315	independently	0.1	0.15	-7,782.91	-	315	48
	7	243	together	15	0.25	-6,165.75	-	222	36
	8	392	independently	0.1	0.15	-11,342.19	**-11,224.64**	392	54
	9	265	together	15	0.25	-6,308.35	-	265	45
	10	327	independently	0.1	0.15	-7,708.27	-	303	25
	11	260	independently	0.1	0.15	-8,465.66	-9,211.12	260	35
	12	338	together	15	0.25	-9,874.55	-	316	47
	13	340	together	15	0.25	-4,384.34	-	340	38
	14	466	together	15	0.25	-12,223.42	-	466	69
	Global	4503	-	-	-	-	-	4389	606
CAC415 RILs	1	186	together	15	0.25	-5,020.23	-	174	41
	2	314	together	15	0.25	-6,706.58	-	314	44
	3	302	independently	0.1	0.15	-7,280.74	-	289	34
	4	364	independently	0.1	0.15	-8,592.37	-	363	54
	5	327	independently	0.1	0.15	-7,690.35	-	325	50
	6	323	independently	0.1	0.15	-7,628.57	-	322	51
	7	245	together	15	0.25	-7,388.27	-	237	46
	8	438	together	15	0.25	-12,658.23	-	436	56
	9	268	independently	0.1	0.15	6,441.53	-	266	49
	10	258	together	15	0.25	-5,819.33	-	252	33
	11	289	together	15	0.25	-10,483.63	-11,605.05	255	50
	12	333	independently	0.1	0.15	-7,276.95	-	322	46
	13	343	independently	0.1	0.15	-8,136.78	-	343	58
	14	489	independently	0.1	0.15	-15,535.39	-	481	78
	Global	4479	-	-	-	-	-	4379	690

1001 **Table S3. Positions of significant transmission ratio distortion.** Genetic (cM) and physical (Mb)
1002 position on each chromosome in the three RIL populations that show significant distortion
1003 (Direction) via Chi-Square test at α = 0.01 and Bonferonni-corrected α. Shading indicates
1004 putative contiguous regions of TRD.

Chromosome	cM	Mb	Direction	RIL Population	α Threshold
01	0.000 - 15.128	0.05 - 3.90	*M. guttatus*	CAC110	0.01
01	10.930 - 12.679	3.30 - 3.45	*M. guttatus*	CAC110	0.000167
01	32.397	4.10 - 4.25	*M. guttatus*	CAC110	0.01
01	122.469 - 134.368	11.05 - 12.85	*M. guttatus*	CAC110	0.01
01	124.218 - 134.368	11.10 - 12.85	*M. guttatus*	CAC110	0.000167
01	NA	NA	NA	CAC162	0.01
01	NA	NA	NA	CAC162	0.000278
01	1.220 - 28.693	0.50 - 3.60	*M. guttatus*	CAC415	0.01
01	12.204	3.40 - 3.45	*M. guttatus*	CAC415	0.000244
01	72.640 - 74.470	11.20 - 11.70	*M. nasutus*	CAC415	0.01
02	64.202 - 64.551	18.40 - 18.80	*M. nasutus*	CAC110	0.01
02	74.023 - 86.970	18.95 - 20.55	*M. nasutus*	CAC110	0.01
02	81.370 - 83.468	19.90 - 20.10	*M. nasutus*	CAC110	0.000204
02	34.741 - 36.783	3.40 - 5.25	*M. nasutus*	CAC162	0.01
02	38.823 - 39.844	5.50 - 12.05	*M. nasutus*	CAC162	0.01
02	40.864 - 43.926	12.15 - 15.70	*M. nasutus*	CAC162	0.01
02	NA	NA	NA	CAC162	0.000213
02	56.154	18.50 - 18.75	*M. guttatus*	CAC415	0.01
02	NA	NA	NA	CAC415	0.000227
03	NA	NA	NA	CAC110	0.01
03	NA	NA	NA	CAC110	0.000250
03	22.452 - 31.637	19.65 - 20.85	*M. nasutus*	CAC162	0.01
03	44.449 - 64.360	21.15 - 23.80	*M. nasutus*	CAC162	0.01
03	54.660 - 56.702	22.75 - 23.15	*M. nasutus*	CAC162	0.000185
03	0.000 - 17.078	0.25 - 19.95	*M. guttatus*	CAC415	0.01
03	0.000 - 10.978	1.20 - 19.95	*M. guttatus*	CAC415	0.000294
04	0.000 - 35.719	0.00 - 19.65	*M. guttatus*	CAC110	0.01
04	0.000 - 35.719	0.00 - 19.65	*M. guttatus*	CAC110	0.000213
04	39.221 - 44.119	19.80 - 20.15	*M. guttatus*	CAC110	0.01
04	0.000 - 16.873	0.05 - 3.70	*M. nasutus*	CAC162	0.01
04	0.000	0.05 - 0.45	*M. nasutus*	CAC162	0.000278
04	3.062 - 13.298	1.20 - 3.20	*M. nasutus*	CAC162	0.000278
04	16.873	3.45 - 3.70	*M. nasutus*	CAC162	0.000278
04	42.725 - 54.929	6.45 - 18.95	*M. guttatus*	CAC415	0.01
04	NA	NA	NA	CAC415	0.000185

1005

05	0.000 - 82.002	0.00 - 20.90	*M. guttatus*	CAC110	0.01
05	0.000 - 82.002	0.00 - 20.90	*M. guttatus*	CAC110	0.000238
05	NA	NA	NA	CAC162	0.01
05	NA	NA	NA	CAC162	0.000278
05	2.441 - 9.765	0.50 - 1.75	*M. guttatus*	CAC415	0.01
05	78.303 - 89.303	19.45 - 21.25	*M. nasutus*	CAC415	0.01
05	NA	NA	NA	CAC415	0.000200
06	NA	NA	NA	CAC110	0.01
06	NA	NA	NA	CAC110	0.000175
06	0.000 - 27.785	0.00 - 4.05	*M. guttatus*	CAC162	0.01
06	8.689 - 27.785	1.80 - 4.05	*M. guttatus*	CAC162	0.000208
06	67.161	8.50 - 9.25	*M. guttatus*	CAC162	0.01
06	69.203	13.90 - 14.30	*M. guttatus*	CAC162	0.01
06	69.713	14.35 - 14.40	*M. guttatus*	CAC162	0.01
06	69.713	14.60 - 14.70	*M. guttatus*	CAC162	0.01
06	57.782	6.9 - 7.05	*M. nasutus*	CAC415	0.01
06	60.221	7.60 - 9.20	*M. nasutus*	CAC415	0.01
06	60.221	9.5 - 9.65	*M. nasutus*	CAC415	0.01
06	60.221	10.25 - 15.40	*M. nasutus*	CAC415	0.01
06	NA	NA	NA	CAC415	0.000196
07	45.655 - 72.643	3.05 - 21.80	*M. guttatus*	CAC110	0.01
07	53.409 - 64.250	3.10 - 8.75	*M. guttatus*	CAC110	0.000217
07	65.299 - 72.643	15.00 - 21.80	*M. guttatus*	CAC110	0.000217
07	NA	NA	NA	CAC162	0.01
07	NA	NA	NA	CAC162	0.000278
07	56.933	6.90 - 6.95	*M. nasutus*	CAC415	0.01
07	55.713 - 73.440	8.30 - 14.40	*M. nasutus*	CAC415	0.01
07	64.900	12.85 - 13.05	*M. nasutus*	CAC415	0.000217
07	68.561 - 72.22	15.20 - 16.25	*M. nasutus*	CAC415	0.01
08	56.691 - 67.882	6.60 - 9.00	*M. nasutus*	CAC110	0.01
08	56.691 - 62.287	6.60 - 7.20	*M. nasutus*	CAC110	0.000114
08	63.686	7.90 - 7.95	*M. nasutus*	CAC110	0.000114
08	63.686	8.95 - 9.00	*M. nasutus*	CAC110	0.000114
08	53.543 - 53.893	14.90 - 15.15	*M. nasutus*	CAC110	0.01
08	50.745 - 66.133	15.85 - 17.05	*M. nasutus*	CAC110	0.01
08	65.084 - 66.133	15.85 - 16.05	*M. nasutus*	CAC110	0.000114
08	72.088 - 109.184	18.35 - 27.70	*M. nasutus*	CAC110	0.01
08	82.934 - 87.492	21.25 - 21.65	*M. nasutus*	CAC110	0.000114
08	93.096 - 100.091	21.95 - 23.80	*M. nasutus*	CAC110	0.000114
08	102.889	24.10 - 24.25	*M. nasutus*	CAC110	0.000114
08	104.288	25.35 - 26.40	*M. nasutus*	CAC110	0.000114
08	39.841 - 55.513	4.25 - 7.55	*M. nasutus*	CAC162	0.01
08	71.385 - 117.963	21.50 - 27.35	*M. nasutus*	CAC162	0.01
08	80.576 - 83.129	22.10 - 22.20	*M. nasutus*	CAC162	0.000185
08	95.938 - 117.963	22.70 - 27.35	*M. nasutus*	CAC162	0.000185
08	9.765	1.70 - 1.80	*M. nasutus*	CAC415	0.01
08	NA	NA	NA	CAC415	0.000179

09	NA	NA	NA	CAC110	0.01
09	NA	NA	NA	CAC110	0.000244
09	NA	NA	NA	CAC162	0.01
09	NA	NA	NA	CAC162	0.000222
09	NA	NA	NA	CAC415	0.01
09	NA	NA	NA	CAC415	0.000204
10	19.249 - 20.648	5.10 - 5.30	*M. nasutus*	CAC110	0.01
10	88.257 - 89.656	14.90 - 15.80	*M. guttatus*	CAC110	0.01
10	NA	NA	NA	CAC110	0.000182
10	NA	NA	NA	CAC162	0.01
10	NA	NA	NA	CAC162	0.000400
10	0.000 - 1.220	0.00 - 0.77	*M. nasutus*	CAC415	0.01
10	53.554 - 104.91	1.80 - 22.00	*M. guttatus*	CAC415	0.01
10	53.554 - 95.746	1.80 - 20.25	*M. guttatus*	CAC415	0.000303
10	98.797	20.30 - 20.40	*M. guttatus*	CAC415	0.000303
11	54.170 - 56.618	5.05 - 5.75	*M. guttatus*	CAC110	0.01
11	82.175 - 85.323	9.60 - 9.90	*M. nasutus*	CAC110	0.01
11	94.429 - 132.951	10.35 - 26.70	*M. nasutus*	CAC110	0.01
11	102.823 - 103.523	23.50 - 23.65	*M. nasutus*	CAC110	0.000149
11	119.282 - 124.889	25.30 - 26.60	*M. nasutus*	CAC110	0.000149
11	0.000 - 2.551	0.05 - 1.10	*M. nasutus*	CAC162	0.01
11	1.021 - 2.551	0.75 - 1.10	*M. nasutus*	CAC162	0.000286
11	NA	NA	NA	CAC415	0.01
11	NA	NA	NA	CAC415	0.000200
12	15.399 - 87.186	1.05 - 24.50	*M. nasutus*	CAC110	0.01
12	21.705 - 25.202	1.70 - 5.20	*M. nasutus*	CAC110	0.000147
12	22.404 - 29.398	5.30 - 17.60	*M. nasutus*	CAC110	0.000147
12	38.49 - 60.193	18.60 - 21.70	*M. nasutus*	CAC110	0.000147
12	65.090	22.55 - 22.70	*M. nasutus*	CAC110	0.000147
12	68.239 - 80.538	22.75 - 23.60	*M. nasutus*	CAC110	0.000147
12	8.168 - 9.188	1.30 - 1.90	*M. nasutus*	CAC162	0.01
12	15.823 - 16.334	2.00 - 2.55	*M. nasutus*	CAC162	0.01
12	18.375 - 18.885	2.70 - 3.10	*M. nasutus*	CAC162	0.01
12	17.864 - 30.110	5.05 - 7.95	*M. nasutus*	CAC162	0.01
12	30.110	6.20 - 6.25	*M. nasutus*	CAC162	0.000213
12	30.621	18.55 - 18.60	*M. nasutus*	CAC162	0.01
12	30.621	18.55 - 18.60	*M. nasutus*	CAC162	0.000213
12	32.152 - 67.944	18.65 - 24.20	*M. nasutus*	CAC162	0.01
12	32.152 - 32.152	18.65 - 19.20	*M. nasutus*	CAC162	0.000213
12	37.259 - 45.425	19.80 - 23.40	*M. nasutus*	CAC162	0.000213
12	69.986 - 75.611	24.30 - 24.90	*M. nasutus*	CAC162	0.01
12	NA	NA	NA	CAC415	0.01
12	NA	NA	NA	CAC415	0.000217

13	0.000 - 53.932	2.10 - 25.00	*M. guttatus*	CAC110	0.01
13	0.000 - 45.185	2.10 - 24.00	*M. guttatus*	CAC110	0.000200
13	88.949 - 117.730	26.50 - 30.80	*M. nasutus*	CAC110	0.01
13	88.949 - 117.730	26.50 - 30.80	*M. nasutus*	CAC110	0.000200
13	38.986 - 78.866	25.55 - 30.80	*M. nasutus*	CAC162	0.01
13	54.367 - 78.866	26.30 - 30.80	*M. nasutus*	CAC162	0.000263
13	61.649	25.50 - 25.55	*M. guttatus*	CAC415	0.01
13	NA	NA	NA	CAC415	0.000172
14	0.000 - 22.761	0.00 - 2.35	*M. guttatus*	CAC110	0.01
14	0.000 - 9.099	0.00 - 1.90	*M. guttatus*	CAC110	0.000119
14	0.000 - 3.062	0.00 - 0.60	*M. guttatus*	CAC162	0.01
14	NA	NA	NA	CAC162	0.000145
14	0.000 - 13.422	0.00 - 2.65	*M. guttatus*	CAC415	0.01
14	NA	NA	NA	CAC415	0.000128

1008

Table S4. Average Interchromosomal linkage disequilibrium (r) across all pairwise marker comparisons for each chromosome pair in each RIL population. N is the total number of pairwise marker comparisons. Average ILD of those marker comparisons which are greater than the 95% quantile (r95). N95 is the number of those pairwise comparisons that are greater than the 95% quantile. NA indicates there were no pairwise marker comparisons greater than the 95% quantile.

LG Comparison	r	N	r95	N95	Proportion	RIL Population
01,02	0.1003	2940	NA	0	0.0000	CAC110
01,02	0.0871	1692	NA	0	0.0000	CAC162
01,02	0.0822	1804	NA	0	0.0000	CAC415
01,03	0.0948	2400	NA	0	0.0000	CAC110
01,03	**0.2244**	**1944**	**0.4251**	**25**	**0.0129**	**CAC162**
01,03	0.0618	1394	NA	0	0.0000	CAC415
01,04	**0.0991**	**2820**	**0.4027**	**69**	**0.0245**	**CAC110**
01,04	0.1335	1296	NA	0	0.0000	CAC162
01,04	**0.1431**	**2214**	**0.4041**	**19**	**0.0086**	**CAC415**
01,05	0.1085	2520	NA	0	0.0000	CAC110
01,05	0.1097	1296	NA	0	0.0000	CAC162
01,05	0.1040	2050	NA	0	0.0000	CAC415
01,06	0.0697	3420	NA	0	0.0000	CAC110
01,06	0.0808	1728	NA	0	0.0000	CAC162
01,06	0.0677	2091	NA	0	0.0000	CAC415
01,07	0.1052	2760	NA	0	0.0000	CAC110
01,07	0.0818	1296	NA	0	0.0000	CAC162
01,07	0.0673	1886	NA	0	0.0000	CAC415
01,08	0.0745	5280	NA	0	0.0000	CAC110
01,08	0.1135	1944	NA	0	0.0000	CAC162
01,08	0.1408	2296	NA	0	0.0000	CAC415
01,09	0.0883	2460	NA	0	0.0000	CAC110
01,09	0.1120	1620	NA	0	0.0000	CAC162
01,09	0.0620	2009	NA	0	0.0000	CAC415
01,10	0.0722	3300	NA	0	0.0000	CAC110
01,10	**0.1510**	**900**	**0.4638**	**43**	**0.0478**	**CAC162**
01,10	0.0770	1353	NA	0	0.0000	CAC415
01,11	**0.1260**	**4020**	**0.3961**	**64**	**0.0159**	**CAC110**
01,11	0.0539	1260	NA	0	0.0000	CAC162
01,11	0.0785	2050	NA	0	0.0000	CAC415
01,12	0.0832	4080	NA	0	0.0000	CAC110

01,12	0.1656	1692	NA	0	0.0000	CAC162
01,12	0.0490	1886	NA	0	0.0000	CAC415
01,13	**0.1026**	**3000**	**0.3831**	**24**	**0.0080**	**CAC110**
01,13	0.0816	1368	NA	0	0.0000	CAC162
01,13	**0.1492**	**2378**	**0.4022**	**9**	**0.0038**	**CAC415**
01,14	0.0864	5040	NA	0	0.0000	CAC110
01,14	0.1142	2484	NA	0	0.0000	CAC162
01,14	**0.1319**	**3198**	**0.3934**	**5**	**0.0016**	**CAC415**
02,03	0.0867	1960	NA	0	0.0000	CAC110
02,03	0.0784	2538	NA	0	0.0000	CAC162
02,03	0.0911	1496	NA	0	0.0000	CAC415
02,04	0.0808	2303	NA	0	0.0000	CAC110
02,04	0.0946	1692	NA	0	0.0000	CAC162
02,04	0.0634	2376	NA	0	0.0000	CAC415
02,05	0.0616	2058	NA	0	0.0000	CAC110
02,05	0.1019	1692	NA	0	0.0000	CAC162
02,05	0.0842	2200	NA	0	0.0000	CAC415
02,06	0.0682	2793	NA	0	0.0000	CAC110
02,06	0.0975	2256	NA	0	0.0000	CAC162
02,06	0.0884	2244	NA	0	0.0000	CAC415
02,07	0.0848	2254	NA	0	0.0000	CAC110
02,07	0.0742	1692	NA	0	0.0000	CAC162
02,07	0.1123	2024	NA	0	0.0000	CAC415
02,08	0.0958	4312	NA	0	0.0000	CAC110
02,08	0.1219	2538	NA	0	0.0000	CAC162
02,08	0.0753	2464	NA	0	0.0000	CAC415
02,09	0.0952	2009	NA	0	0.0000	CAC110
02,09	0.0915	2115	NA	0	0.0000	CAC162
02,09	0.0974	2156	NA	0	0.0000	CAC415
02,10	0.0520	2695	NA	0	0.0000	CAC110
02,10	0.0531	1175	NA	0	0.0000	CAC162
02,10	0.1337	1452	NA	0	0.0000	CAC415
02,11	0.0792	3283	NA	0	0.0000	CAC110
02,11	0.1718	1645	NA	0	0.0000	CAC162
02,11	0.0674	2200	NA	0	0.0000	CAC415
02,12	0.0401	3332	NA	0	0.0000	CAC110
02,12	0.0882	2209	NA	0	0.0000	CAC162
02,12	0.0780	2024	NA	0	0.0000	CAC415
02,13	**0.1408**	**2450**	**0.4083**	**90**	**0.0367**	**CAC110**
02,13	0.1008	1786	NA	0	0.0000	CAC162

02,13	0.0684	2552	NA	0	0.0000	CAC415
02,14	0.0945	4116	NA	0	0.0000	CAC110
02,14	0.1041	3243	NA	0	0.0000	CAC162
02,14	0.0707	3432	NA	0	0.0000	CAC415
03,04	0.0496	1880	NA	0	0.0000	CAC110
03,04	0.0856	1944	NA	0	0.0000	CAC162
03,04	0.1287	1836	NA	0	0.0000	CAC415
03,05	0.1039	1680	NA	0	0.0000	CAC110
03,05	0.1435	1944	NA	0	0.0000	CAC162
03,05	0.0768	1700	NA	0	0.0000	CAC415
03,06	0.0940	2280	NA	0	0.0000	CAC110
03,06	0.0809	2592	NA	0	0.0000	CAC162
03,06	**0.1284**	**1734**	**0.4024**	**5**	**0.0029**	**CAC415**
03,07	0.0752	1840	NA	0	0.0000	CAC110
03,07	0.0582	1944	NA	0	0.0000	CAC162
03,07	0.1069	1564	NA	0	0.0000	CAC415
03,08	0.0851	3520	NA	0	0.0000	CAC110
03,08	0.1265	2916	NA	0	0.0000	CAC162
03,08	0.0799	1904	NA	0	0.0000	CAC415
03,09	0.0865	1640	NA	0	0.0000	CAC110
03,09	0.1260	2430	NA	0	0.0000	CAC162
03,09	0.1058	1666	NA	0	0.0000	CAC415
03,10	0.0897	2200	NA	0	0.0000	CAC110
03,10	0.1326	1350	NA	0	0.0000	CAC162
03,10	0.0958	1122	NA	0	0.0000	CAC415
03,11	**0.1867**	**2680**	**0.3860**	**69**	**0.0257**	**CAC110**
03,11	0.1129	1890	NA	0	0.0000	CAC162
03,11	0.0647	1700	NA	0	0.0000	CAC415
03,12	0.0964	2720	NA	0	0.0000	CAC110
03,12	0.0840	2538	NA	0	0.0000	CAC162
03,12	0.0761	1564	NA	0	0.0000	CAC415
03,13	**0.1453**	**2000**	**0.4824**	**64**	**0.0320**	**CAC110**
03,13	0.0684	2052	NA	0	0.0000	CAC162
03,13	0.1268	1972	NA	0	0.0000	CAC415
03,14	0.0543	3360	NA	0	0.0000	CAC110
03,14	0.1271	3726	NA	0	0.0000	CAC162
03,14	0.0718	2652	NA	0	0.0000	CAC415
04,05	0.0623	1974	NA	0	0.0000	CAC110
04,05	0.0706	1296	NA	0	0.0000	CAC162
04,05	**0.1399**	**2700**	**0.3988**	**3**	**0.0011**	**CAC415**

04,06	0.0690	2679	NA	0	0.0000	CAC110
04,06	0.0548	1728	NA	0	0.0000	CAC162
04,06	0.0895	2754	NA	0	0.0000	CAC415
04,07	0.0548	2162	NA	0	0.0000	CAC110
04,07	0.1111	1296	NA	0	0.0000	CAC162
04,07	0.0962	2484	NA	0	0.0000	CAC415
04,08	0.0768	4136	NA	0	0.0000	CAC110
04,08	0.1041	1944	NA	0	0.0000	CAC162
04,08	**0.1439**	**3024**	**0.3979**	**1**	**0.0003**	**CAC415**
04,09	0.0735	1927	NA	0	0.0000	CAC110
04,09	0.1238	1620	NA	0	0.0000	CAC162
04,09	0.1040	2646	NA	0	0.0000	CAC415
04,10	0.0626	2585	NA	0	0.0000	CAC110
04,10	0.1461	900	NA	0	0.0000	CAC162
04,10	0.0672	1782	NA	0	0.0000	CAC415
04,11	0.0755	3149	NA	0	0.0000	CAC110
04,11	0.0728	1260	NA	0	0.0000	CAC162
04,11	0.1005	2700	NA	0	0.0000	CAC415
04,12	0.0470	3196	NA	0	0.0000	CAC110
04,12	0.1031	1692	NA	0	0.0000	CAC162
04,12	0.1035	2484	NA	0	0.0000	CAC415
04,13	**0.1303**	**2350**	**0.3716**	**2**	**0.0009**	**CAC110**
04,13	0.1510	1368	NA	0	0.0000	CAC162
04,13	0.1289	3132	NA	0	0.0000	CAC415
04,14	0.0531	3948	NA	0	0.0000	CAC110
04,14	**0.1708**	**2484**	**0.4401**	**17**	**0.0068**	**CAC162**
04,14	**0.2961**	**4212**	**0.4512**	**832**	**0.1975**	**CAC415**
05,06	0.0675	2394	NA	0	0.0000	CAC110
05,06	0.1297	1728	NA	0	0.0000	CAC162
05,06	**0.0983**	**2550**	**0.4037**	**15**	**0.0059**	**CAC415**
05,07	0.0628	1932	NA	0	0.0000	CAC110
05,07	0.1130	1296	NA	0	0.0000	CAC162
05,07	**0.1240**	**2300**	**0.4012**	**4**	**0.0017**	**CAC415**
05,08	0.0508	3696	NA	0	0.0000	CAC110
05,08	0.0812	1944	NA	0	0.0000	CAC162
05,08	**0.1105**	**2800**	**0.3940**	**1**	**0.0004**	**CAC415**
05,09	0.0724	1722	NA	0	0.0000	CAC110
05,09	0.1111	1620	NA	0	0.0000	CAC162
05,09	0.1016	2450	NA	0	0.0000	CAC415
05,10	0.0599	2310	NA	0	0.0000	CAC110

05,10	0.0734	900	NA	0	0.0000	CAC162
05,10	0.1091	1650	NA	0	0.0000	CAC415
05,11	**0.2175**	**2814**	**0.4226**	**474**	**0.1684**	**CAC110**
05,11	0.1003	1260	NA	0	0.0000	CAC162
05,11	0.1079	2500	NA	0	0.0000	CAC415
05,12	0.0704	2856	NA	0	0.0000	CAC110
05,12	0.1033	1692	NA	0	0.0000	CAC162
05,12	**0.1176**	**2300**	**0.3957**	**4**	**0.0017**	**CAC415**
05,13	**0.1133**	**2100**	**0.3957**	**13**	**0.0062**	**CAC110**
05,13	0.0733	1368	NA	0	0.0000	CAC162
05,13	0.1121	2900	NA	0	0.0000	CAC415
05,14	0.0616	3528	NA	0	0.0000	CAC110
05,14	0.0864	2484	NA	0	0.0000	CAC162
05,14	**0.1589**	**3900**	**0.4167**	**94**	**0.0241**	**CAC415**
06,07	0.0763	2622	NA	0	0.0000	CAC110
06,07	0.0821	1728	NA	0	0.0000	CAC162
06,07	0.1154	2346	NA	0	0.0000	CAC415
06,08	0.0677	5016	NA	0	0.0000	CAC110
06,08	0.1192	2592	NA	0	0.0000	CAC162
06,08	**0.1273**	**2856**	**0.4106**	**23**	**0.0081**	**CAC415**
06,09	0.0496	2337	NA	0	0.0000	CAC110
06,09	0.1248	2160	NA	0	0.0000	CAC162
06,09	0.0741	2499	NA	0	0.0000	CAC415
06,10	0.0717	3135	NA	0	0.0000	CAC110
06,10	0.0845	1200	NA	0	0.0000	CAC162
06,10	**0.1326**	**1683**	**0.4304**	**10**	**0.0059**	**CAC415**
06,11	0.1348	3819	NA	0	0.0000	CAC110
06,11	0.0890	1680	NA	0	0.0000	CAC162
06,11	0.0867	2550	NA	0	0.0000	CAC415
06,12	0.0634	3876	NA	0	0.0000	CAC110
06,12	**0.2184**	**2256**	**0.4341**	**83**	**0.0368**	**CAC162**
06,12	0.1248	2346	NA	0	0.0000	CAC415
06,13	0.0843	2850	NA	0	0.0000	CAC110
06,13	0.0812	1824	NA	0	0.0000	CAC162
06,13	0.0995	2958	NA	0	0.0000	CAC415
06,14	0.0485	4788	NA	0	0.0000	CAC110
06,14	0.0892	3312	NA	0	0.0000	CAC162
06,14	**0.1300**	**3978**	**0.4029**	**1**	**0.0003**	**CAC415**
07,08	0.0530	4048	NA	0	0.0000	CAC110
07,08	0.1047	1944	NA	0	0.0000	CAC162

07,08	**0.1350**	**2576**	**0.4180**	**32**	**0.0124**	**CAC415**
07,09	0.0974	1886	NA	0	0.0000	CAC110
07,09	0.1520	1620	NA	0	0.0000	CAC162
07,09	0.0977	2254	NA	0	0.0000	CAC415
07,10	0.0691	2530	NA	0	0.0000	CAC110
07,10	0.0948	900	NA	0	0.0000	CAC162
07,10	0.0828	1518	NA	0	0.0000	CAC415
07,11	0.0750	3082	NA	0	0.0000	CAC110
07,11	0.0862	1260	NA	0	0.0000	CAC162
07,11	0.1393	2300	NA	0	0.0000	CAC415
07,12	0.0747	3128	NA	0	0.0000	CAC110
07,12	0.0811	1692	NA	0	0.0000	CAC162
07,12	0.0939	2116	NA	0	0.0000	CAC415
07,13	0.0689	2300	NA	0	0.0000	CAC110
07,13	0.1137	1368	NA	0	0.0000	CAC162
07,13	0.0472	2668	NA	0	0.0000	CAC415
07,14	0.0760	3864	NA	0	0.0000	CAC110
07,14	0.1120	2484	NA	0	0.0000	CAC162
07,14	0.0740	3588	NA	0	0.0000	CAC415
08,09	0.0781	3608	NA	0	0.0000	CAC110
08,09	0.1185	2430	NA	0	0.0000	CAC162
08,09	0.1120	2744	NA	0	0.0000	CAC415
08,10	0.0597	4840	NA	0	0.0000	CAC110
08,10	0.1139	1350	NA	0	0.0000	CAC162
08,10	0.0935	1848	NA	0	0.0000	CAC415
08,11	0.0939	5896	NA	0	0.0000	CAC110
08,11	0.0979	1890	NA	0	0.0000	CAC162
08,11	0.0908	2800	NA	0	0.0000	CAC415
08,12	0.0849	5984	NA	0	0.0000	CAC110
08,12	0.0863	2538	NA	0	0.0000	CAC162
08,12	0.0740	2576	NA	0	0.0000	CAC415
08,13	0.1100	4400	NA	0	0.0000	CAC110
08,13	0.0866	2052	NA	0	0.0000	CAC162
08,13	0.1011	3248	NA	0	0.0000	CAC415
08,14	0.0686	7392	NA	0	0.0000	CAC110
08,14	0.1274	3726	NA	0	0.0000	CAC162
08,14	0.0995	4368	NA	0	0.0000	CAC415
09,10	0.0904	2255	NA	0	0.0000	CAC110
09,10	0.1074	1125	NA	0	0.0000	CAC162
09,10	0.0758	1617	NA	0	0.0000	CAC415

09,11	**0.1469**	**2747**	**0.3752**	**2**	**0.0007**	**CAC110**
09,11	0.0711	1575	NA	0	0.0000	CAC162
09,11	0.0896	2450	NA	0	0.0000	CAC415
09,12	0.0639	2788	NA	0	0.0000	CAC110
09,12	0.1226	2115	NA	0	0.0000	CAC162
09,12	0.1003	2254	NA	0	0.0000	CAC415
09,13	0.0699	2050	NA	0	0.0000	CAC110
09,13	0.0717	1710	NA	0	0.0000	CAC162
09,13	**0.1417**	**2842**	**0.4009**	**1**	**0.0004**	**CAC415**
09,14	0.0612	3444	NA	0	0.0000	CAC110
09,14	0.1531	3105	NA	0	0.0000	CAC162
09,14	0.0679	3822	NA	0	0.0000	CAC415
10,11	0.0930	3685	NA	0	0.0000	CAC110
10,11	0.1011	875	NA	0	0.0000	CAC162
10,11	0.0721	1650	NA	0	0.0000	CAC415
10,12	0.0570	3740	NA	0	0.0000	CAC110
10,12	0.0980	1175	NA	0	0.0000	CAC162
10,12	0.1084	1518	NA	0	0.0000	CAC415
10,13	0.0757	2750	NA	0	0.0000	CAC110
10,13	0.1372	950	NA	0	0.0000	CAC162
10,13	0.0864	1914	NA	0	0.0000	CAC415
10,14	0.0664	4620	NA	0	0.0000	CAC110
10,14	0.1520	1725	NA	0	0.0000	CAC162
10,14	0.1194	2574	NA	0	0.0000	CAC415
11,12	**0.1682**	**4556**	**0.3902**	**135**	**0.0296**	**CAC110**
11,12	0.0680	1645	NA	0	0.0000	CAC162
11,12	0.0685	2300	NA	0	0.0000	CAC415
11,13	0.0919	3350	NA	0	0.0000	CAC110
11,13	0.0740	1330	NA	0	0.0000	CAC162
11,13	0.0794	2900	NA	0	0.0000	CAC415
11,14	0.0930	5628	NA	0	0.0000	CAC110
11,14	0.1356	2415	NA	0	0.0000	CAC162
11,14	**0.1458**	**3900**	**0.3904**	**1**	**0.0003**	**CAC415**
12,13	0.0909	3400	NA	0	0.0000	CAC110
12,13	0.0714	1786	NA	0	0.0000	CAC162
12,13	0.0941	2668	NA	0	0.0000	CAC415
12,14	0.1328	5712	NA	0	0.0000	CAC110
12,14	0.1018	3243	NA	0	0.0000	CAC162
12,14	0.1522	3588	NA	0	0.0000	CAC415
13,14	**0.1047**	**4200**	**0.3966**	**10**	**0.0024**	**CAC110**

13,14	0.1072	2622	NA	0	0.0000	CAC162
13,14	**0.1665**	**4524**	**0.4149**	**50**	**0.0111**	**CAC415**

1015

Table S5. Positions of two-locus epistasis. Physical (Mb) positions of pairs of loci on each linkage group (LG) in the three RIL populations that show LD (r) in the 95th percentile. Counts of each genotypic class in the population and Chi-Square statistics from likelihood ratio tests, with p<0.0001 are shown in bold. Loci marked with an asterisk have peak r and χ^2 values at adjacent markers. Single locus proportions of *M. guttatus* alleles (G Prop.) were used to determine if the pattern of TRD at each epistatic locus could be explained by a two locus hybrid incompatibility (NG- or GN-), or if single locus distortion in the same direction better explains the pattern (GG++, GG+, NN++, or NN+). The best candidates for two locus hybrid incompatibilities are shaded grey.

	Locus 1		Locus 2										Locus 1	Locus 2	
Population	LG	Mb	LG	Mb	r	GG	GN	NG	NN	N	χ2	p	G Prop.	G Prop.	Pattern
	03	**20.40 - 22.65**	**13**	**3.05 - 5.20**	**0.56**	**64**	**3**	**17**	**19**	**103**	**32.552**	**<0.0001**	**0.65**	**0.79**	**GG++**
	05	**3.10 - 20.75**	**11**	**2.55 - 4.90**	**0.54**	**39**	**21**	**1**	**22**	**83**	**29.035**	**<0.0001**	**0.72**	**0.48**	**NG-**
	01	**11.15 - 12.85**	**04**	**1.20 - 19.65**	**0.46**	**73**	**13**	**12**	**19**	**117**	**22.858**	**<0.0001**	**0.74**	**0.73**	**GG++**
	02	**2.85 - 18.95**	**13**	**21.75 - 23.65**	**0.45**	**54**	**1**	**26**	**14**	**95**	**21.079**	**<0.0001**	**0.58**	**0.84**	**GG++**
	09	**0.80 - 0.90**	**11**	**26.30 - 26.60**	**0.38**	**29**	**37**	**6**	**54**	**126**	**19.359**	**<0.0001**	**0.52**	**0.28**	**NG-**
	05	**2.40 - 20.90**	**11**	**5.05 - 10.20***	**0.50**	**43**	**14**	**5**	**17**	**79**	**18.697**	**<0.0001**	**0.72**	**0.61**	**GG++**
	03	**0.15 - 18.95**	**11**	**24.35 - 25.30**	**0.40**	**29**	**24**	**12**	**56**	**121**	**18.567**	**<0.0001**	**0.44**	**0.34**	**NN++**
CAC110	**11**	**8.80 - 24.40**	**12**	**1.00 - 19.2**	**0.44**	**18**	**12**	**12**	**59**	**101**	**17.988**	**<0.0001**	**0.30**	**0.30**	**NN++**
	01	**3.30 - 5.50**	**11**	**4.00 - 5.75**	**0.47**	**29**	**9**	**10**	**24**	**72**	**16.515**	**<0.0001**	**0.53**	**0.54**	**GG+**
	05	**2.25 - 3.50**	**13**	**24.00 - 25.00**	**0.44**	**54**	**13**	**7**	**14**	**88**	**15.846**	**<0.0001**	**0.76**	**0.69**	**GG++**
	13	25.00 - 25.70	14	1.25 - 2.15	0.41	41	7	15	17	80	13.622	0.0002	0.60	0.70	GG+
	03	18.40 - 21.55	11	3.35 - 6.25	0.42	34	7	12	17	70	13.194	0.0003	0.59	0.66	GG+
	01	7.80 - 9.60	13	21.75 - 23.65	0.42	40	2	25	12	79	11.101	0.0009	0.53	0.82	GG+
	04	3.80 - 3.90	13	21.40 - 21.55	0.37	60	1	16	5	82	9.671	0.0019	0.74	0.93	GG++
	01	11.10 - 11.15	11	4.10 - 4.55	0.39	26	13	5	15	59	9.497	0.0021	0.66	0.53	GG+
	04	**19.90 - 22.80**	**14**	**2.35 - 18.15**	**0.50**	**29**	**10**	**14**	**44**	**97**	**24.708**	**<0.0001**	**0.40**	**0.44**	**NN+**
CAC162	**01**	**1.40 - 5.55**	**10**	**19.65 - 19.95**	**0.54**	**27**	**9**	**8**	**31**	**75**	**23.571**	**<0.0001**	**0.48**	**0.47**	**NN+**
	06	**6.30 - 15.10**	**12**	**6.20 - 7.75**	**0.47**	**9**	**50**	**23**	**15**	**97**	**21.637**	**<0.0001**	**0.61**	**0.33**	**HV**
	01	**2.35 - 5.45**	**03**	**0.00 - 20.65**	**0.45**	**28**	**21**	**7**	**42**	**98**	**20.628**	**<0.0001**	**0.50**	**0.36**	**NG-**
	04	**1.90 - 22.30**	**14**	**2.15 - 25.60**	**0.61**	**34**	**9**	**7**	**31**	**81**	**31.85**	**<0.0001**	**0.53**	**0.51**	**GG+**
	06	**17.00 - 19.25**	**10**	**19.50 - 20.25**	**0.43**	**38**	**0**	**22**	**13**	**73**	**22.217**	**<0.0001**	**0.52**	**0.82**	**GG+**
	05	**3.50 - 20.40**	**14**	**16.50 - 23.00**	**0.49**	**26**	**5**	**17**	**32**	**80**	**19.799**	**<0.0001**	**0.39**	**0.54**	**GN-**
	07	**13.20 - 21.80**	**08**	**22.30 - 27.70**	**0.48**	**23**	**7**	**14**	**38**	**82**	**19.719**	**<0.0001**	**0.37**	**0.45**	**NN+**
	13	**22.05 - 25.55**	**14**	**0.00 - 3.00**	**0.47**	**41**	**6**	**15**	**20**	**82**	**18.738**	**<0.0001**	**0.57**	**0.68**	**GG+**
	06	**9.65 - 16.00**	**08**	**23.60 - 25.55**	**0.44**	**22**	**10**	**12**	**37**	**81**	**15.892**	**<0.0001**	**0.40**	**0.42**	**NN+**
	01	**5.85 - 7.40**	**04**	**4.10 - 16.55**	**0.43**	**32**	**6**	**18**	**24**	**80**	**15.338**	**<0.0001**	**0.48**	**0.63**	**GN-**
	01	**7.70 - 11.70**	**13**	**24.20 - 25.15**	**0.42**	**24**	**4**	**22**	**30**	**80**	**15.279**	**<0.0001**	**0.35**	**0.58**	**GN-**
	05	**20.85 - 21.75**	**06**	**7.10 - 16.05**	**0.43**	**20**	**11**	**11**	**40**	**82**	**15.242**	**<0.0001**	**0.38**	**0.38**	**NN++**
	05	20.05 - 20.40	07	20.05 - 21.80	0.42	17	7	15	42	81	14.019	0.0002	0.30	0.40	NN+
CAC415	06	6.30 - 6.45	14	8.85 - 9.80	0.49	24	7	18	32	81	13.719	0.0002	0.38	0.52	GN-
	05	8.50 - 17.80	12	0.30 - 0.70	0.40	23	7	18	33	81	13.458	0.0002	0.37	0.51	GN-
	03	15.95 - 19.85	06	17.65 - 20.05	0.41	44	18	5	15	82	13.338	0.0003	0.76	0.60	GG+
	04	19.75 - 19.90	08	2.20 - 2.50	0.40	13	36	22	11	82	13.207	0.0003	0.60	0.43	HV
	05	21.40 - 21.75	08	22.10 - 22.15*	0.39	22	9	16	35	82	12.436	0.0004	0.38	0.46	NN+
	01	3.35 - 3.40	14	20.65 - 22.70	0.40	35	18	5	17	75	12.133	0.0005	0.71	0.53	GG+
	11	24.70 - 25.50	14	25.10 - 25.15*	0.39	32	15	10	24	81	12.119	0.0005	0.58	0.52	GG+
	07	1.00 - 1.45	08	18.50 - 18.55*	0.40	13	30	26	12	81	12.078	0.0005	0.53	0.48	HV
	04	20.05 - 20.10	05	2.40 - 3.50	0.40	33	11	10	19	73	12.024	0.0005	0.60	0.59	GG+
	05	0.50 - 1.20	06	1.45 - 1.50	0.40	23	21	2	18	64	11.726	0.0006	0.69	0.39	NG-
	09	23.70 - 23.85	13	26.20 - 27.70*	0.40	14	25	30	11	80	11.494	0.0007	0.49	0.55	HV

1026